GREEN DIESEL PRODUCTION VIA CATALYTIC HYDROGENATION/DECARBOXYLATION OF TRIGLYCERIDES AND FATTY ACIDS OF VEGETABLE OIL AND BROWN GREASE

by

ELVAN SARI

DISSERTATION

Submitted to the Graduate School

of Wayne State University,

Detroit, Michigan

in partial fulfillment of the requirements

for the degree of

DOCTOR OF PHILOSOPHY

2013

MAJOR: CHEMICAL ENGINEERING

Approved by:

_____

Advisor   Date

_____

_____

_____

ACKNOWLEDGMENTS

TABLE OF CONTENTS

iii

LIST OF TABLES

LIST OF FIGURES

CHAPTER 1

INTRODUCTION

1.1 Overview

Total worldwide energy consumption was 5×10^{20} J in 2008, with the majority (80 - 90 %) being derived from the combustion of fossil fuels.[1] The world energy demand is projected to increase by more than 55% between 2005 and 2030 according to International Energy Agency (IEA) and vast investments will be necessary to meet this increased demand.[2] Assuming fossil fuels prices will remain relatively high in the next few decades, global consumption of those fuels is projected to only increase at an average annual rate of 0.9 percent from 2006 to 2030 making these liquid fuels the slowest growing source of energy. In contrast, renewable energy sources are the world's fastest growing sector of the world's energy resources, with consumption estimated to increase by 3.0 percent per year.[1]

There are several factors that improve the prospects for renewable energy sources worldwide including the projected oil prices, the environmental impact of fossil fuel use, energy security, and strong government incentives. The transportation sector is the world's largest user of fossil energy.[3] While there are several sources of energy, current modes of transportation are still nearly 95% dependent on oil in the US. Today's goals include reducing our dependence on fossil fuels, improving energy efficiency, and pursuing alternative sources of energy.[1] Hydrogen, liquefied petroleum gases, liquefied natural gas, biomass, biodiesel, and green diesel are only some of the alternative energy sources that are being researched and considered as possible fossil fuel replacements. Although, all the alternative energy sources show potential for partially replacing fossil fuels as the next transportation fuel, many also display several disadvantages. However, green diesel has presented the most promising results among biodiesel due to its

superior fuel properties. Therefore, green diesel could potentially be the answer for the future transportation energy demands.

1.2 Why Renewable Fuels?

The world's energy demand has been increasing, especially in the transportation sector. Around 40% of total energy use is related to transportation fuels, which will experience additional demand for liquid fuels in the future[4] due to a movement toward motorized transportation in developing countries . The motivation for seeking environmentally friendly, renewable and alternative fuels is based on three main concerns: environment, economy, and energy security.

The environmental concerns are mostly related to air pollution, thereby global warming. Greenhouse gas (GHG) emissions from the energy sector are significantly increasing, which is causing climate change. While power production is the main contributor to GHG emissions, the second largest source is motorized transportation[5]. According to the EPA, carbon dioxide (CO_2) emissions, the major GHG associated with vehicle transportation, rose by 29% between 1990 and 2007[6]. Approximately 20% of the total CO_2 currently released into the atmosphere by human activities such as transport related emissions and they are expected to rise in the future.[7] Transportation utilizes petroleum-based products with gasoline making up more than 50 % of the emissions with diesel and jet fuel contributing the remainder. Therefore, fossil fuel usage is a major component of the climate change problem. Although CO_2 capturing and storage (CCS) technology is believed to help alleviate environmental impact of GHG, CCS is inappropriate for mobile applications.[5] On the other hand, GHG emissions reduction can be achieved by changing transportation fuel resources from fossil fuel to renewable fuel[5]. Not only global climate change, but also local air pollution in metropolitan cities can be prevented by use of renewable fuels. The

above mentioned environmental concerns turn alternative renewable fuels into key elements of an energy solution for the future. [7]

In order to help deal with environmental, economical, and energy security issues, petroleum alternatives should be expanded. The more renewable resources are employed; a cleaner atmosphere, stable economy, and consistent energy solution will be provided to the next generations.

1.3 Liquid Biofuels

Liquid transportation fuels obtained from renewable agricultural sources, such as corn starch, vegetable oils, animal fats, grasses, trees, and so on, are called biofuels. [4] The biofuel initiative was started by Rudolph Diesel with his engine invention that was fueled with peanut oil more than a century ago and has been repeatedly utilized during shortage periods such as conflict and civil unrest. [8]

Moreover, , sustainability and reliability can be deemed as other unique advantages of biofuels[9]. Apart from that, biofuels are the only effective alternatives to petroleum because they have the potential for large volume production.[10]

The raw material for biofuels is biomass. Biomass resources comprise of carbohydrates, lignin, and lipids.[4] There are several mechanisms to produce biofuel from biomass such as pyrolysis, gasification, chemical, and biochemical processes. Pyrolysis and gasification processes generate syngas (CO, H_2), which is then turned into hydrocarbons as fuel. Chemically processing biomass produces biofuels through homogeneous or heterogeneous catalysis; while biochemical processes occur via enzymatic catalysis such as fermentation of biomass.[4]

Liquid biofuels can be classified into two main categories including traditional (first generation) biofuels and next generation (second generation) biofuels.[5] The fuels obtained from

food sources such as sugar crops, corn, wheat, and oilseed crops are called first generation biofuels.[8] Bioethanol and biodiesel are two examples of commercial, traditional liquid biofuels.[11] Bioethanol is produced via fermentation of carbohydrates. It can be used as a petroleum substitute or in a petroleum blend. Ethanol obtained from corn is the current leader in the U.S. biofuels market with production at 6.4 billion gallons per year in 2007 as shown in Figure 1.[12] Around 14% of the U.S. corn crop was used for producing ethanol which corresponds to nearly 4% of total gasoline consumed based on its energy in the U.S. in 2006.[12] On the other hand, its energy density is low comparing to that of petroleum since ethanol has lower carbon number.[8] Secondly, producing bioethanol from sugar or corn crops causes rivalry of food and fuel sources just like any other first generation biofuels.[8] Even though bioethanol fuel production is expected to increase in the future, its growth will depend on the improvements of new production technologies of bioethanol because of the agricultural limitations.[12]
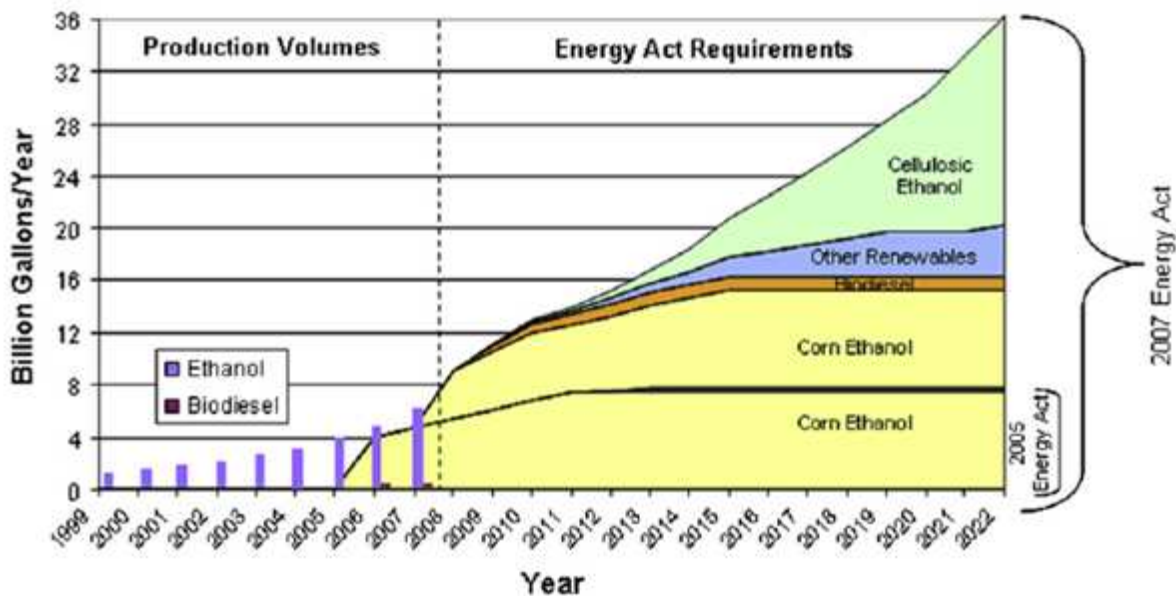
Figure 1. U.S. renewable fuels production and requirements [12]

Although production of ethanol derived from corn is the current focus in the U.S., a new biofuel that can be produced from different lignocellulosic feedstocks, animal fats and oils is emerging.[12] These biofuels based on non-food crops biofuels are called ''2nd generation biofuels'' or "next generation biofuels".[8] Next generation liquid biofuels involve ethanol from cellulosic feedstock, synthetic ethers, and diesel such as ethyl tert-butyl ether (ETBE), bio-methyl tert-butyl ether (bio-MTBE), and green diesel.

Cellulosic ethanol is a biofuel produced from lignocellulosic sources such as wood, grasses or non-edible plants by either fermentation or gasification processes. Both production technologies have multiple steps and require pretreatment and distillation. Cellulosic ethanol production by fermentation consists of hydrolysis, where complex cellulose is broken into glucose, and then microbial fermentation is employed to produce ethanol.[13] Gasification, the second way to cellulosic ethanol production, transforms the lignocellulosic material into carbon monoxide, carbon dioxide and hydrogen which are called syngas. Syngas can then be converted, in a catalytic reactor, to ethanol along other higher alcohols. Although cellulosic ethanol can be derived from a variety of raw materials relative to ethanol from corn and sugar cane, both fermentation and gasification require significant processing.

Bio-ethyl tert-butyl ether (bio-ETBE) is an oxygenated hydrocarbon extensively used worldwide as a gasoline additive similar to ethanol. It is produced by reacting bio- ethanol with fossil isobutylene in the presence of heat and a catalyst. Bio-ETBE offers the same benefits as bioethanol including reduced air pollution, increased fuel octane, and reduced oil imports without the technical and logistic difficulties shown by the alcohol. Unlike bio-ethanol, bio-ETBE does not induce evaporation of gasoline, which is one of the causes of smog, and does not absorb moisture from the atmosphere. Furthermore, bio-ETBE characteristics are superior to

other ethers and include: low volatility, low water solubility and higher water tolerance, very low sulfur content, no dangerous commingling or azeotrope formation, high octane value, and reduced tailpipe CO and hydrocarbon emissions. ETBE is also superior to bio-methyl tert butyl ether (bio-MTBE), another fuel oxygenate used worldwide. Bio-MTBE is produced by reacting bio-methanol and isobutylene in the presence of a catalyst and heat.[14] Although it reduces ozone precursors emission and has similar octane value to ETBE, MTBE is highly soluble in water and has high resistance to biodegradation. These last two characteristics makes MTBE a less likely candidate compared to bio- ETBE which has partially replaced it, since it transfers readily to groundwater and causes contamination problems when fuel spills and leaks occur.[15] Although these two ether based fuels look promising, both require the use of a fossil fuel for their production. The use of fossil fuel by large petroleum companies make bio-ETBE and bio-MTBE further removed from a "true" biofuel.

It is possible to produce diesel-like fuel by using either lignocellulosic biomass, vegetable oils, or animal fats as feedstocks. Diesel like biofuel production from lignocellulosic feedstock requires two stages. The first stage includes synthesis gas production via the Fischer-Tropsch process or pyrolysis. These gases are then converted to a diesel-like fuel by means of hydroprocessing.[11] On the other hand, it is possible to produce diesel-like fuel using relatively simple processes in two different paths starting from vegetable oils and animal fats. The first pathway is transesterification for biodiesel, and the second way is hydrogenation of green diesel or hydrogenation derived renewable diesel (HDRD).[11] The current status of the biomass to biofuel conversion technologies are shown in Table 1.[11] Biodiesel and HDRD are already in the market while the Fischer-Tropsch and pyrolysis derived diesel are still in the developing stages. In 2009, there were about 170 biodiesel plants in the U.S., and the list is expected to rise in the

coming years [12]assuming they are cost competitive. For the Fischer-Tropsch and pyrolysis processes much more research is needed in order to make these processes more feasible.

Table 1. Biomass-to- biofuel conversion technologies: current development stages.[11]

Technologies	Laboratory	Pilot Plant	Demonstration Plant	Market
Sugar/Starch ethanol				
Lignocellulosic ethanol				
P-Series				
Biodiesel & HDRD				
Syn. bio FT diesel				
Methanol				
DME				
Biomethane				
Bio-SNG				
Green pyrolysis diesel				

#HDRD: Hydrogenation derived renewable diesel (i.e., NExBTL)   DME: Dimethyl ether   Bio-SNG: Bio-Synthetic natural gas

Diesel type fuels including green diesel, other synthetic diesels, and biodiesel have a great number of benefits over conventional diesel fuel in terms of fuel properties. Comparison of NExBTL as an example of green diesel, GTL (gas to liquid) as a synthetic fuel, FAME as a biodiesel, and petroleum diesel fuel properties are given in Table 2. NExBTL is a green diesel product of Neste Oil, which is paraffinic and clean burning fuel reducing NOx and PM emissions when compared with conventional diesel fuel.[5] The most significant characteristic of NExBTL is its increased cetane number which is as high as 99 while diesel EN590 has a cetane number of 53 and biodiesel has a value of 51. Biodiesel (FAME) is has lower particulate matter emission than petroleum diesel, but produces a slightly higher NOx emission.[5] Overall, synthetic diesel fuels possess similar properties such as viscosity, cloud point, lower heating value, oxygen and sulfur

contents, while FAME differs from diesel in terms of fuel composition, viscosity, lower heating value and oxygen content.

Table 2. Properties of selected diesel-type fuels 5

FUEL PROPERTIES	NExBTL biodiesel	GTL diesel	FAME (RME)	Diesel EN590/2005
Density @15°C [kg/m3]	775...785	770....785	≈ 885	≈ 835
Viscosity @40°C [mm2/s]	2.9...3.5	3.2...4.5	≈ 4.5	≈ 3.5
Cetane number	84...99 **)	73...81	≈ 51	≈ 53
Distillation 10 vol% [°C]	260...270	≈ 260	≈ 340	≈ 200
Distillation 90 vol% [°C]	295...300	325...330	≈ 355	≈ 350
Cloud point [°C]	- 5...- 30	0...- 25	≈ - 5	≈ - 5
Lower heating value [MJ/kg]	≈ 44	≈ 44	≈ 38	≈ 43
Lower heating value [MJ/litres]	≈ 34	≈ 34	≈ 34	≈ 36
Polyaromatics [wt%]	0	0	0	≈ 4
Oxygen [wt%]	0	0	≈ 11	0
Sulfur [mg/kg]	<10	< 10	< 10	< 10

Germany is one of the largest biodiesel producers worldwide and held a 0.9 % biodiesel share of the entire fuel market and 2.2 % share of the diesel fuel market in 2003.[7] Now, only rapeseed methyl esters as biofuels are available in the German fuel market with over 1700 public fueling stations.[7] After becoming widespread in Europe, biodiesel now is gaining more popularity in the U.S. Table 3 projects biodiesel consumption in the U.S. and Europe based on soybean oil and rapeseed oil respectively in 2006. Although today FAME enjoys a larger share of the fuel market of renewable fuels, next generation biofuels will likely take their place because of their high quality and better efficiency.[5]

Table 3. Biodiesel consumption in the USA and Europe 11.

Biodiesel	USA	Europe
Consumption 2006 (billion gallons)[1]	0.263	1.2
Main sources	Soybean	Rapeseed

1.3.1 Second Generation Biofuel Challenges

There are several factors that make commercialization of second-generation biofuels viable.[11] An important factor is the wide variety of biomass feedstocks that are available to be converted into biofuels by multiple processing technologies. This provides the option of using whatever feedstock is available in a certain region to be utilized to maximize biofuel production leading to a greater energy security. Furthermore, the wide array of feedstocks that can be used for the production of second-generation biofuels allows for less land to be utilized in order to grow crops making biofuel fabrication more sustainable. It is also important to note that these energy-crops are not explicitly harvested in areas destined for food crops and can be grown in low quality environments. [8,11] Moreover, efforts are continuously being employed to improve the production processes by reducing the utility (electrical power and heat) and chemical (oxygen, hydrogen and others) costs needed to process biomass into the desired form of energy. Furthermore, although there are differences between the chemical and physical properties of biofuels according to the different processing technologies, all biofuels are generally more environmentally friendly than conventional fuels. Another important driving force is the option of using already available processing plants where little or no modification is required for full implementation of the process necessary for manufacturing second-generation biofuels. If an already existing facility is modified for new processes, the cost of building new facilities can be eliminated and the capital cost substantially reduced. However, despite these advantages, main

challenge hindering second-generation biofuels still exists.[11] The initial capital investment cost
for second-generation biofuels is still higher than that of first generation biofuels.[8]

1.4. Introduction to Feedstock

There is a large biomass feedstock variety available to produce liquid transportation
biofuels [9]. The biomass feedstocks can be classified into three basic categories: lignocellulosics,
amorphous sugars, and triglycerides (Figure 2).[4]
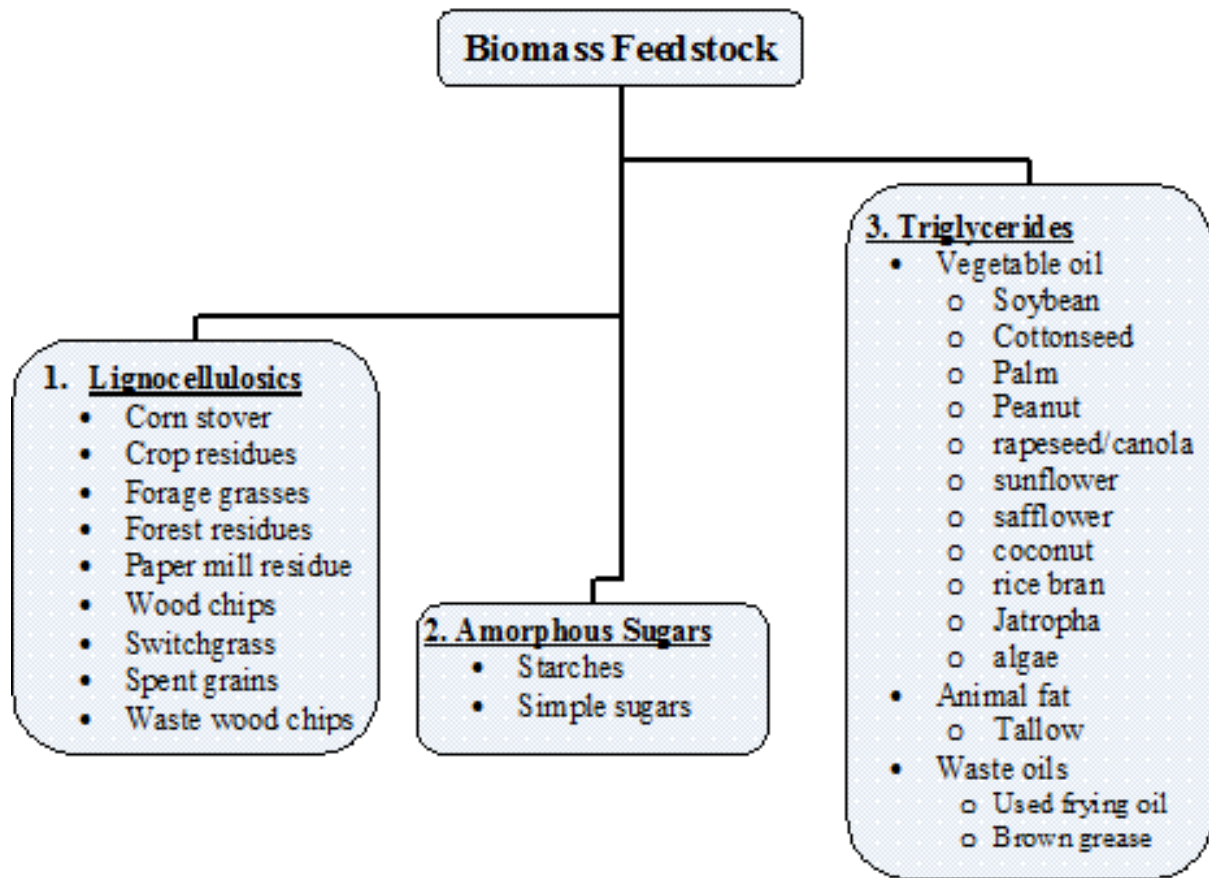
Figure 2. Biomass feedstock classification for liquid transportation biofuel production.

Lignocellulose is a composite material of rigid cellulose fibers which are very large polymers composed of many glucose molecules; lignin which is a polymer constructed of non-carbohydrate and alcohol units; and hemicelluloses which consist of short, highly branched, sugar chains.[16] Depending on the proportions of cellulose, hemicellulose, and lignin in the composition, diverse lignocellulose materials can result. Typical biomass contains 40% - 60% cellulose, 10% - 25% lignin, and 20% - 40% hemicelluloses.[16] Corn stover , crop residues , forage grasses, forest residues, paper mill residue, wood chips, switchgrass, spent grains, and waste wood chips are suitable foodstock examples of lignocellulosic biomass to utilize in next generation biofuel production.[16] Although lignocellulosic biomass is inexpensive as a feedstock and easy to find, it is an expensive transportation fuel because it is a low-energy-density feedstock. [4]

Amorphous sugars such as starches and simple sugars can also be used as biomass feedstocks in order to produce liquid alternative biofuels. However, one of the main arguments against its use is the food versus fuel debate.[17] First generation biofuels made from food crops (starch or sugars) utilize crop sources that could otherwise be used for feeding people or livestock. Many support the idea that diverting crops away from food usage will create several adverse effects. Among these are the loss of farmable land to harvesting crops for starch and sugar based biofuels instead of food supplies for the population and livestock.[18] In addition, loss of crops to fuel production will lead to price inflation of food items because of the lack of availability of crops for food consumption.[17,18]

Triglycerides which are the main constituents of vegetable oil and animal fats represent the third group of biomass feedstock for transportation fuels. Vegetable oils are composed of

triglycerides which have glycerin in their structure. The structure of a triglyceride molecule includes glycerol and three fatty acids is shown in Figure 3.[8]
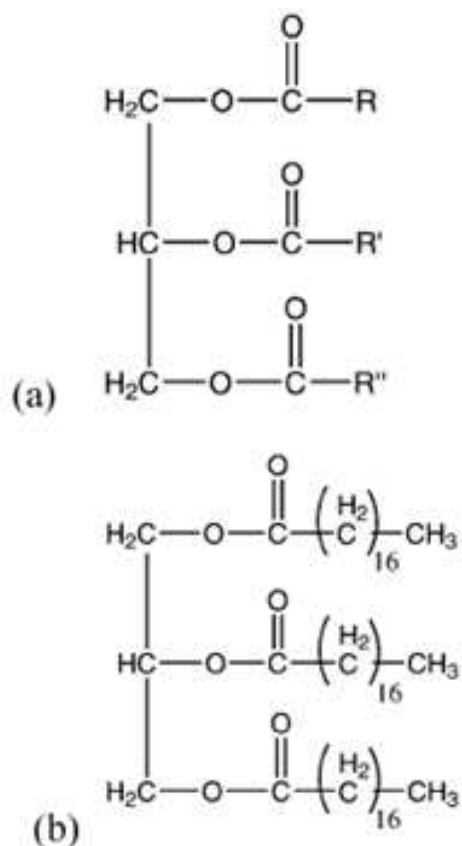
Figure 3. (a) Structure of a triglyceride molecule, (b) the triacylglyceride of stearic acid (octadecanoic acid) .[8]

Figure 4 shows the structure of a saturated and an unsaturated fatty acid molecule which are carboxylic acids with long unbranched aliphatic tails. [8]
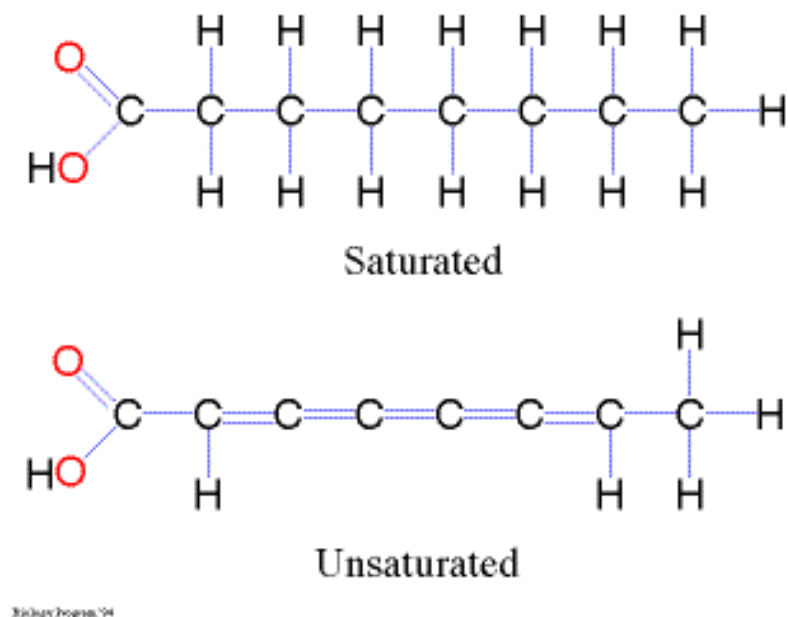
Figure 4. Saturated and unsaturated fatty acids

The three fatty acids in a triglyceride structure can all be the same or different. The most common carbon chain lengths are even numbered containing 16, 18, or 20 carbon atoms.[8] The triglycerides in vegetable oils typically contain a mixture of fatty acids.[4] For instance, typical soybean oil is comprised of 7% linolenic acid (C18:3) (C18:3 indicates an carboxylic acid with 18 carbon atoms and 3 carbon-carbon double bonds), 51% linoleic acid (C18:2), 23% oleic acid (C18:1), 4% stearic acid (C18:0), and 10% palmitic acid (C16:0).[4]

Most common vegetable oil sources are soybean, cottonseed, palm, peanut, rapeseed/canola, sunflower, safflower, coconut, and rice bran. When selecting a feedstock for biofuel production, financial manageability, local availability of the feedstock, and hence geography are important considerations.[9] Based on these criteria, rapeseed and sunflower oils are preferred in the European Union, palm oil is primarily used for biodiesel production in Asian countries, and soybean oil is the most common feedstock in the United States.[5,9] However, other seed oils have been investigated as well.[4] In addition, two new candidates have emerged as non-food biofuel

feedstocks: jatropha and algae [5] because they can be grown and harvested in non-traditional farming areas.

Jatropha curcas is the plant mainly grown in Asia, Africa, India, Central and South America, where it can grow well in marginal and poor soils of tropical and subtropical countries.[5,19] It has several advantages including undemanding cultivation, high oil content and non-food feedstock. Jatropha seeds contain 27-40% oil which allows producing a high-quality biofuel.[20] Jatropha oil is not a food based feedstock because it is inappropriate for human diets due to adverse effects associated with its consumption. It is believed that Jatropha oil can not only meet local biofuel requirements, but can also be exported to Europe, where domestic feedstocks are insufficient for the projected biodiesel demand of 10 Mt per year.[19]

Nowadays, there is a growing interest in utilizing algal oils as a biodiesel feedstock because algae also yields much higher oil production per acre than other triglycerides feedstocks.[11] The oil yield of microalgae can be as high as 80% with certain species based on dry weight.[8] Algae can be obtained from a variety of microbes' photosynthetic activity where sunlight, carbon dioxide, and nitrogen are converted into triglycerides, carbohydrates, and lignin.[11] Thus, algae can easily grow in low quality water which makes algae production easily manageable.[12] Moreover, seawater and coastal land, where conventional agriculture does not exist, are preferred for algae cultivation.[11] Since it does not compete with food for land use or water resources, algae oil is a potential solution to the concerns regarding the use of agricultural land for energy generation rather than food production.[8] In addition, it has been estimated that microalgae, which grow extremely fast, can double in mass in less than 24 hours. This suggests that it would only take 3% of the corp land in the USA to supply the domestic fuel needs while first generation biomass would take nearly 61% of farming land for the same purpose.[8] Shell and Hawaiian

based HR BioPetroleum recently declared they would produce biodiesel from algae. According to HR BioPetroleum, cultivation of algae yields nearly 15 times more oil per hectare than those of terrestrial crops such as rapeseed, palm, and soybean.[11] Additional news regarding algae commercialization comes from a AlgaeLink and KLM cooperative effort to develop the next generation alternative jet fuel for the operation of the Air France/KLM aircraft.[21] AlgaeLink has been selling its systems since 2007, and it claims that making commercial algae farming interesting for a large number of markets can be achieved.[21] Algae oil is even more attractive as an alternative fuel because of its low production cost, 50 cents per gallon, in a demonstration plant in the Netherlands.[5] Despite its numerous advantages over the other vegetable oil resources, algae oil has not yet been extensively carried out in a commercial scale.[12]

In addition to vegetable oil, many biodiesel plants utilize animal fats like tallow as feedstocks.[12] Biodiesel production has been demonstrated using lard and fish oil as animal fat resources.[9] The rising prize of soybean oil, which is the main biodiesel feedstock in the USA, became a great driving force for the use of chicken fat for biodiesel feedstock where the industry needs cheaper biomass resources.[22] The largest US producer of leftover fat from chicken, Tyson, announced that they produce about 300 million gallons of animal fat that could potentially be converted to fuel.[22] However, there are some technical drawbacks that come with the use of animal fat.[22] Since it clouds up (having high cloud point) more at higher temperatures than soybased biodiesel and thickens when used in colder climates, its use would be limited to areas where temperatures don't fall below 40 degrees F.[22]

Triglyceride feedstocks contain not only vegetable oils and animal fats, but also waste oils such as used frying oils and brown grease.[9] Since waste cooking oils are lower-cost lipid feedstocks, they are currently very important sources for economical production-oriented

approaches. However, inconsistencies in the composition of the oil due to the source and quality of the feedstock make it difficult to process.[9] Depending on the variations in free fatty acid (FFA) composition, triglycerides, water content, and impurities, the conversion method will have to altered to obtain high grade biodiesel.[9] In fact, quality variability of waste oil is recognized as more problematic than that of vegetable oils.[5]

Choice of the biomass used as a source of biofuels is an important consideration.[8] To determine if a feedstock is suitable for commercial biofuel production, its chemical and physical characteristics as well as supply, cost, storage properties, and engine performance will be considered [9]. The main reason of the economic defeat of biofuels against petroleum based fuels is the relatively high cost of the triglyceride feedstock. Even with the least expensive triglyceride feedstocks, the 70 - 85 % of the total production expense is related to the feedstock cost.[9] With currently available technologies, the lowest cost biodiesel is produced from waste oil and animal grease.[19] With respect to other available biomass feedstocks, generally, the most expensive are triglyceride based followed by amorphous sugars with lignocellulosic feedstocks the least expensive.[4]

1.5. Lipid derived biofuels

Lipids are another biomass source that can be used to produce biofuels in the form of biodiesel and green diesel.[8] Biodiesel and green diesel have an advantage over other alernative fuel sources since they can be directly integrated in current trasportation infrastruture without any engine modifications. [8]

1.5.1. Biodiesel

Due to their high viscosity, the raw oils cause operational problems in the diesel engine when it is used as a fuel. To overcome this issue, they are converted into biodiesel, bringing its

kinematic viscosity closer to that of petroleum diesel.[9] Biodiesel is mainly composed of mono-alkyl esters of long chain fatty acids derived from triglycerides feedstocks such as vegetable oils, animal fats or waste oils.

The alkyl esters that make up biodiesel vary in degree of saturation and chain length.[9] Unsaturated esters have lower energy content per unit weight compared to saturated esters, but their energy per volume is higher due to their high density.[9] However, variation in the energy content of saturated and unsaturated esters is not large enough to allow detection of different types of oil in the feedstock.[9] For instance, at 40°C, methyl stearate (C18:0) has an energy content of 34.07 MJ/L while methyl oleate (C18:1)'s energy content is 34.32 MJ/L, only a 0.7% difference. [23]

The reaction where triglycerides are transformed into biodiesel is transesterification.[24] In the transesterification reaction, triacylglycerol (TAG) reacts with an alcohol in the presence of a catalyst to form alkyl esters of the fatty acids (Figure 5).[9] In order to achieve as high yields of alkyl esters as 99.7 %, typically 50 % - 200 % excess alcohol is needed.[4] The alcohol is typically methanol. Although it is possible to get better biodiesel in terms of fuel properties with ethanol or iso-propanol, in most cases methanol is preferred for biodiesel production since it is lower-priced.[9] In the U.S. methanol costs half compare to ethanol.[9] When methanol is used in the reaction, the derived biodiesel product is composed of fatty acid methyl esters (FAME). On the other hand, other alcohols can be relatively less expensive in some countries such as Brazil so that they produce ethyl esters as biofuel from ethanol.[9]
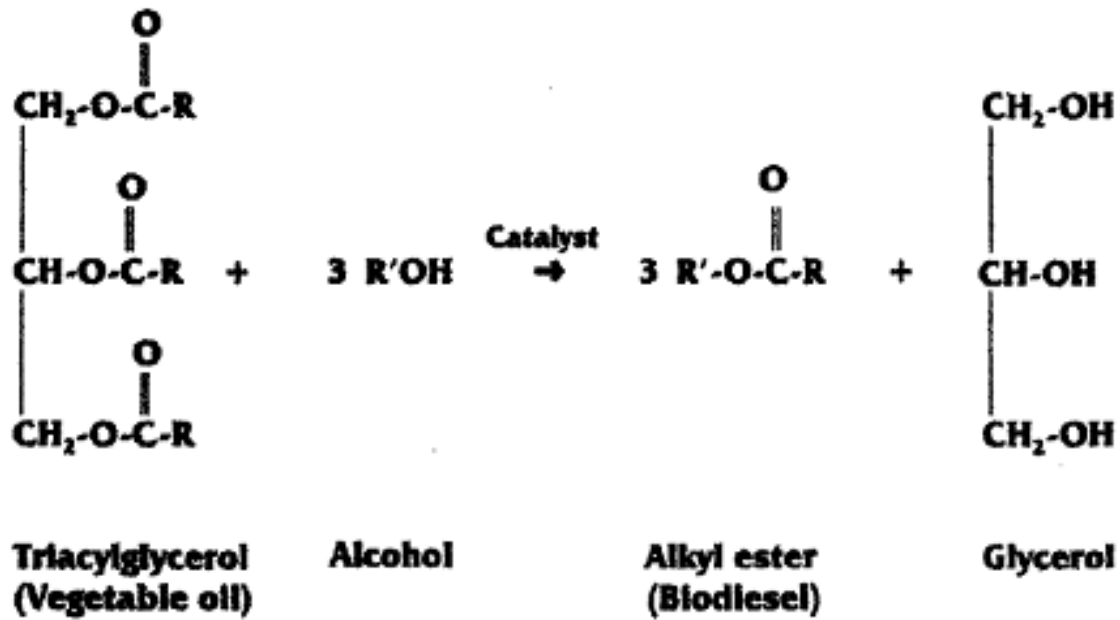
Figure 5. The transesterification reaction. (R= various fatty acid chain, R'= CH_3).[9]

Transesterification can utilize both base or acid catalysts, but most of the current biodiesel technologies rely on base catalysts including sodium hydroxide, potassium hydroxide, and sodium methoxide, which is the catalyst used by more than 60 % of biodiesel plants.[4,9,24] The base or acid catalysis can be either homogeneous or heterogeneous. In the case of homogeneous catalysis, reactants are in solution with the catalyst, which increases the reaction rate. However, after reaction, separating the catalyst from the reaction products causes material loss and incurs additional production expense related to neutralization and waste reclamation.[8] Unlike homogeneous catalysts, though, an active heterogeneous catalyst has an economic advantage in biofuel production since it can be readily removed from the reaction mixture after transesterification and reused without significant post treatment.[8]

A schematic of biodiesel production from low FFA containing feedstock via base catalyst transesterification is shown in Figure 6. Oil, alcohol and catalyst are mixed in a reactor for 1

hour at 60 °C. After the reaction is completed, glycerol is separated from the FAME products. FAMEs proceed in a neutralizer with acid in order to deactivate any residual catalyst and then methanol is removed. Any remaining catalyst, soap, salts, methanol, or free glycerol is removed from FAME during water washing step. At the end, biodiesel product is obtained after the drying process.[9]
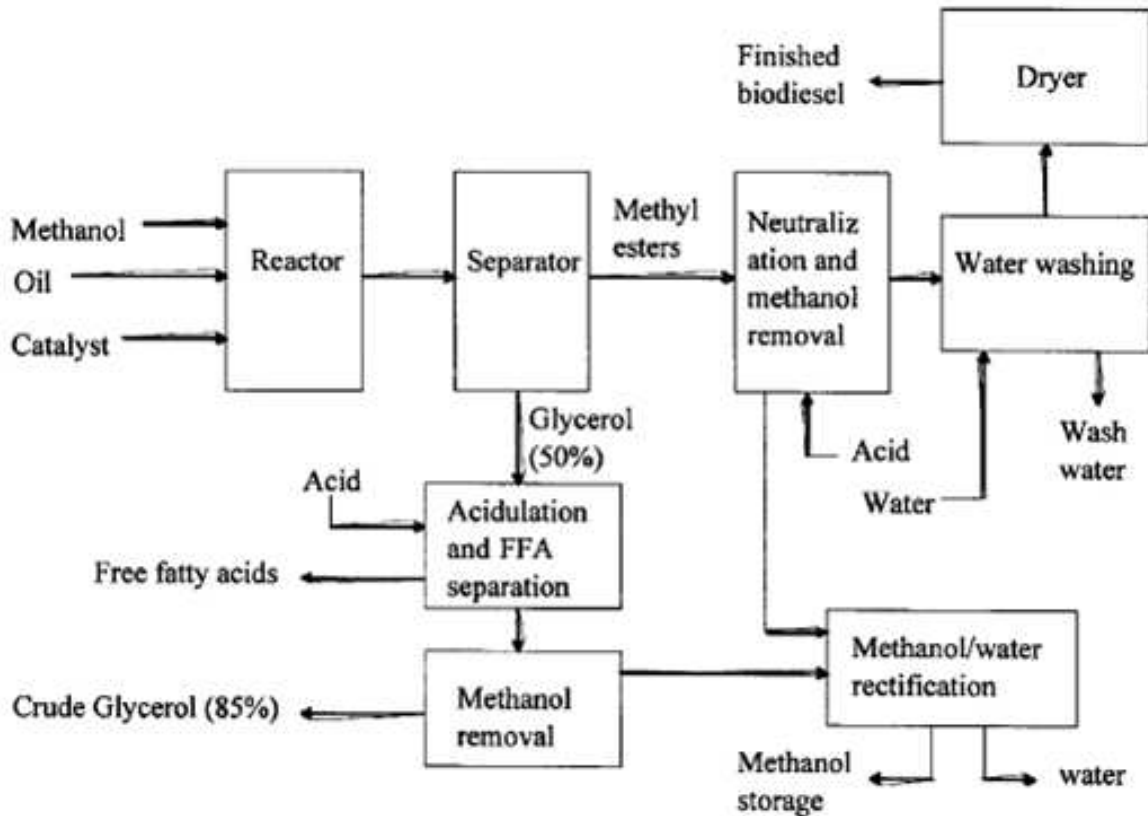
Figure 6. Process flow diagram for biodiesel production.[9]

The biodiesel quality generally depends on the quality of the feedstock, the other materials used in the process and the transesterification process.[9] For an efficient transesterification process, not only the alcohol should be moisture free, but also feedstock should have less than 0.5% of FFA.[25] Moisture that can come from alcohol has a potential of reacting with alkyl esters, triglycerides, diglycerides, and monoglycerides to form FFAs.[4] Because FFA contents of

vegetable oil and waste oil are usually high, the raw material should be pretreated (esterified).[8] Otherwise, during transesterification, they can form soap (only in homogeneous processes), which causes separation problems in the biodiesel production process.[8] Usually low cost feedstocks such as waste oil and animal fats have higher amounts of FFA, thus biodiesel production from these raw materials become economically unfeasible.[26] Another factor that influences the quality of biodiesel is the side products that can form during the transesterification reaction such as intermediate glycerols, mono- and diacylglycerols as well as unreacted triacylglycerols, FFA, residual alcohol, and catalyst contamination in the final product.[9]

Biodiesel has several advantages including environmental, safety and comparable fuel properties to regular diesel fuel. Firstly, all biodiesel fuels, independent of their feedstock origin, diminish greenhouse gases.[9] By using vegetable oil obtained from plants that consumes CO_2, biodiesel decreases CO_2 in the atmosphere.[9] In addition, biodiesel has extremely low sulfur comparing with the petroleum diesel so that SO_X emissions from biodiesel combustion is reduced.[8] Furthermore, when biodiesel is used in existing diesel engines, considerable decline in unburned hydrocarbons (HC), carbon monoxide (CO), and particulate matter (PM) are observed.[9] Secondly, biodiesel has advantage of having a high flashpoint greater than 150 ºC which guaranties lower fire hazard than other fuels like diesel, gasoline and jet fuel.[9] Thirdly, according to engine tests, the actual efficiency of fuel is equivalent for biodiesel and petroleum diesel.[27] Moreover, the cetane number is comparable to that of diesel fuel.[9]

Despite its above mentioned benefits, there are some disadvantages associated with biodiesel including its high cost, slightly , oxidative stability, and cold flow properties.[9] Other than these drawbacks, biodiesel's energy content (32.9 MJ/L) is lower than that of No. 2 diesel fuel (36.0 MJ/L) which may lead around 8.4% of power loss in diesel engine.[9] Moreover, the fuel

properties of biodiesel change depending on the chemical composition of the source oils.[19] Another aspect of biodiesel production that must be addressed is the accumulation of glycerol, the more biodiesel produced, the more glycerol accumulates. Therefore, an expanded market for glycerol is needed to make biodiesel production more feasible economically.[12]

1.5.2 Green Diesel

Like biodiesel, green diesel is a next generation transportation fuel which emerged because of the need for a renewable fuel replacement that is compatible with existing automotive powertrains. Unlike biodiesel, however, green diesel can be produced in large volumes at existing centralized petroleum refineries (need references). Biodiesel, on the other hand, is more suited for smaller scale production plants in rural areas close to the source of oil used in the process. Green diesel or renewable diesel is a mixture of diesel-like hydrocarbons produced via a catalytic reaction involving hydroprocessing and/or decarboxylation/ decarbonylation of triglycerides from various agricultural feedstocks[12,28]. While hydrodeoxygenation eliminates oxygen by reacting triglycerides and FFAs with hydrogen to form water and n-paraffins, decarboxylation or decarbonylation eliminates oxygen to form of carbon dioxide or carbon monoxide and n-paraffins.[4,7] This leads to a diesel product that is indistinguishable from petroleum diesel whereas biodiesel is chiefly composed of oxygenated species that can have vastly different properties than traditional petroleum diesel.[8,12] Although both biodiesel and green diesel are lipid- derived liquid transportation biofuels, there are significant differences between them. The first difference is between the molecular structures of the two fuels. While biodiesel is comprised of alkyl ester molecules, green diesel's main constituents are hydrocarbons. Therefore, unlike biodiesel, green diesel does not have oxygen based molecules. This characteristic of green diesel results in high heating value and high energy density.[4]

Secondly, green diesel has an extremely higher cetane number (80-90), while biodiesel has cetane number on the order of 50. Thirdly, green diesel has lower NO_x emissions compared to biodiesel.[4] Besides, hydroprocessing is a feed-flexible process being not sensitive to FFA content of feedstock while transesterification is very sensitive to FFA level.[4] In regards to their side products, hydroprocessing produces propane which is a gaseous fuel itself and can be utilized in the system.[4] Furthermore, the outstanding energy density of hydrocarbons as fuel makes them a powerful transportation fuel option (Figure 7).[29] Overall, based on the above arguments green diesel seems to be superior product over biodiesel.[4]
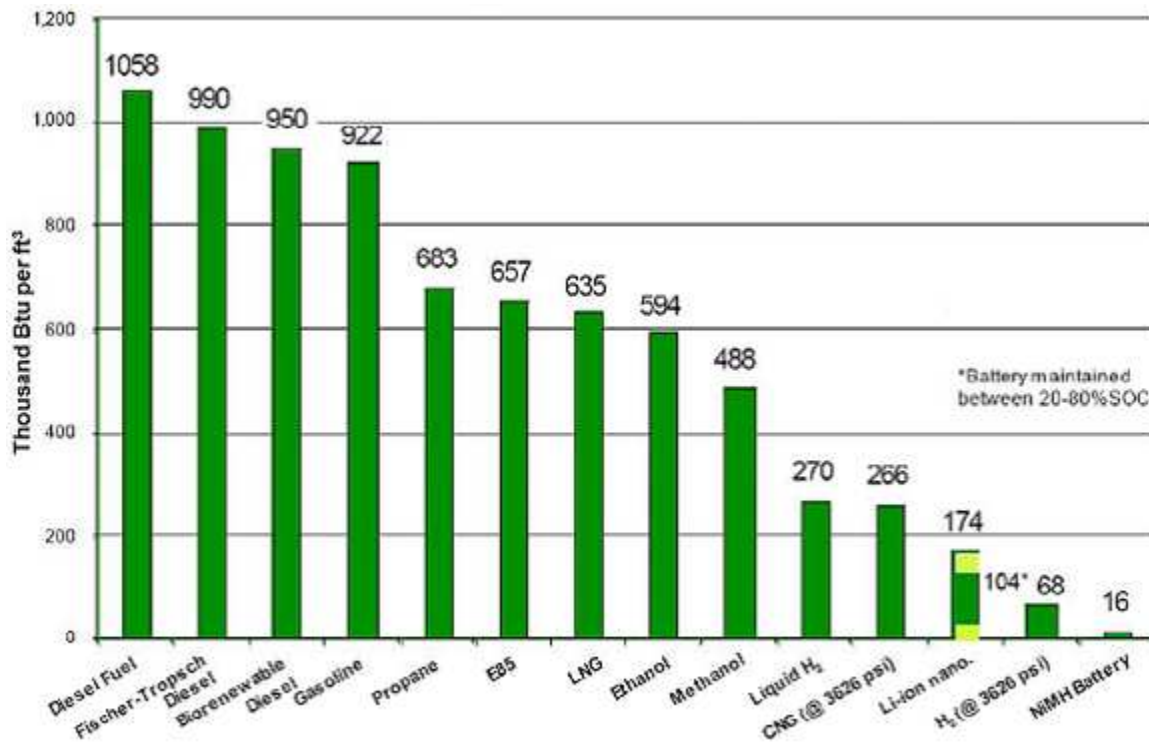
Figure 7. Energy density of various fuels. [29]

Green diesel commercialization has already started. Currently green diesel is industrially produced in Finland by Neste Oil having two plants with a combined capacity of 170 000 ton/year (Figure 8).[28] In addition, Neste Oil announced that they would start green diesel

production in Singapore in 2010 and in Rotterdam in 2011 with plants that have an 800 000 ton/year capacity.[30]
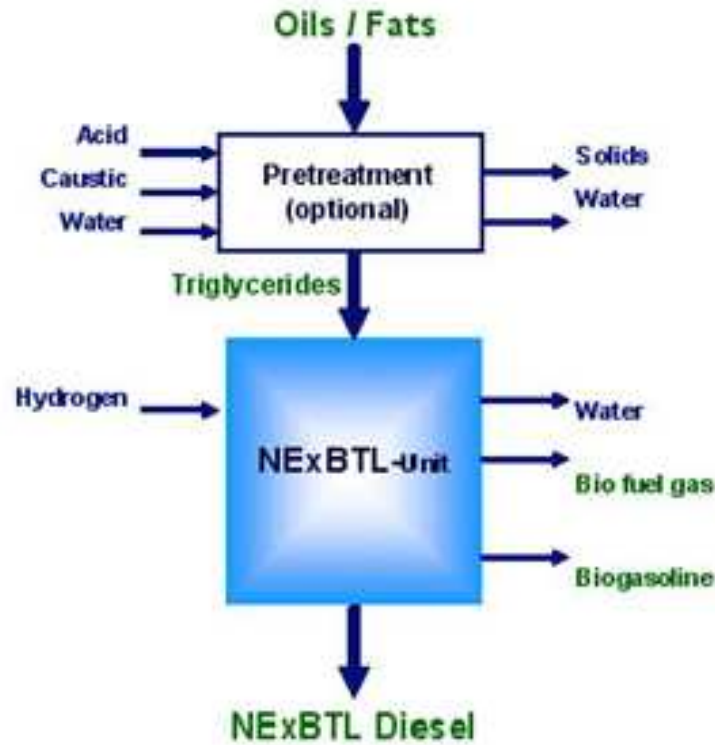
Figure 8. NExBTL process.[28]

Another green diesel commercialization effort using vegetable oils is led by UOP LLC and Eni cooperation. Ecofining technology planned to start its renewable diesel fuel production using a catalytic hydroprocessing technology to convert vegetable oils to a green diesel fuel in Italy in 2009.[31] The product having a high cetane value, has been proposed as a direct substitute for diesel fuel.[31] Separately, Petrobras/H-BIO developed a hydrotreating process to convert vegetable oil and mineral diesel fractions blends into green diesel which can be utilized as a diesel fuel cetane enhancer with the added benefit of reducing the sulfur content and density (Figure 9).[31]
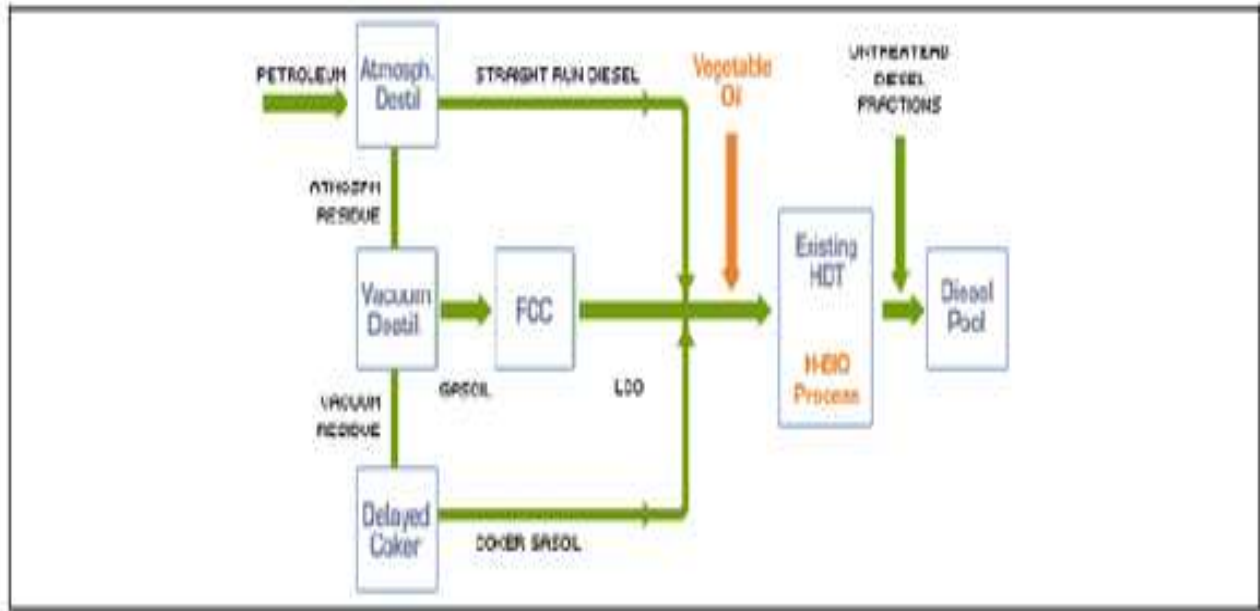
Figure 9. H-Bio/Petrobras Process.[31]

Advances in the production of green diesel have been slow to appear due to a lack of process knowledge. A better understanding of the processing conditions is required to further develop the current green diesel process, including catalyst composition, catalyst preconditioning/hydrotreating, and the optimization of the reaction conditions. Additionally, process economics will need to be improved to make green diesel production more competitive with petroleum diesel production.

1.5.2.1 Green Diesel Production from Triglycerides Feedstock- Deoxygenation

Green diesel or renewable diesel is a mixture of diesel-like hydrocarbons produced via a catalytic reaction involving hydroprocessing and/or decarboxylation/ decarbonylation of triglycerides from various agricultural feedstocks [12,28]. Biomass-derived feedstocks contain oxygenated compounds that lower the chemical stability and energy content of the fuel.[4] Therefore, the oxygen must be removed from the feedstock to achieve a liquid fuel with a high

thermal stability and combustion properties similar to petroleum fuels. The process whereby oxygen is removed from the feedstock is called deoxygenation which includes hydrodeoxygenation, decarboxylation and decarbonylation.

1.5.2.2 Hydrodeoxygenation (HDO) For Hydrogenation-Derived Renewable Diesel (HDRD) Production

Hydroprocessing is a general term used for the catalytic reactions that use hydrogen to eliminate the heteroatoms such as sulfur, nitrogen, oxygen, and metals, and also to saturate the olefins and aromatics.[4] Typical hydroprocessing reactions include hydrodesulfurization (HDS) where the sulfur is removed by breaking C-S bonds and hydrogen sulfide is formed; hydrodenitrogenation (HDN) which targets the removal of nitrogen as ammonia; hydrodeoxygenation (HDO) which removes oxygen as water; and hydrodemetalization (HDM) to remove metals such as metal sulfides. [4]

Hydrogenation-derived renewable diesel (HDRD) production focuses on the oxygen removal from the bio-oils/fats, which correspond to a HDO reaction, to obtain hydrocarbons in diesel fuel range (Figure 10). HDO reactions of bio- oils/fats operate at moderate temperatures, between 300-600 °C, and under high hydrogen pressure in the presence of a heterogeneous catalyst.[4] However, the reaction conditions such as temperature and pressure should be adjusted depending on the feedstock.[4] The catalysts used for HDO are in fact the same as those that are used for HDS and HDN such as sulfided Co-Mo or Ni-Mo because the hydrogenation processes are very similar in petroleum refineries.[4]
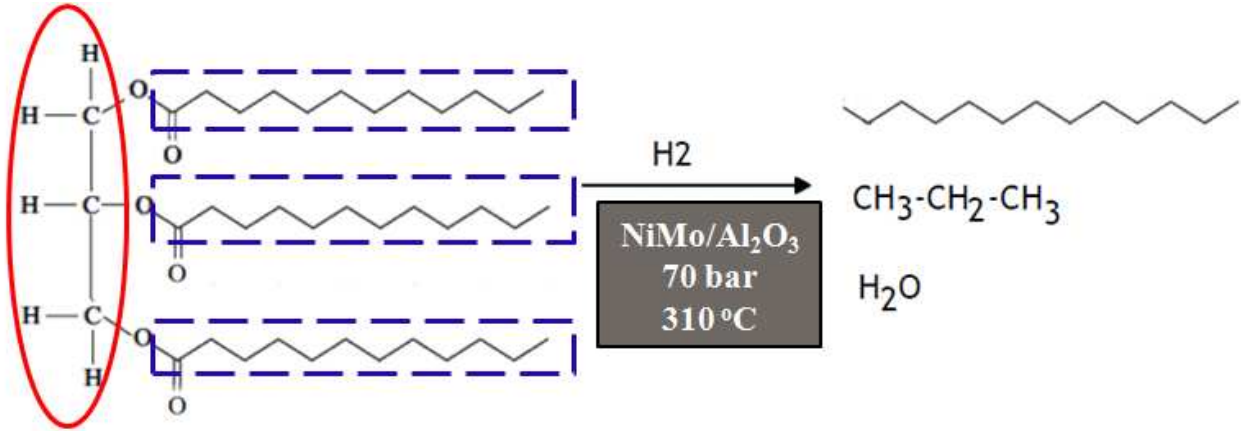
Figure 10. The oxygen removal from the triglycerides (HDO reaction)

It has been shown that it is possible to produce an alternative diesel fuel (green diesel) via hydrogenation of triglycerides, which can be also called HDRD.[32] Because HDRD is characterized by a high cetane number, it's preferred use is a diesel fuel additive to improve fuel ignition.[33] Craig and Soveran showed in U.S. Pat. No. 4,992,605 that hydroprocessing of vegetable oils such as canola, sunflower, soybean and, rapeseed oils, will produce hydrocarbons in the diesel boiling range (mainly C_{15} - C_{18} paraffins) which can act as a fuel ignition improvers.[33] They carried out the process at a temperature of 350°-450° C and 4.8-15.2 MPa with a liquid hour space velocity (LHSV) of 0.5-5.0 hr^{-1} by using a commercially available hydroprocessing catalyst such as Co-Mo and Ni-Mo[33]. In their study they determined the optimum temperatures and pressures for selected vegetable oil hydrogenation shown in Table 4.[33]

Table 4. Optimum hydroprocessing temperatures and pressures.[33]

Feedstock	Canola oil	Sunflower oil	Soybean oil	Rapeseed oil	Tall oil fatty acid	Palm oil
Optimum temperature (^{o}C)	370	360	360	390	390	370
Optimum pressure (MPa)	4.8	4.8	4.8	4.8	4.8	4.8

Based on their results, it appears that hydroprocessing of vegetable oil may also yield up to 11 wt. % water as in the case of canola oil hydrogenation over a Co-Mo catalyst at 375 ^{o}C and 5.5 MPa with LHSV of 0.99 h^{-1}. [33] Moreover, it can be seen that hydroprocessing of vegetable oil produces not only water, but also gaseous byproducts including methane (CH_4), ethane (C_2H_6), propane (C_3H_8), propylene (C_3H_6), butane (C_4H_{10}), carbon dioxide (CO_2), carbon monoxide (CO), and in some cases hydrogen sulfide (H_2S) in varying degrees depending on the source feedstock.[33] It is concluded that, in higher temperature runs, a mixture of straight and branched chain aliphatic (C6-C18) hydrocarbon formation is significant indicating that the hydroprocessing products are exclusively associated with the process conditions.[33]

Another process for green diesel production of diesel fuel ignition improvers is outlined in US Pat. No. 5,705,722.[34] According to Monnier et. al., it is possible to produce HDRD with a cetane number of more than 90 and yield of 80 wt. %.[34] In their work, they processed a biomass feedstock at 8.3 MPa of hydrogen pressure and 370 ºC.[34] The catalyst employed in this process was a commercial nickel-molybdenum/alumina (Ni-Mo/Al) catalyst with silicon carbide (SiC) in a 1:2 volume ratio.[34] They concluded that hydrogenation of a mixture of tall oil with

vegetable oil or animal fat showed a better yield of cetane improvers compared to a single feedstock.[34] Even though this process claims very high yields and cetane numbers, using such high hydrogen pressures is not compatible with commercially feasible processes.

1.5.2.3 Decarboxylation of Fatty Acids

Decarboxylation is the chemical reaction where a carboxyl group (-COOH) is removed from a molecule as carbon dioxide (CO_2), while the chemical reaction where carbonyl group (C=O) is split off from a molecule is called decarbonylation. Many carboxylic acids can be decarboxylated with heat by suspending the acid in an immiscible and high boiling-point liquid:

$$\text{(1)}$$

Because fatty acids are carboxylic acids, they can be processed in the same way to form straight chain hydrocarbons (n-hydrocarbons). For fatty acids, fatty acid esters, and triglycerides, decarboxylation proceeds by the following reactions:

$$\text{(2)}$$

$$\text{(3)}$$

$$\text{(4)}$$
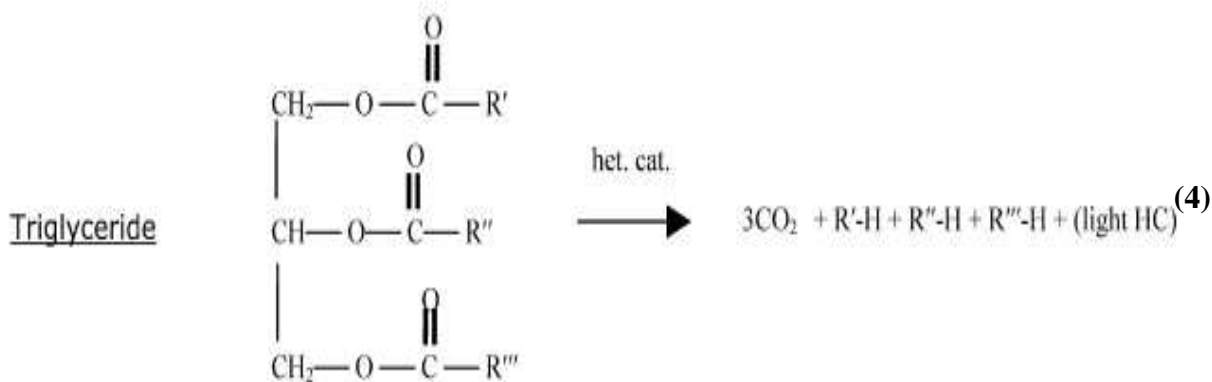
Immer proposed the following sequence of elementary steps of decarboxylation of free fatty acids on Pd/C catalyst:

$$RCOOH + 2* \rightleftharpoons RCOO* + H*$$
$$RCOO* \rightarrow CO_2 + R*$$
$$R* \rightleftharpoons R' + H*$$
$$R* + H* \rightleftharpoons RH + 2*$$
$$H* + H* \rightleftharpoons H_2 + 2*$$
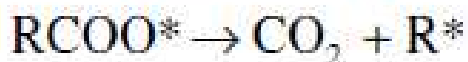
where * is a catalytic site or ensemble, and R′ is an olefinic hydrocarbon.[35]

Although both hydrogenation and decarboxylation successfully produce deoxygenated n-hydrocarbons (green diesel), there are several benefits of decarboxylation over hydrodeoxygenation. Decarboxylation requires hydrogen only to saturate olefins, while hydrogenation uses hydrogen not only to saturate olefins but also to remove oxygen as water. Thus, hydrogen consumption is lower for the decarboxylation reaction. Less hydrogen consumption leads to less capital and operational costs due to the reduced size of the hydrogen compressor and hydrogen purchases. In addition, the capital and operational costs are lower because decarboxylation is favored at lower pressures than hydrogenation.[4] Another advantage of the decarboxylation process over hydrogenation is that catalytic stability increases because water does not form in the reaction.[4] Even though both reactions have additional CO_2 production potential, CO_2 from decarboxylation can be captured in a relatively pure state, which provides an additional benefit to the decarboxylation process.[4]

It has been shown that it is possible to produce mainly n-heptadecane as a product when compounds of stearic acid, ethyl stearate, or tristearine were deoxygenated using a commercial

activated carbon supported palladium (5 wt.% Pd, Aldrich) catalyst (Reaction 5).[36] During the decarboxylation of stearic acid, heptadecenes were observed as intermediates.

Stearic acid decarboxylation at 300 ^{o}C and 17 bar, however, shows that the best conversion efficiency (62 %) when 5 volume % hydrogen and 95 volume % argon are used as the reaction atmosphere compared 100 % helium (41 % conversion) or 100 % hydrogen (49 %). During deoxygenation, ethyl stearate was first converted into stearic acid, and then further decarboxylated to n-heptadecane. At the same reaction conditions (5 vol. % H_2 - 95 vol. % Ar) with stearic acid decarboxylation, the best conversion of ethyl stearate decarboxylation was achieved. The selectivity to n-heptadecane decreased when aromatics, which are not desirable in diesel fuel, began forming at 300-360 ^{o}C. In one study, the reaction kinetics for ethyl stearate and stearic acid decarboxylation for production of diesel fuel hydrocarbons was studied over a palladium/carbon (Pd/C) catalyst in a semi-batch reactor.[37] According to the study, ethyl stearate was coverted with first order kinetics to stearic acid intermediates, which were further converted n-heptadecane following an ~zero order reaction rate at 300 ^{0}C. At high intermediate product concentrations it was found that the catalyst was deactivated by decarboxylation pathway.[37]

$$CH_3-(CH_2)_{16}-C\overset{O}{\underset{OH}{\big<}} \longrightarrow CH_3-(CH_2)_{15}-CH_3 + CO_2 \quad \textbf{(5)}$$

stearic acid   n-heptadecane
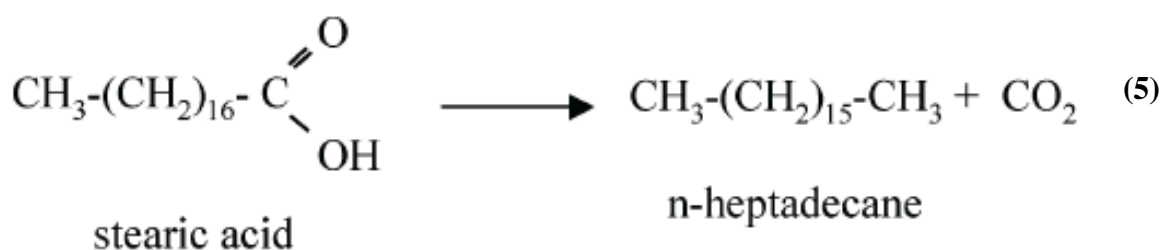
Further studies into better understanding the catalyst effect in heterogeneous decarboxylation were carried out without a catalyst versus a set of diferent catalyst.[38] It was found that thermal decarboxylation without any catalyst only leads to 5% conversion in a semibatch reactor under a helium atmosphere at 300 ^{o}C and 6 bar. A series of catalysts including cabon supported catalysts,

metal oxides of Ir, Mo, Ni, Os, Pd, Pt, Rh and Ru, as well as a Raney nickel catalyst, were tried under the same reaction conditions. It was concluded that decarboxylation of stearic acid with carbon supported catalysts generally lead to higher rates most probably because of the metal-support interaction. The initial reaction rate was the highest for 5% Pd/C (1.9 mmol/s/g_{met}) which showed the best performance. With Ru/C and Rh/C catalysts it was observed that their selectivity towards unsaturated side products was higher, which resulted in their deactivation.[38]

Another study of catalytic deoxygenation to produce diesel fuel hydrocarbons was carried out in a semi-batch reactor using unsaturated fatty acids including monounsaturated fatty acids, oleic acid, the di-unsaturated fatty acid, linoleic acid, and the monounsaturated fatty acid ester, methyl oleate. [38] In this study, Pd/C catalyst was employed at a pressure between 15–27 bar and a temperature of 300–360 °C.

A later study demonstrated that for green diesel production via decarboxylation of stearic acid over 4 wt. % Pd catalyst supported on sibunit (a new class of mesoporous carbon-carbon composite materials combining advantages of chemical stability and electric conductivity of graphite and high specific surface area and adsorption capacity of active coals) is possible.[39] This process was carried out in a semi-batch reactor with 300 mL volume at 17 bar helium and 300 °C, using dodecane as a solvent . Under these conditions, the catalytic decarboxylation of stearic acid resulted in n-pentadecane formation as well as n-heptadecane as the main products. Thus, it is concluded that the product distribution in catalytic decarboxylation of stearic acid changes depending on the type of the support and the nature of the surface groups in carbon material.[39] Some of the tested decarboxylation reactions for conversions of fatty acids are shown in Table 5.[8]

Table 5. Literature summary of decarboxylation reactions of fatty acids.[8]

Author	Year	Catalyst	Reaction conditions[a]	Main product	Reported yields (%)
Almon[66]	1975	Ca–montmorillonite	250 °C, excess water	n-Heneicosane	
Lestari[73]	2008	Pd/C (Sibunit)	330 °C, 17 bar helium, 4% catalyst (wt%) t = 20 min	n-Heptadecane	100
Kubrickova[70]	2008	Activated carbon supported palladium (5 wt%, Aldrich)	300 °C, 17 bar hydrogen (5 vol%) + argon (95 vol%), 4% catalyst (wt%) t = 360 min	n-Heptadecane	62
Snare[72]	2006	5% Pd/C	300 °C, 6 bar helium, 1 g catalyst, t = 360 min	n-Heptadecane	100

[a] t = reaction time.

1.6. Heterogeneous Catalyst

1.6.1 Catalyst Support Properties

Chemical manufacturing processes employ catalysts in order to increase the reaction rate and control the selectivity to the desired products. Generally, catalysts are a combination of an inert support and an active surface component residing on the support surface. The purpose of the support is to keep the active phase of the catalyst material in a highly dispersed state[40] to maximize reaction rates and to provide a stable platform for reactions in a chemical process. Additional benefits of a support include: dissipation of reaction heat and improved poisoning resistance.[40]

The catalyst- support surface interaction is significantly important because it has an effect on the catalytic activity.[40] For example, sulfide metal catalysts supported on alumina (γ-Al$_2$O$_3$), which is employed in HDS processes, can effectively disperse large amounts of metal sulfides. However, because of the strong interactions between the transition metal oxides and the γ-Al$_2$O$_3$ support, the HDS activity is reduced. Therefore, a much more inert support such as SiO$_2$ or carbon could be more suitable for sulfide catalysts. Moreover, alumina-supported sulfide catalysts have a much higher coking tendency since they have stronger surface acid sites

compared to carbon-supported catalysts, which are less acidic and, therefore, show weaker metal- support interactions.[40]

There are several parameters that must be considered in selecting a suitable support: inertness, stability, mechanical properties, physical form, surface area, and porosity.[40] The support should also help inhibit unwanted reactions. Usually granulated and pelleted supports are suitable for packed bed reactors while powder supports are appropriate for liquid phase batch, slurry, or fluidized bed reactors.[40] The high surface area of a support may also improve the catalytic activity or affect diffusion rates of reactants and products. However, high surface area is not always desirable.[40] For instance, porous structures and the pore size of the catalyst are very important in terms of accessibility. While large pores favor gas- liquid heterogeneous catalysis which has a slow diffusion in the liquid phase, small pore and particle size increase the number of possible active sites.[41] This is the main reason why the porous structure and the pore size distribution should be adjusted.

Because of these factors, there are three catalyst support materials that are typically considered as an optimum support for deoxygenating applications utilized in HDRD production: alumina, silica, and activated carbon.

1.6.2 Carbon Supports

Carbon supports have several benefits in catalytic reactions such as its resistance to acidic/ basic atmospheres, its flexibility of being more / less hydrophilic based on the preparation method and the precursor, and the ease of recycling the used expensive metal catalysts by burning away the carbon support.[40] As an example, it has been shown that the $Co-Mo-Al_2O_3$ catalyst has a significantly greater coking tendency than the Co-Mo-carbon black catalyst due to the lower surface acidity of carbon compared with alumina.[42] Furthermore, sintering of the active

phase on the surface of the carbon support is minimized due to its high temperature stability (up to 1425 ^{o}C).[40] In addition, it is possible to modify the pore structure of a carbon support to achieve a desired pore size distribution by changing the precursor and the preparation methods [40] Conversely, it should be noted that carbon supports can only be used under conditions where the carbon is non-reactive. For example, carbon supported iron catalysts display large weight losses in the presence of hydrogen due to methane formation above 425 ^{0}C.[40]

1.6.2.1 Activated Carbon Support

Activated carbon supports, which are carbonaceous materials having high internal surface area and porosity, are common adsorbents in many applications such as vehicle exhaust emission control, solvent recovery, catalyst support, air separation, and purification.[24] Their large surface area makes them ideal for adsorbing selective gases and liquids with high capacity.[24] This property is the reason why activated carbon has the largest share of the carbon support market of any carbon specie.[40]

The source of carbon for these applications is always biological in nature. For example, carbon derived from coconut shells, wood, peat, and coal can be carbonized and then activated in order to create desired pore structure of the carbon material.[40] Activation of carbon can be either a chemical or physical process. Chemical activation is a single step reaction which takes place using chemical agents such as alkali metal hydroxides (KOH, NaOH), alkali metal carbonates (Li_2CO_3, Na_2CO_3, K_2CO_3, Rb_2CO_3, Cs_2CO_3) and transition metal salts ($ZnCI_2$) during carbonization of the carbonaceous precursor.[43] On the other hand, physical activation is a two step process which involves carbonization of the carbonaceous precursor under an inert gas following activation in carbon dioxide (CO_2), steam or air atmosphere.[43] During this reaction, the closed micropores are opened.[43]

According to the International Union of Pure and Applied Chemistry (IUPAC), activated carbon can be classified into three groups depending on their pore sizes: micro-porous (less than 2 nm), mesa-porous (2 - 50 nm), and macro-porous (more than 50 nm).[44] Typical microporous activated carbon, which consists of aromatic sheets and strips, is shown in Figure 11.[43] While activated carbon usually has a BET surface area around 1000 m^2/g, some highly activated carbon can be as high as 3000 m^2/g.[40] Although the surface area and pore size are a measure for adsorption behavior of catalysts, the adsorption characteristics of an activated carbon cannot be explained strictly by these two parameters.[40]; The preparation method and the activation treatment [40]are also important. In addition, the porosity of a carbon support must be matched to the application. In practice, the microporous structures of activated carbon supports are not always feasible for an applicable because large molecules associated with some industrial feedstocks cannot access the micro-pores.[40] For instance, large molecules such as triglycerides and FFAs will not be able to access a microporous activated carbon support leading to poor deoxygenation conversion activity for green diesel production.

Figure 11. Structure of a typical microporous activated carbon.[43]

1.6.2.2 Carbon Supported Metal Catalyst

Supported metal catalyst preparation is one of the most important areas in processes that employ chemical reactions. Usually Group 8-11 metals of the periodic table are supported on carbon such as platinum, palladium, rhodium, ruthenium and iridium.[40] The metal-carbon supported catalyst can be prepared by adsorption from solution, impregnation, precipitation, and vapor phase deposition.[40] In Petroleum refineries, non-precious metal sulfide catalysts such as sulfided Ni-Mo/Al_2O_3 are used for hydrotreating applications. This is because the presence of sulfur in these catalysts prevents deactivation [4] where precious metal catalysts would be susceptible to poisoning from sulfur present in the feedstock. In 1976, it was proven that even sulfide catalyst on carbon support could be successfully used for hydroprosessing.[40] However, future work in deoxygenation of low sulfur oil/fat feedstocks will focus on developing non-sulfur-based catalysts with enhanced stability that do not require high-pressure hydrogen.

1.6.2.3 Carbon Coated Monoliths as Catalyst Supports

The composition of one type of common monolithic support structures is cordierite (2MgO . 2Al_2O_3 . 5SiO_2) which has 51 wt.% silica, 35 wt.% alumina and 14 wt.% magnesia.[41] In practice, a monolith is cylindrical in shape with many straight and parallel channels (Figure 12).[45]
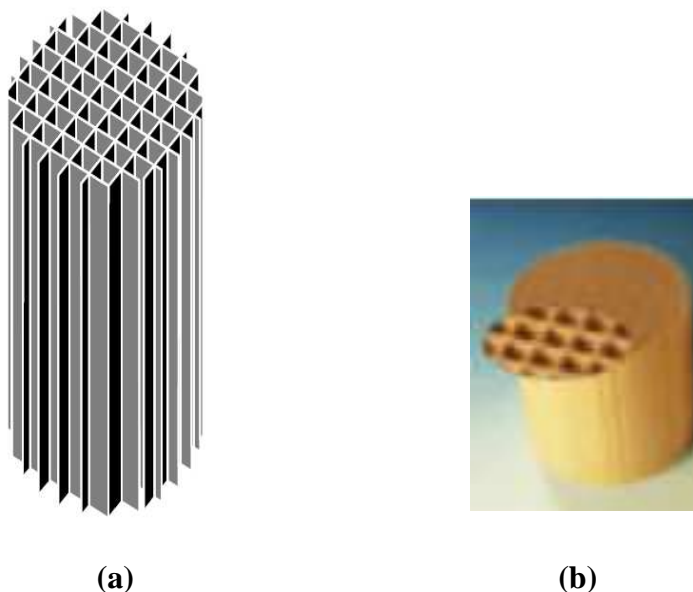
Figure 12. a) Schematic of a monolith, b) A cylindrical monolith

Monoliths are commonly used in automotive aftertreatment systems to reduce or eliminate toxic exhaust gases. In this application, hydrocarbons (HCs), carbon monoxide (CO), and nitrogen oxides (NOx) are converted to carbon dioxide (CO_2), water (H_2O), and nitrogen (N_2) by precious metal formulations coated on a monolith support.[45] Another application where monoliths are used is in the cleaning of industrial flue gases by placing the monolith in the exhaust stack[45], forcing the gas emissions to pass directly through the supported catalyst.

Monoliths have several characteristics that make them attractive as catalyst supports in heterogeneous gas – liquid reactions: a low pressure drop, high geometric surface area, short diffusion lengths, and mechanical strengths and thermal shock tolerance.[41] When a monolithic supported catalyst is compared with a trickle bed reactor packed with a powder catalyst, the monolith exhibits much less pressure drop per external surface area of the catalyst.[46] According to their study, Garcia-Bordeje et al. showed that carbon supported on a monolith has higher BET surface areas and pore volumes than those of unsupported carbon. This is due to the fact that

during carbonization, the cordierite prevents the carbon material from shrinking.[41] Also, having many channels creates a large contact area between the catalyst layer and the reactant fluid inside the monolithic structure catalyst.[45] Another advantage of monolithic catalyst is having a short diffusion length due to the deposition of the catalyst on the thin monolith walls.[47]
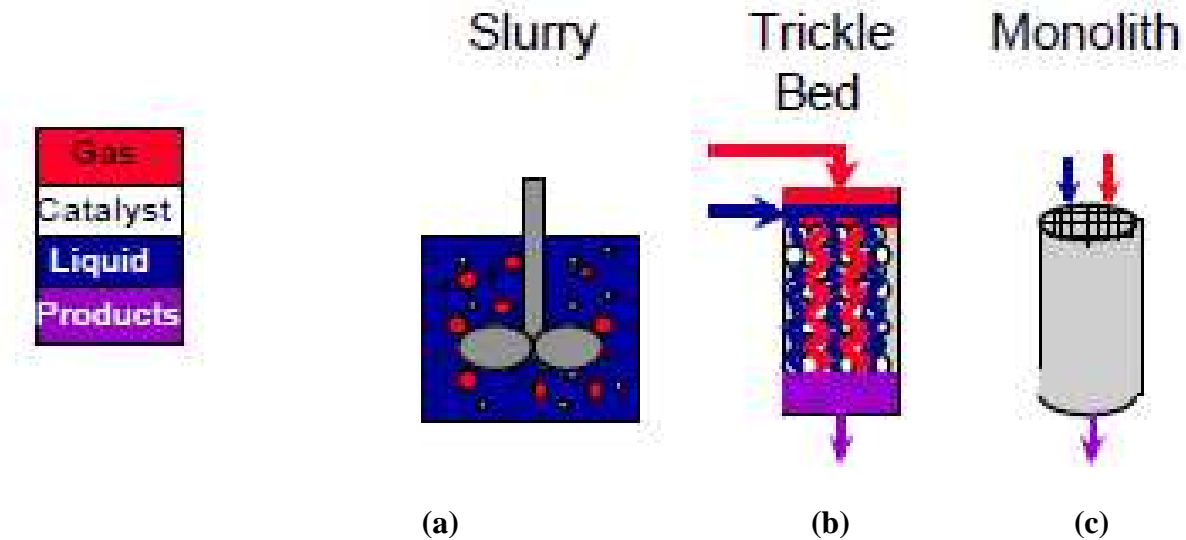
Figure 13. a) Slurry (batch) reactor, b) Trickle bed (fixed bed) reactor, c) Monolithic reactor

In slurry reactors (Figure 13.a), powder catalysts are preferred to overcome mass transfer limitations. However, powder catalyst separation from the products can be a tedious and time consuming process. In addition, catalyst separation is a costly process which creates extra waste streams and loss of catalyst and product during filtration.[48] Monolith supported catalysts offer the advantage of avoiding catalyst separation in slurry reactors. Boger et al. evaluated the economics of a monolithic reactor versus a conventional slurry reactor. He found that the monolithic reactor promised significantly reduced production costs.[48] A fixed- bed reactor (Figure 13.b) design is not always a good choice either. The powder catalyst used in the bed can be easily plugged with reactor products and byproducts. However, pelletized catalyst in a fixed- bed reactors can be a

potential solution for this problem, but catalyst pellets, which only have the active phase in a thin surface layer, may not allow a high reaction throughput.[47] Moreover, Kreutzer M. T, et al. proved that monolithic reactor (Figure 13.c) provides a higher reaction rate for hydrogenation than a trickle bed reactor with the similar external surface area.[49] Another study was carried out to compare the productivity (reaction rate) of α-methylstyrene (AMS) hydrogenation to cumene in monolithic and trickle - bed reactors. Figure 14a shows that it's possible to perform AMS hydrogenation to cumene in a monolithic reactor with a higher reaction rate than in a trickle – bed reactor having the same reactor size.[50] Therefore, it can be concluded that can be controlled by adjusting the channel size and catalyst wash-coat layer.

cpsi: cells per square inch **(a)**   **(b)**
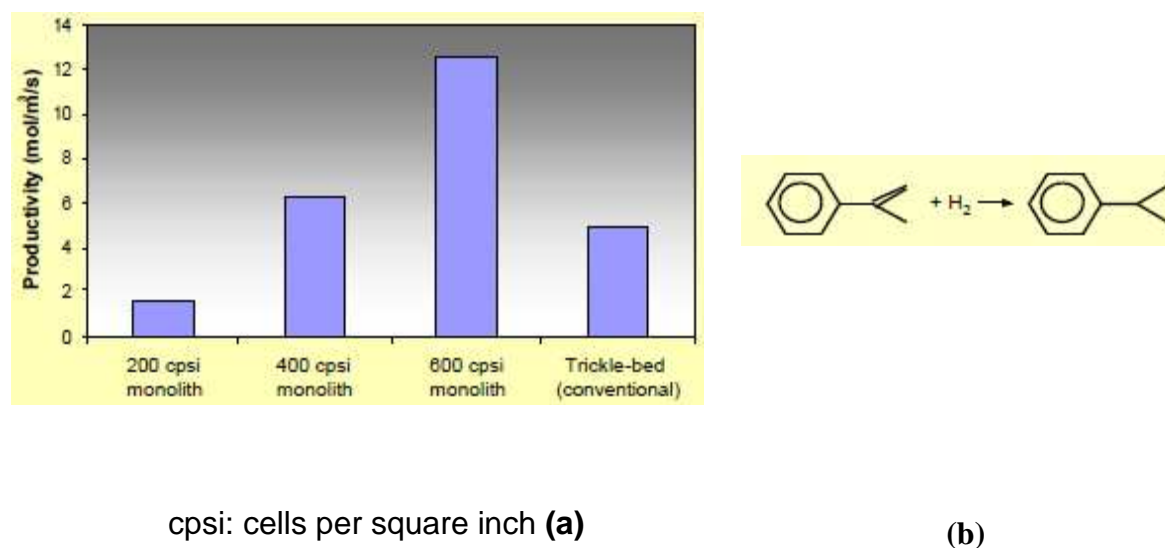
Figure 14. a) Comparison of the reaction rate of AMS hydrogenation using a monolithic reactor with different cell densities and a trickle bed reactor, b) Schematic of AMS hydrogenation to cumen.[50]

1.7 Challenges in Green Diesel Production

Current commercial green diesel production technology is based on hydrogenation of vegetable oil / animal fat or their blend with plant oil. During hydroprocessing of triglycerides to hydrocarbons, consecutive reactions proceed in a series.[51] Figure 15 demonstrates the reactions during conversion of TAG over $NiMo/Al_2O_3$ catalyst in a high pressure atmosphere of H_2. The first reaction is hydrogenation of the triglyceride molecule where all the double bonds are saturated. The second reaction involves removal of oxygen atoms which can be hydrodeoxygenation, decarboxylation and/or decarbonylation. Additionally side reactions taking place such as the hydrocracking of TAG, the water – gas shift reaction, methanization, cyclization, and aromatization are referred to as the third reaction. The forth reaction is isomerization of n-paraffins. According to the hydrotreating process, O_2 containing groups in TAG are eliminated by reacting with H_2 in order to produce hydrocarbons. Moreover, the hydrogenation reaction has to proceed in an excess H_2 atmosphere to avoid unwanted side reactions such as polymerization, ketonization, cyclization and aromatization.[52] Insufficient H_2 results in coke formation on the catalyst surface and catalyst deactivation. As a result, the green diesel yield decreases and the profile of green diesel species changes.[53]
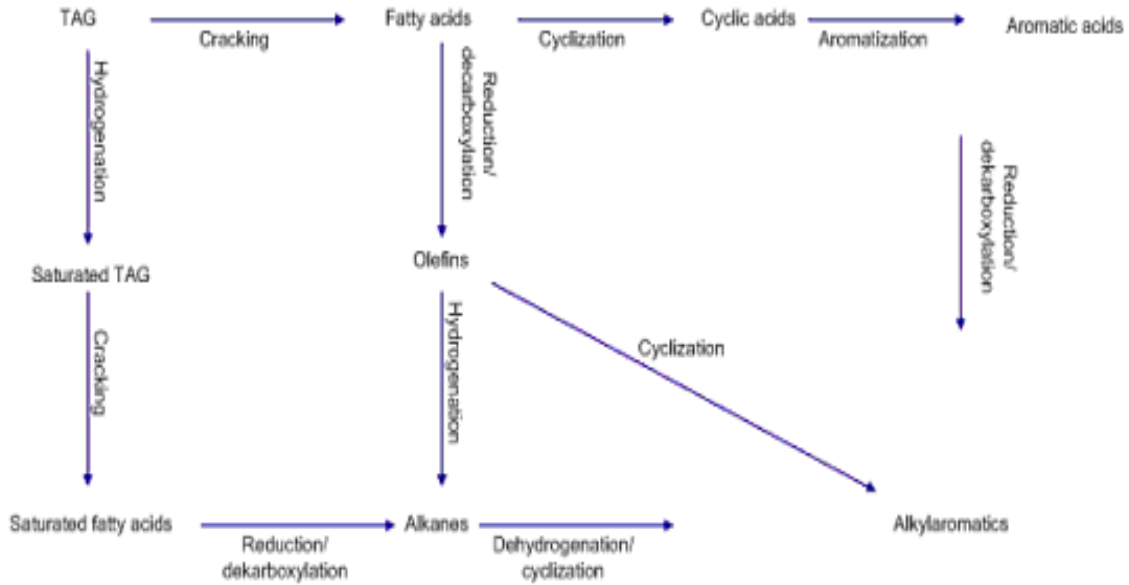
Figure 15. TAG conversion to green diesel in the presence of hydrogen and a NiMo/Al$_2$O$_3$ catalyst.[54]

Therefore, to avoid catalyst coking and deactivation problems, high H$_2$ pressure operations are preferred, but from an economics standpoint, this is not easily feasible due to the cost of H$_2$ and building high pressure systems.

CHAPTER 2

Catalytic Conversion of Brown Grease to Green Diesel via Decarboxylation

The decarboxylation of brown grease (BG) to green diesel hydrocarbons over a 5 wt.% Pd/C catalyst was investigated in semi-batch and batch reactors. Catalytic deoxygenation of BG under H_2-Ar occurs primarily via decarboxylation with the liquid products of primarily n-heptadecane and n-pentadecane. A 90% conversion of BG in a semi-batch mode was obtained in 7 hours. In contrast, in a batch reaction the conversion was roughly 40% in the same reaction time. However, by pre-treating the "as received" BG with H_2, the conversion in a batch reactor was increased 1.4-fold; and when the H_2 to BG ratio was increased to 3/1 (mol/mol), the conversion was further improved. A complete conversion of BG into green diesel via decarboxylation is possible over 5% Pd/C catalyst at 300 ^{o}C and 1.5 MPa. This study demonstrates the feasibility of obtaining valuable green diesel biofuel from waste oil.

2.1. Introduction

Environmental, economic, and energy security concerns have been the motivation for seeking environmentally friendly, renewable alternative fuels. The major feedstocks for non-ethanol liquid biofuel production are vegetable oils and animal fats. Waste oils, such as used frying oils and brown grease, are lower-cost lipid feedstocks and currently an important potential sources for economical production-oriented approaches [9].

There is a tremendous amount of waste cooking oil and grease, collected from restaurant traps, that may be exploited for fuel use. According to the National Renewable Energy Laboratory (NREL), the total volume of trap grease (brown grease) produced is ~3,800 million lbs per year in the U.S [55]. Disposing of brown grease is a costly process. On the other hand, brown grease is known to possess a high energy value of around 12,000 Btu per pound [55].

Furthermore, brown grease is an inexpensive feedstock in comparison with food grade vegetable oils [56]. For all these reasons, there is a need for catalytic processes for the conversion of unwanted brown grease into valuable products such as biofuels. However, the high free fatty acid (FFA) content of brown grease (50 - 100%) can be problematic for biofuel production [57] and there is no proven biofuel production technology for a feedstock having 50-100% FFA content [58]. The presence of FFA in the feedstock of vegetable oils also creates processing problems. When 10 wt.% FFA- 90 wt.% triglycerides were used in a hydrotreating process to produce green diesel, the fraction of high molecular weight hydrocarbons products not in the diesel fuel boiling range gradually increased compared to a feedstock containing only triglycerides. This resulted in a loss of diesel yield and reduction in catalyst life [59].

Brown grease is comprised of both saturated and unsaturated FFAs. Almost 40% of brown grease is oleic acid (C18:1), which is a monounsaturated fatty acid, and around 70% is total unsaturated fatty acids [60]. Due to its high FFA content (50-100%), BG is potentially a good candidate for a decarboxylation reaction where the oxygen is removed as carbon dioxide, producing green diesel. Currently, hydrodeoxygenation (HDO) is the only proven technology to convert waste oil into green diesel. However, this technique requires high pressure (~5 MPa) and excess H_2 (H_2/oil ratio of ~1000/1) in order to remove oxygen as water, leading to high production costs. In comparison, decarboxylation does not require additional H_2 to form hydrocarbons. Although several studies of hydrocarbon production from waste oil and vegetable oil (or refinery oil) mixtures have been reported [61,62], no selective decarboxylation of brown grease for the production of diesel fuel hydrocarbons has been demonstrated.

Saturated fatty acids have been successfully converted to hydrocarbons via decarboxylation under inert gas [63-68]. Screening of heterogeneous catalysts for decarboxylation of

stearic acid as the model FFA compound has been performed with different metals (Ni, NiMo, Ru, Pd, PdPt, Pt, Ir, Os, Rh) on different supports (Al_2O_3, SiO_2, Cr_2O_3, MgO, C) under a helium inert gas atmosphere. A 5% Pd on activated carbon supported catalyst provided the best conversion of stearic acid to C_{17} "green diesel like" hydrocarbons (mainly n-heptadecane), with 100% conversion of stearic acid and 99% selectivity to total C_{17} hydrocarbons. [38]

There has been considerable study of the conversion of unsaturated FFAs to hydrocarbons. [64,69,70] However, there is not yet an active and selective catalyst that can handle direct decarboxylation of unsaturated FFAs to hydrocarbons. The best results demonstrated so far are 99% conversion of oleic acid to stearic acid (selectivity (S) = 36%), heptadecane (S = 26%) and other side products after 6 hours over Pd/C catalyst under Ar-H_2 flow, at 300 ^{o}C and 2.7 MPa [69]. Because of the competitive adsorption and reaction of active C=C double bonds on the catalyst surface, the decarboxylation yield of total FFAs decreased while yield of the side reactions increased, leading to an increased H_2 consumption and a decreased diesel yield [59].

During the reaction to convert oleic acid to n-paraffins over 5% Pd/C in the presence of 10% H_2 and solvent (dodecane) at 1.5 MPa and 300 ^{o}C, the primary reactions are hydrogenation of C=C double bonds followed by decarboxylation of the resulting stearic acid. However, in the absence of H_2, oleic acid decarboxylation was inhibited by adsorbed cis- C=C double bonds in its alkyl chain [64].

The objectives of this study are to investigate the effect of reaction parameters on the activity and the selectivity of brown grease decarboxylation with minimum H_2 consumption over an activated carbon supported palladium catalyst, and to gain a better understanding of the reaction pathways.

2.2 Experimental

2.2.1 Materials

The FFAs used in this investigation were: stearic acid (≥95%), oleic acid (technical grade, 90%) and linoleic acid (60%) purchased from Sigma Aldrich (St. Louis, MO). Dodecane ($CH_3(CH_2)_{10}CH_3$, anhydrous, ≥99%), used as a solvent, and carbon disulfide (CS_2) were purchased from Sigma Aldrich. Ultra high purity grade argon (Ar) and hydrogen (H_2) were purchased from Cryogenic Gases (Detroit, MI). A commercial catalyst in powder form with 5 wt.% palladium on activated carbon support (Pd/C) was purchased from Sigma Aldrich. Methyl arachidate purchased from Nu-Chek Prep Inc. (Elysian, MN) was used as an internal standard. Brown grease was obtained from NextDiesel (Adrian, MI).

2.3 Brown Grease Decarboxylation Procedure

2.3.1 Semi-batch and Batch Reactions

The decarboxylation of brown grease over 5 wt.% Pd/C commercial powder catalyst was investigated in a 100 mL Hanwoul (Geumjeong-dong, South Korea) stirred batch reactor which was also employed in a semi-batch mode for selected experiments. Gas flow rates were controlled by metal sealed mass flow controllers (Brooks, Warren, MI). In all experiments, the catalyst was soaked in dodecane (solvent) prior to the reduction of the catalyst under H_2 flow of 60 mL/ min [64]. During the reduction step the agitation speed was kept at 250 ± 2 rpm, and the pressure was 0.5 MPa. As soon as the desired pressure was reached, the temperature was increased to 200 °C with a temperature ramp of 10 °C/min and kept under flowing H_2 for 1 hour at 200 °C. After cooling the reactor under H_2 flow, excess H_2 was purged with inert gas and the reactor was opened to add reactants into the vessel. For selected experiments, a pre-hydrotreatment of BG was employed in semi-batch mode before the decarboxylation step.

During the pre-treatment, 0.45 g of 5% Pd/C catalyst and 2 g of BG were used under a gas flow of 30 ml/min H_2 and 30 ml/min Ar. The pre-treatment was completed in 2 hours at 100 ^{o}C and 1.5 MPa.

In a majority of the studies, 7 wt.% brown grease in solvent with 65/1 (wt./wt.) ratio of solvent/catalyst was used. The catalyst loading (catalyst/feed = 0.2 (wt./wt.)) was comparable with those reported in the literature [64,69]. Throughout the reaction, the agitation speed was kept at 1000 $\pm$ 4 rpm. In the batch mode reactions, 10 or 50 vol.% H_2 balanced with Ar was added into the vessel at room temperature in order to obtain 1.5 MPa at 300 ^{o}C. While in the semi-batch mode, gases were flowed continuously through the reactor at a flow rate of 60 mL/min. After the reaction, the reactor was cooled down to room temperature and the final liquid product was analyzed. In some cases, a liquid sampling condenser was used.

2.4 Analysis Method

Liquid samples were obtained by centrifuging the product and separating the catalyst powder from the liquid product. After dissolving in carbon disulfide, liquid samples were analyzed using a Perkin Elmer Clarus 500 gas chromatograph (GC) equipped with flame ionization detector (FID) and a Restek (Rtx-65 TG) column (length: 30 m, internal diameter: 0.25 mm, phase film thickness: 0.10 μm) which provided a good separation for both hydrocarbons and FFAs without any derivatization requirement for sample preparation. The GC oven temperature was programmed as follows: 2 min hold at 80 ^{o}C, 10 ^{o}C/min ramp to 300 ^{o}C, 10 min hold at 300 ^{o}C. The detector temperature was maintained at 300 ^{o}C. Samples (1 μL) were injected into the column with a 50:1 split ratio, and concentrations were determined relative to a methyl arachidate internal standard. In order to identify the products, a GC-MS (Clarus 500 GC-

MS, Perkin-Elmer) with a capillary wax Rtx-WAX column (length: 60 m, diameter: 0.25 mm, thickness of stationary phase 0.25 μm) was also used.

2.5. Results and discussion

2.5.1 Brown Grease Conversion to Hydrocarbons over Pd/C catalyst: Effect of Reaction Parameters

It was reported that brown grease contains $15 \pm 5\%$ macromolecules [60]. In order to remove the macromolecular components, brown grease dissolved in dodecane solvent was vacuum filtered using a filter paper (Whatman # 42) with a 2.5 μm pore size. After filtration, 75 wt.% of the BG passed through the filter paper with the solvent while the remaining portion was captured in gel form. The filtered BG analyzed by GC-FID yielded approximately 94 wt.% FFAs while 6 wt.% could not be identified (Table 6), which is in good agreement with a previously reported BG analysis [60].

Table 6. Fatty acid composition of brown grease (trap grease).

FFAs (wt.%)	Brown Grease (Kim, et al., 2010)	Trap Grease (Wang, et al., 2008)	[a]Filtered BG (Current Study)
Myristic acid C14:0	1.5	1.16	0-0.3
Palmitic acid C16:0	23.8	30.38	29.7±0.9
Palmitoleic acid C16:1	1.9	1.42	0-0.2
Stearic acid C18:0	4.1	6.02	6.7±0.7
Oleic acid C18:1	48.7	38.39	53.7±6.4
Linoleic acid C18:2	17.8	18.83	6.2±3.7
Linolenic acid C18:3	2.3	1.31	2.5
Unidentified fatty acids	-	2.49	5.7±2.8

[a] FFA content of filtered brown grease analyzed by GC-FID via dilution of brown grease

Brown grease decarboxylation was studied over activated carbon supported palladium catalyst at 300 °C and 1.5 MPa in the semi-batch reaction mode. In Figure 16, 1 hour data point corresponds to the beginning of decarboxylation because the reaction temperature of 300 °C is reached at that moment (West 6100+ Temperature Controller). Since at 1 hour, the FFAs conversion reached almost 50% (

Figure **16**), conversion of FFAs should have started before the temperature reached 300 °C. Also, the GC-FID chromatogram (Figure 17) shows that the selective hydrogenation of C=C double bonds to stearic acid (disappearance of peaks 12, 13, 14 and increase in intensity of peak 11) is taking place during the heating of the reaction mixture to 300 °C. Snare et al. [69] reported formation of stearic acid intermediates from hydrogenation of double bonds during oleic acid decarboxylation under similar reaction conditions. Because the oleic acid content of brown grease can be as high as 50 wt.%, intermediate stearic acid formation is unavoidable. Once all the oleic acid (C18:1), linoleic acid (C18:2) and linolenic acid (C18:3) are saturated (Figure 17), the rate of stearic acid (C18:0) decarboxylation proceeds faster between 1 - 3 hour than between 3-7 hour (

Figure **16**). It should be noted that the increase in intermediates (C16:0 and C18:0) concentration, as a result of selective hydrogenation, leads to an increase in saturated n-C13 – n-C18 HCs selectivity for the first 2 hours of reaction (Figure 18). Figure 18 shows the liquid product selectivities as a function of time in the semi-batch reaction mode. The liquid product selectivity ($S_{i,t}$) is defined as

$$S_{i,t}(\%) = \frac{C_{i,t}}{C_{p,t}} \times 100$$

where $C_{i,t}$ is concentration of product i and $C_{p,t}$ is the liquid product concentration at time t. n-Paraffins obtained in the given range consist of tridecane (n-C13), pentadecane (n-C15) and

heptadecane (n-C17) at 2 hours. The increase in saturated nC13 - nC18 HCs selectivity and decrease in unsaturated nC13 - nC18 selectivity (Figure 18) between 1-2 hours indicates that some of the olefins are getting saturated by H_2 and forming n-paraffins. A similar observation has been reported elsewhere for stearic acid deoxygenation [64].
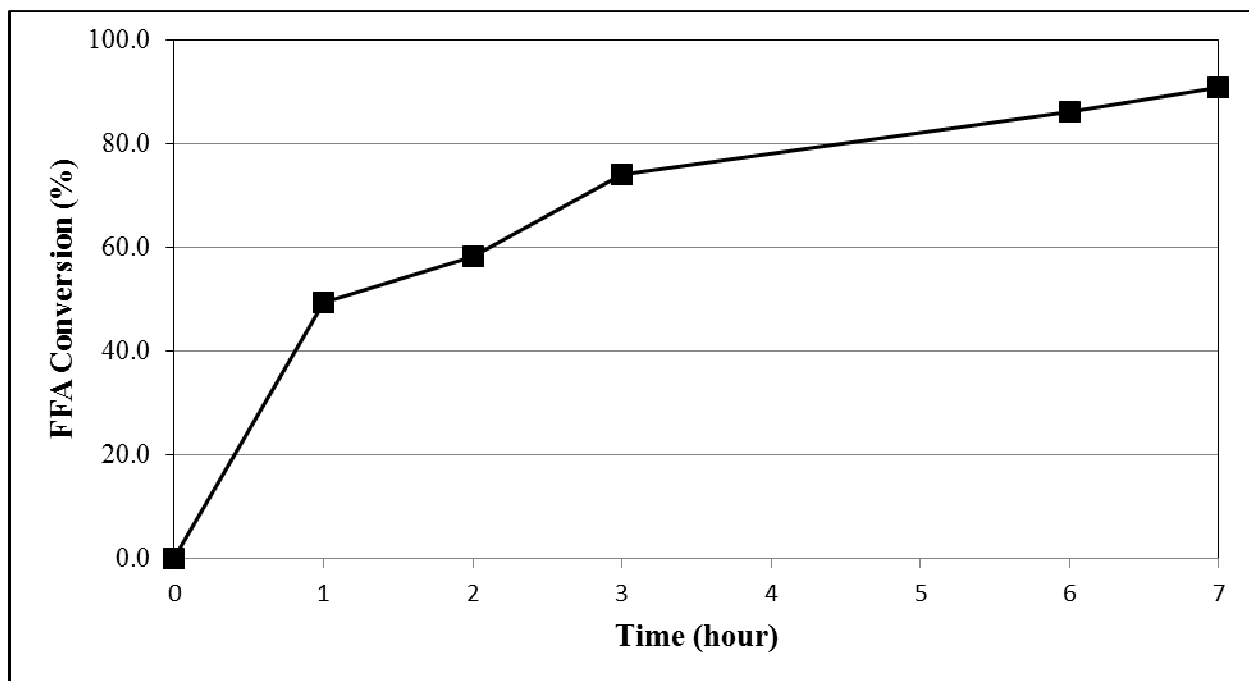
Figure 16. Brown grease decarboxylation over 5% Pd/C catalyst at 300 oC and 1.5 MPa in the semi-batch reaction mode for 7 hours. Reaction conditions: BG=7 wt.% in dodecane, solvent/catalyst=65/1 (wt./wt.), heating rate=5oC/min, 60 ml/min gas flow, 10 vol.% H2 - 90 vol.% Ar. Conversion of brown grease free fatty acids (FFAs) to hydrocarbons (HCs).
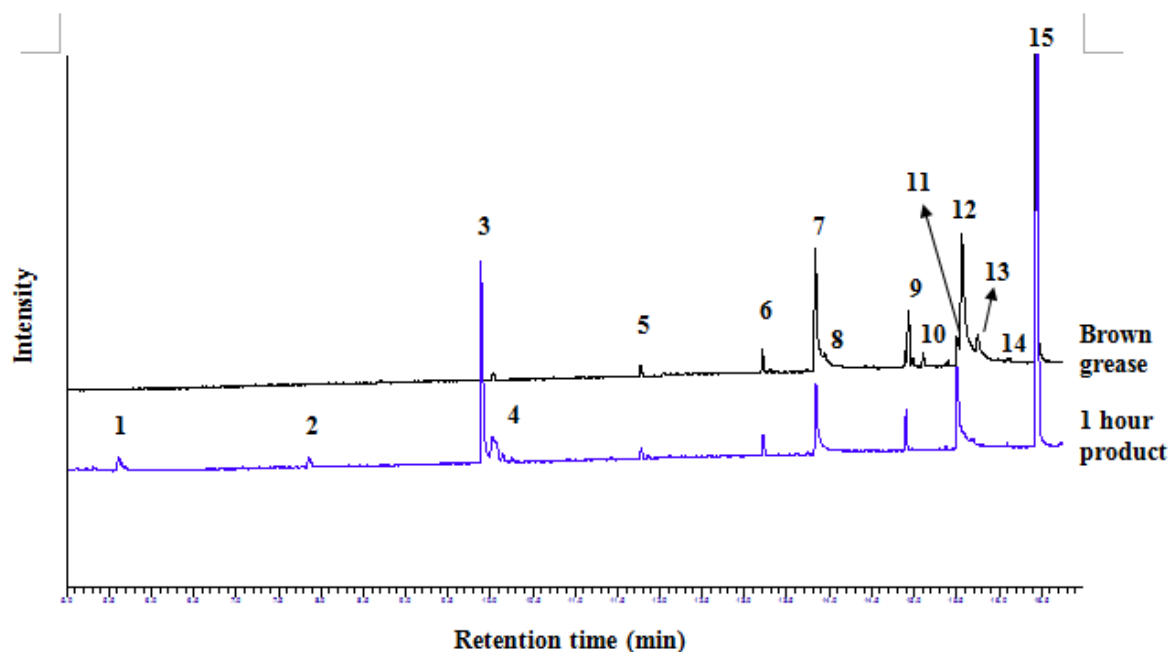
Figure 17. Brown grease decarboxylation over 5% Pd/C catalyst at 300 oC and 1.5 MPa in the semi-batch reaction mode for 7 hours. Reaction conditions: BG=7 wt.% in dodecane, solvent/catalyst=65/1 (wt./wt.), heating rate=5oC/min, 60 ml/min gas flow, 10 vol.% H2 - 90 vol.% Ar. (b) GC-FID chromatogram of the product at 1 hour. Peaks: 1. n-tridecane, 2. n-pentadecane, 3. n-heptadecane, 4. other C17 hydrocarbons, 5&6. unidentified brown grease compound, 7. palmitic acid 8. palmitoleic acid, 9&10. unidentified brown grease compound, 11. stearic acid, 12. oleic acid, 13. linoleic acids, 14. linolenoic acid, 15. ISTD.
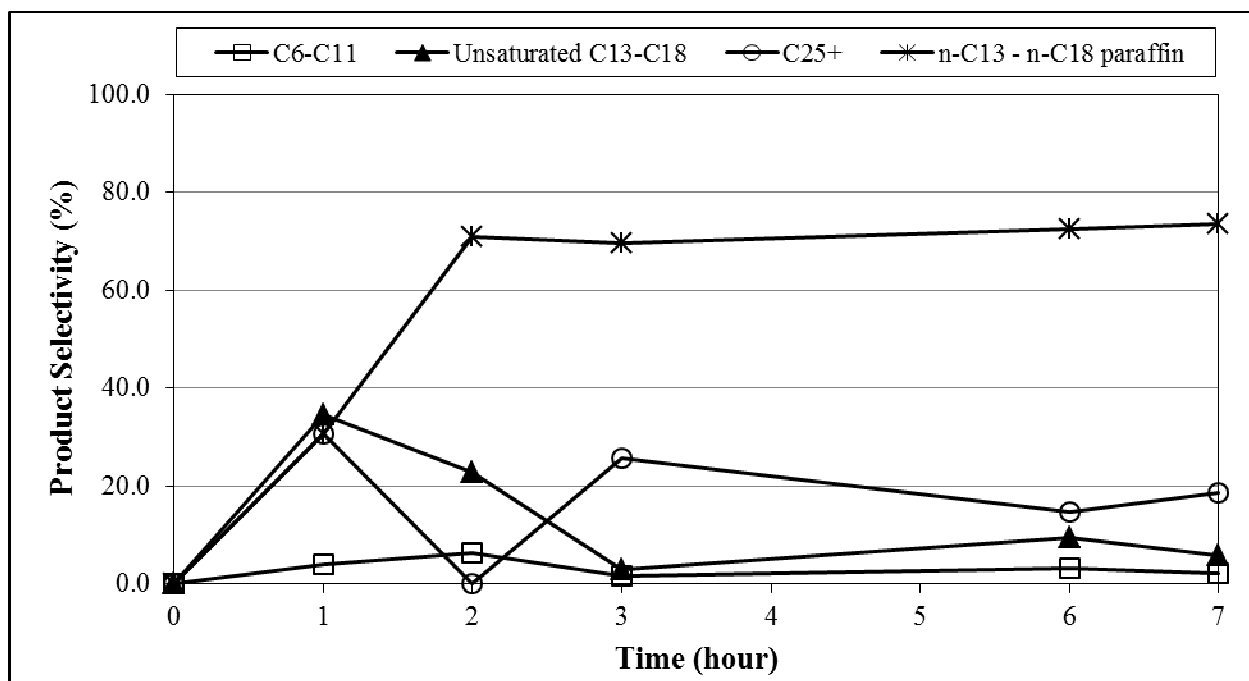
Figure 18. Brown grease decarboxylation over 5% Pd/C catalyst at 300 oC and 1.5 MPa in the

semi-batch reaction mode for 7 hours. Reaction conditions: BG=7 wt.% in dodecane,

solvent/catalyst=65/1 (wt./wt.), heating rate=5oC/min, 60 ml/min gas flow, 10 vol.% H2 - 90

vol.% Ar (c) Liquid product selectivities.
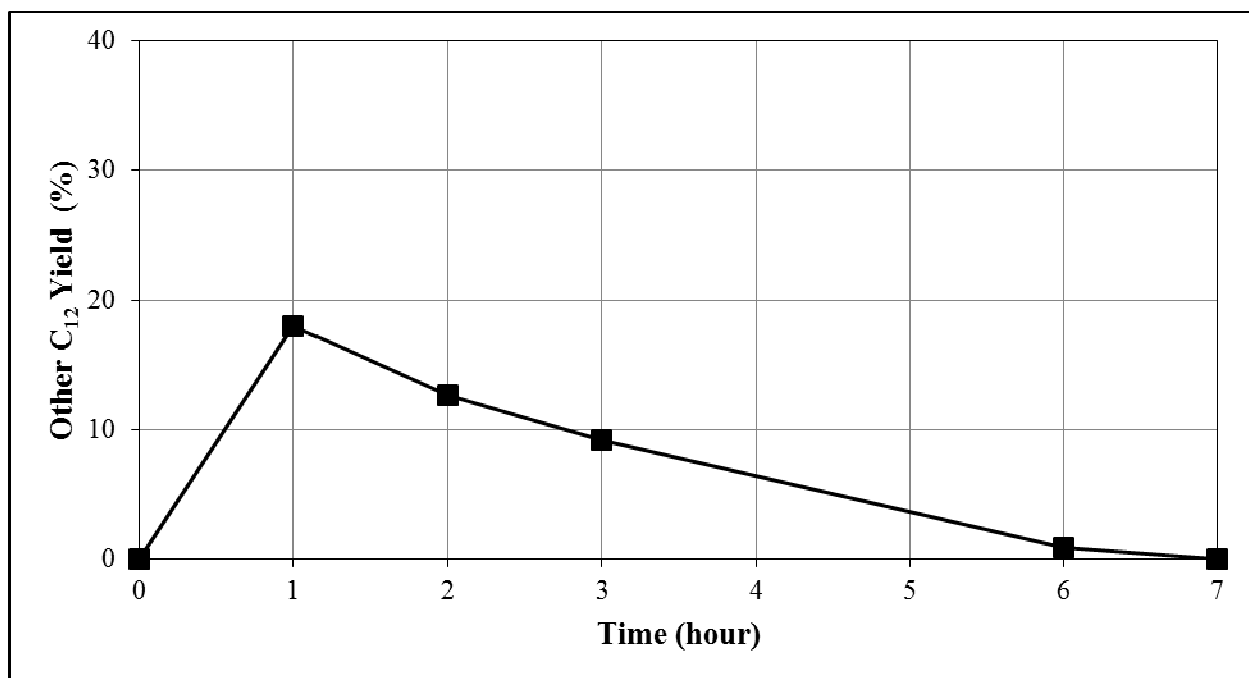
Figure 19. Brown grease decarboxylation over 5% Pd/C catalyst at 300 ^{o}C and 1.5 MPa in the

semi-batch reaction mode for 7 hours. Reaction conditions: BG=7 wt.% in dodecane,

solvent/catalyst=65/1 (wt./wt.), heating rate=5°C/min, 60 ml/min gas flow, 10 vol.% H$_2$ - 90

vol.% Ar. (d) Other C1$_2$ Yield from solvent.

Due to the high unsaturation level of the BG, the formation of heavier products (> C25)

was observed within the first hour (Figure 18). There was a sharp decrease in C25+ selectivity

between 1 - 2 hours which may be attributed to the fact that most unsaturated FFAs become

saturated. However, the later increase in C25+ selectivity between 2-3 hours is likely due to

some olimers transforming into heavier products. Another possible explanation for the presence

of heavy compounds can be attributed to the formation of fatty acid (possibly stearic acid)

dimers. Usually oleic acid is catalyzed in the presence of a clay catalyst or an acid catalyst at

more than 230 ^{o}C to form oleic acid dimers via a Diels-Alder mechanism [71,72]. Pd/C catalyst is

well known for hydrogenation of oleic acid dimer to stearic acid dimer [73]. Also the observation

of a light yellow color in the heavy compound containing products may be indicative of the

formation of stearic acid dimers. Formation of such dimer molecules was also observed by Simakova et al. during deoxygenation of C18 FFAs over mesoporous Pd/C catalyst [74]. However, a more detailed investigation of dimer formation from pure FFAs in the presence of Pd/C catalyst is needed in order to have a better understanding of the BG conversion process.

After 7 hours of reaction, the product also contains n-hexadecane (n-C16) and n-octadecane (n-C18) with selectivities of 1.3% and 0.6% respectively. One possible reaction pathway for formation of n-C16 and n-C18 hydrocarbons from C16:0 and C18:0 FFAs is hydrodeoxygenation (Figure 20). Although water was not captured in the liquid product, it was detected in the reactor effluent with gaseous products coming through the relief valve which was used to maintain the set pressure by continuously releasing the gaseous products, inert gas and unreacted H_2. Also, some of the water produced by HDO may participate in the water-gas shift reaction. In the beginning of the reaction, the low initial H_2 partial pressure (0.09 MPa) resulted in higher selectivity towards decarboxylation reaction pathway over HDO. On the other hand, after 7 hours of reaction, most FFAs have been converted resulted in excess hydrogen to FFA, which favors the HDO reaction.

Apart from the BG conversion, reaction of the dodecane solvent was also observed. Yield of other C12 hydrocarbons is shown as a function of time in Figure 1-d. Within the first hour of reaction, dehydrogenation of solvent to other C12 hydrocarbons is increasing. However, continuous H_2 supply in the semi-batch reaction saturates these components back to dodecane. Possible reaction pathways and products from solvent conversion are shown in Reactions III-VI and a detailed discussion is provided in Section 3.1.1.
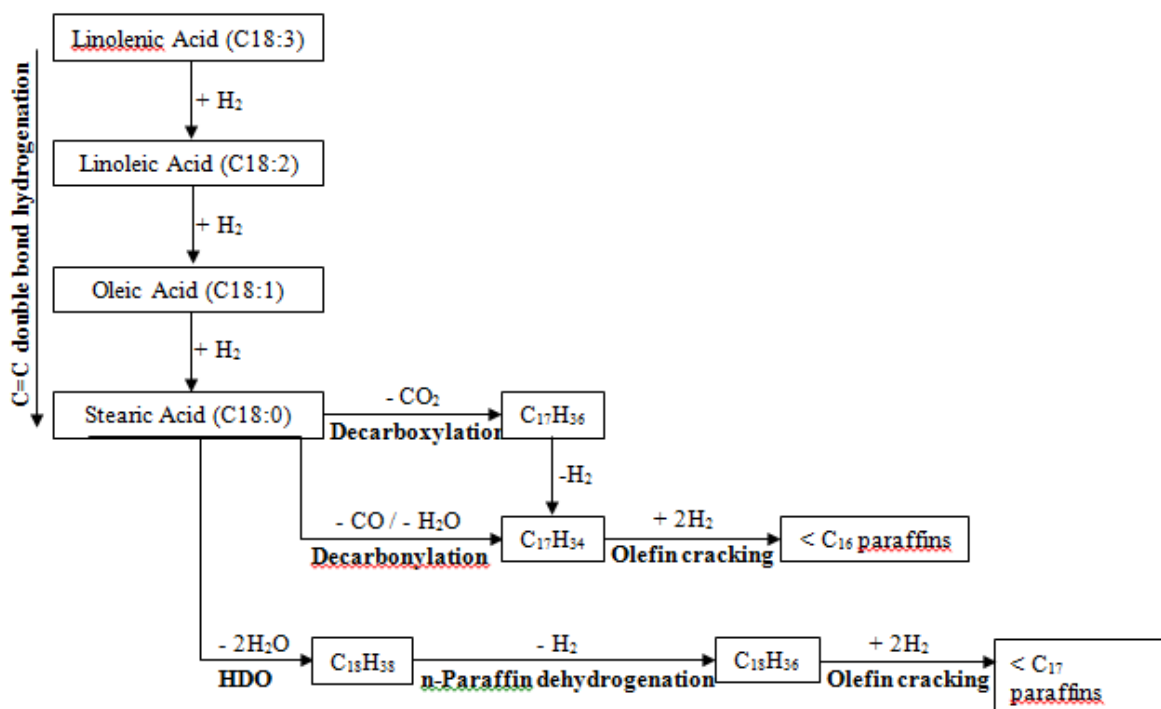
Figure 20. Liquid phase reactions of brown grease conversion to diesel fuel at 300 ^{o}C and 1.5 MPa

2.5.2 Effect of Solvent Dilution

The effect of solvent dilution on the reaction was investigated in both a semi-batch reactor under continuous flow ratio of 1/1 (vol./vol.) H_2/Ar and a batch reactor. Liquid product selectivities and FFA conversions after 6 hours of reaction are given in Figure 21. It is clear that solvent dilution does not show any significant impact on FFA conversion. Regardless of BG concentration in the solvent, semi-batch operation can yield over 95% BG conversion while batch can only yield 40% conversion under similar reaction conditions. This can be attributed to a continuous fresh H_2 supply and removal of gaseous products in semi-batch mode. The highest green diesel hydrocarbon (n-C13 – n-C18) selectivity was obtained with 7 wt.% BG in semi-batch mode; and increasing BG concentration from 7 wt.% to either 25 wt.% or 50 wt.% in semi-

batch mode resulted in a decrease in green diesel hydrocarbons selectivity and in an increase in C25+ selectivity. This is because the higher BG concentration means higher unsaturated FFAs concentration. As discussed in Section 3.1, more unsaturated FFAs will yield more C25+ molecules.

The most significant effect of increasing BG concentration in the batch reactor was a decrease in n-C13 – n-C18 range paraffin selectivity and increase in the C13 – C18 range olefin. In contrast to semi-batch mode, the lack of H_2 apparently causes an increase in C13-C18 olefins selectivity. This suggests that the main reaction pathway for unsaturated HC formation is decarbonylation (Reaction II) for a H_2 rich environment while dehydrogenation (Reaction I) plays a significant role in a low H_2 concentration containing system.

The selectivities of the liquid phase reactions (Figure 22) were calculated based on the liquid products; for instance odd carbon number containing n-paraffins were products of decarboxylation while even carbon number containing n-paraffins resulted from hydrodeoxygenation. Although long-chain paraffins are known to be highly prone to cracking [75], cracking selectivity was very low under our experimental conditions (Figure 22). On the other hand, for batch reaction, there was a high olefin (especially unsaturated C17) selectivity which was attributed to the decarboxylation of unsaturated FFAs [69] or to the decarbonylation of FFAs [64]. Our gas phase GC-FID analysis (CO and CO_2 generation) indicates both decarbonylation as well as decarboxylation are taking place under these reaction conditions. Moreover, palladium is known to have a high catalytic activity for dehydrogenation as well as hydrogenation reactions. In order to obtain 10% conversion of n-paraffin ($>C_{12}$) via dehydrogenation, operation at mild reaction conditions (below 350 ^{o}C and 1 atm) is needed over a noble metal catalyst [76]. Paraffin dehydrogenation is an endothermic reaction with a heat of reaction of about 125 kJ/mol [76].

Therefore, it is likely that olefins are produced via both dehydrogenation (Reaction I) of paraffins and decarbonylation (Reaction II) of BG FFAs (Figure 17). Whether produced via dehydrogenation or decarbonylation, the n-monoolefins can be further hydrogenated in the presence of H_2.

I. Dehydrogenation: $C_nH_{2n+2} \rightleftharpoons C_nH_{2n}+H_2$ ($\Delta H=125$ kJ/mol)[76]

II. Decarbonylation: $C_nH_{2n}O_2 \longrightarrow C_{n-1}H_{2(n-1)}+H_2O+CO$ ($\Delta H=179.1$ kJ/mol)[38]
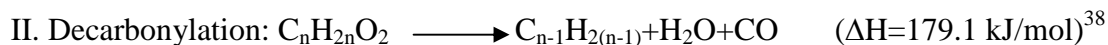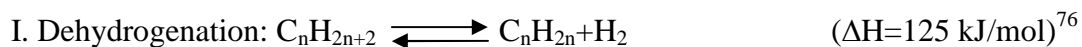
Decarboxylation of BG is the primary reaction with a selectivity of 87% for a 7 wt.% BG - 93 wt.% solvent system under 50 vol.% H_2 – 50 vol.% Ar flow in semi-batch mode (Figure 3-b). When brown grease concentration was increased, selectivity to decarboxylation and decarbonylation/dehydrogenation decreased significantly; while HDO and oligomerization increased (Figure 3-b). Therefore, with a dilute solution of BG, side reactions are minimized and primary n-pentadecane (n-C15) and n-heptadecane (n-C17) products increase. Similar solvent dilution effects are also observed in various hydrogenation processes [77].

Under the same reaction conditions the solvent dodecane (n-C_{12}) undergoes a chemical transformation to other forms of C_{12} hydrocarbons such as olefins, dienes, aromatics and olefin cracking as follows [78]:

III. Olefin formation: $C_{12}H_{26} \rightleftharpoons C_{12}H_{24} + H_2$

IV. Diene formation: $C_{12}H_{24} \rightleftharpoons C_{12}H_{22} + H_2$

V. Aromatic formation: $C_{12}H_{22} \rightleftharpoons C_{12}H_{18} + 2H_2$

VI. Olefin cracking: $C_{12}H_{24} + 2H_2 \rightleftharpoons\ < C_{11}$ hydrocarbons
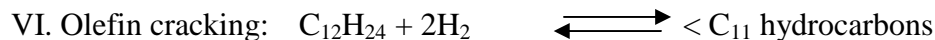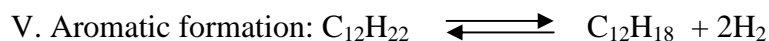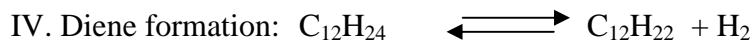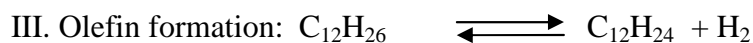
Also, in a blank solvent (dodecane) experiment under the similar reaction conditions, Immer et al. observed H_2 generation which confirmed the dehydrogenation of dodecane [64]. The other C_{12} yield decreased from 46% (batch, 7% BG) to 30% (semi-batch, 7% BG); while

increasing BG concentration from 7% to 50% in semi-batch mode resulted in a total elimination

of other C_{12} hydrocarbon formation (Figure 23). Thus, the H_2 concentration has a small effect on

the other C_{12} hydrocarbon yields, while the solvent dilution has a strong effect.
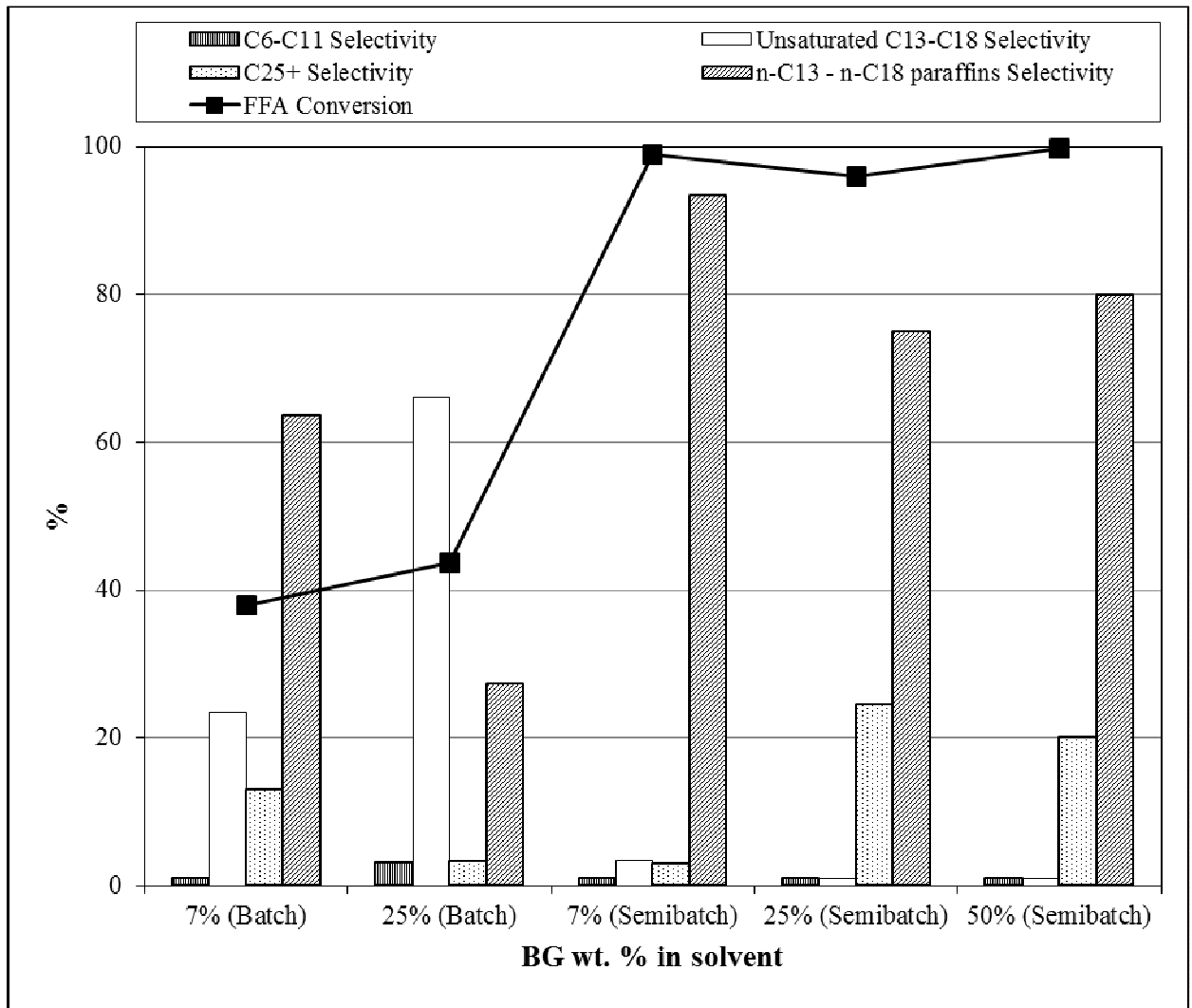
Figure 21. The effect of solvent dilution on Liquid product selectivities and FFAs conversions.
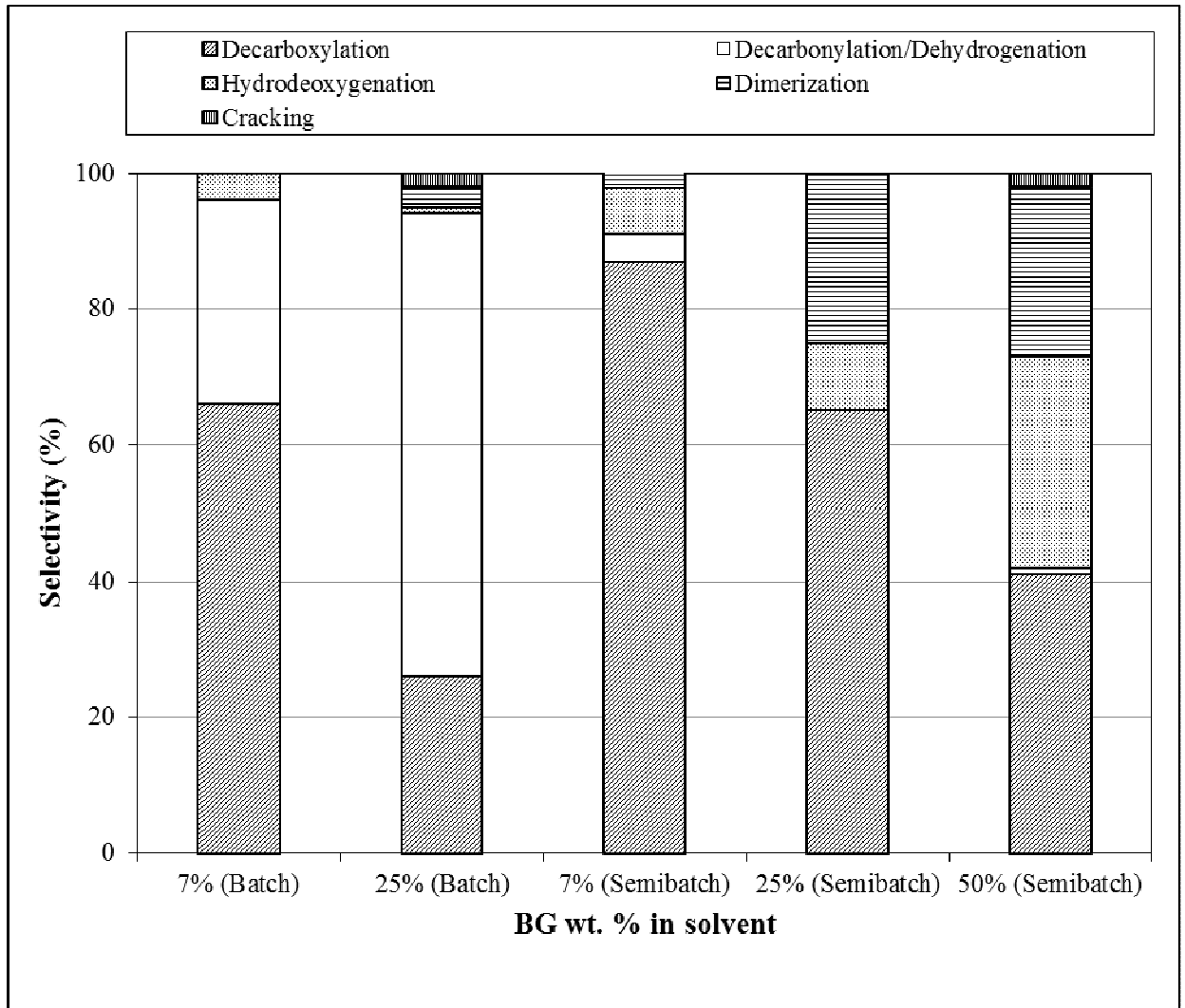
Figure 22. The effect of solvent dilution on selectivities of liquid phase reactions.
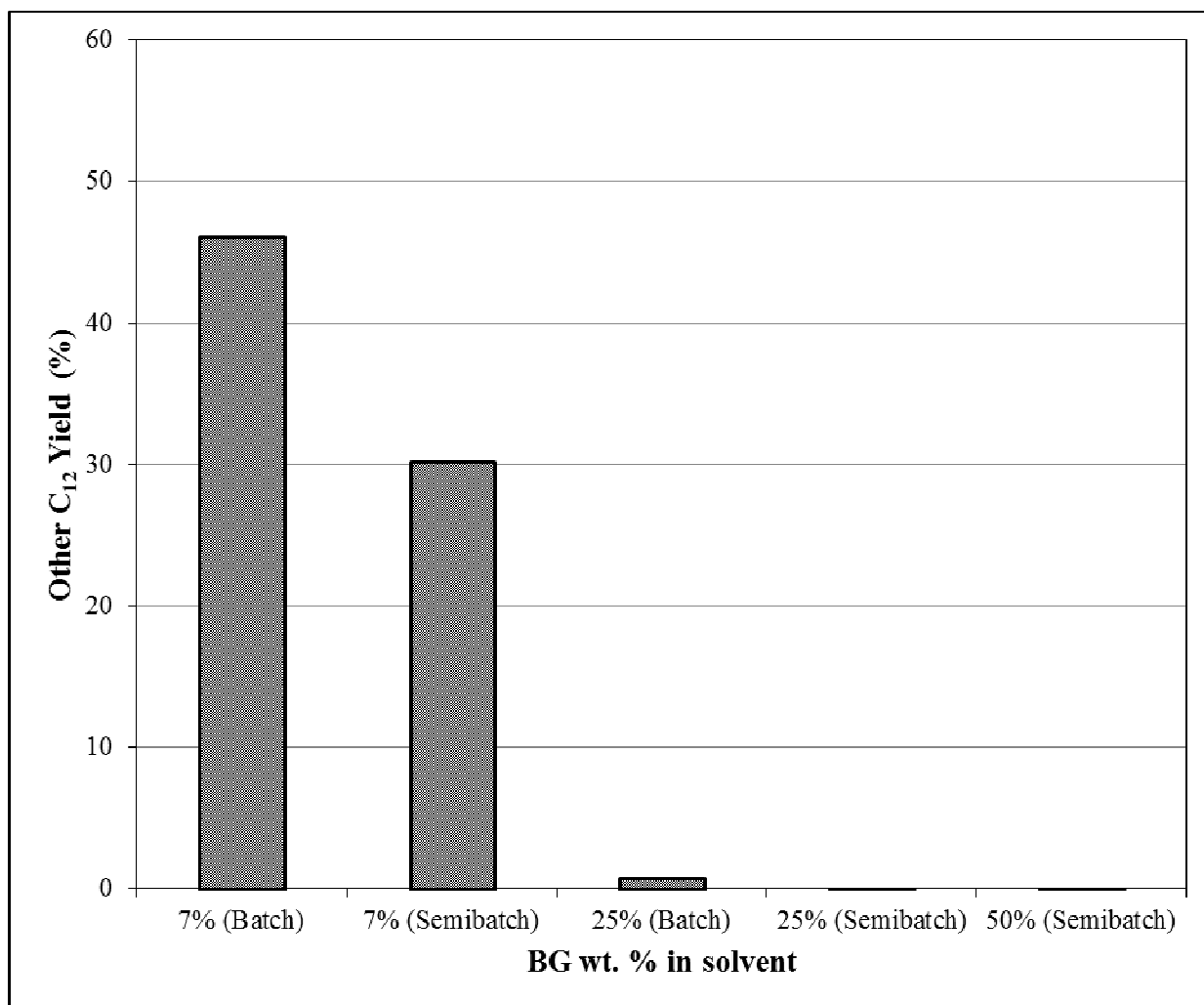
Figure 23. The effect of solvent dilution on yield to other C_{12} hydrocarbons from solvent, under following reaction conditions: 5%Pd/C catalyst, BG/Catalyst=5/1(wt./wt.), heating rate 9°C/min, 300 ^{o}C, 1.5 MPa, 6 hour; For batch mode: initial H_2/BG= 0.4/1 (mol/mol); For semi-batch mode: 48 ml/min gas flow of 1/1 (vol./vol.) H_2 / Ar.

3.1.2 Effect of Degree of Unsaturation of Brown Grease Free Fatty Acids

In an effort to investigate the effect of the degree of unsaturation of BG FFAs on decarboxylation, pure stearic (C18:0), oleic (C18:1) and linoleic (C18:2) acids as well as a mixture of these components were used in separate batch reactions as representative FFA compounds of BG. The results are shown in Table 2. Stearic acid batch decarboxylation yielded 94.8% conversion to mainly n-heptadecane (S= 93.8%) in 1 hour at 300 ^{o}C, and a 100% conversion was achieved within 2 hours. This suggests that, under the same conditions, pre-hydrotreated BG which consists of mainly stearic acid should be completely converted to mainly n-C$_{17}$ within 2 hours. In contrast, pre-hydrotreated BG conversion was only 52% and n-paraffin selectivity decreased to 59.8% after 6 hours (Table 7). This can possibly be attributed to catalyst poisoning by BG impurities. In oleic acid decarboxylation, FFA conversion was 99.4% after 6 hours of reaction in the presence of 1/9 (vol./vol.) H$_2$/Ar gas (Table 7). Similar to the BG results (section 3.1.1), increasing the H$_2$/Ar ratio to 1/1 (vol./vol.) leads to an increase in n-paraffin selectivity (99.6%) with no observable unsaturated hydrocarbons and C25+ products. When only linoleic acid was used in a batch reaction, the conversion slightly decreases to 90. However, there was a bigger impact on product distribution. The selectivity of n-paraffins and olefins in the diesel range changed from 95.4% and 3.3% to 68.6% and 28.3% respectively, when reactant was switched from a saturated FFA (stearic acid) to an unsaturated FFA (linoleic acid). When a mixture of stearic, oleic and linoleic acids was reacted, the conversion of FFAs and the product selectivities were in good agreement with the weighted average of the individual component results. Pre-hydrotreating the FFA mixture improved the conversion and n-paraffin selectivity slightly, but neither FFA conversion nor product selectivities were the same as that of stearic acid.

A separate experiment of BG partial hydrogenation was conducted to determine how long it takes to obtain saturated FFA intermediates such as C16:0 and C18:0 from BG. As observed in the GC-FID results (data not shown), within 2 hours all of the unsaturated FFA compounds of BG are saturated at 100 ^{o}C and 1.5 MPa in a solvent free system and under a flowing 1/1 (vol./vol.) ratio of H_2/Ar gases. The GC-FID analysis confirmed formation of palmitic acid and stearic acids along with n-pentadecane (2.9% yield) and n-heptadecane (46% yield), indicating the partial hydrogenation of BG along with decarboxylation reaction at a lower temperature (100 ^{o}C). Although it is reported elsewhere that pure FFA compounds do not show any decarboxylation activity at 100 ^{o}C, here we observe a different phenomenon in a solvent free reaction atmosphere comparing with approximately 99 wt.% solvent use [70]. Another important finding in this investigation is the formation of heptadecenes (7.3% yield). It is believed that this dehydrogenation/decarbonylation step must occur due to the solvent free atmosphere where the products were not removed quickly from the catalyst surface; therefore n-C17 product further reacted to form heptadecene isomers. Kubickova et al. also observed formation of such isomers during decarboxylation of stearic acid with Pd/C catalyst at 300 ^{o}C and 1.7 MPa [79], conditions much higher than reported here.

Assuming the mixture of FFAs given in Table 7 represents BG, we compare reactions of FFA mixture and BG. The conversion of BG is significantly lower than that of the FFA mixture. However, after pre-hydrogenation, the BG conversion improves by 27% while conversion of the FFA mixture improves by 5%. Moreover, pre-hydrogenation helps to increase selectivity of diesel range n-paraffins and to decrease diesel range olefins for the FFA mixture. On the other hand, pre-hydrogenation of BG has an adverse effect on the product selectivities. The selectivity to olefins in the diesel range is about 80% higher and the selectivity to n-paraffins in the diesel

range is 35% lower for pre-hydrogenated BG conversion than that of the pre-hydrogenated FFA

mixture. These results suggest that the decarboxylation reaction sites of the Pd/C catalyst might

be partially poisoned by impurities in BG.

Table 7. Conversion and liquid product selectivities of batch decarboxylation of brown grease

and pure FFAs with different unsaturation levels. Reaction conditions: 6 wt. % reactant in

dodecane, solvent/catalyst=66/1 (wt./wt.), initial H2/Ar ratio of 1/9 (vol./vol.), 6 hr batch

reaction at 300 oC and 1.5 MPa over 5 % Pd/C catalyst.

Reactant	FFA Conversion (%)	C_6-C_{11} Selectivity (%)	nC_{13}-nC_{18} paraffin Selectivity (%)	Unsaturated C_{13}-C_{18} Selectivity (%)	C_{25+} Selectivity (%)
[a]Stearic Acid (C18:0)	94.8	0	95.4	3.3	1.3
Oleic Acid (C18:1)	99.4	0	94.3	4.4	1.3
[b]Oleic Acid (C18:1)	95.5	0.4	99.6	0	0
Linoleic Acid (C18:2)	90.0	0	68.6	28.3	3.2
Mixture of: Stearic Acid (10wt.%) Oleic Acid (65wt.%) Linoleic Acid (25wt.%)	93.5	0	87.4	12.6	0
Pre-hydrotreated Mixture of: Stearic Acid (10wt.%) Oleic Acid (65wt.%) Linoleic Acid (25wt.%)	98.4	0	91.4	8.6	0
Brown Grease (BG)	37.9	0	63.6	23.4	13.0
Pre-hydrotreated BG	52.0	0	59.8	40.2	0

[a]: 1 hour

[b]: Initial H_2 /Ar ratio= 1/1 (vol./vol.)

2.5.3 Effect of Pre-treating Brown Grease with H_2

The effect of pre-treatment of brown grease with H_2 on the decarboxylation activity was investigated at 300 $^{\circ}$C and 1.5 MPa in a batch mode reaction. Figures 4-a and b show the effect of H_2-treatment of BG on FFA conversion and product selectivities. Although, pre-hydrogenation of BG improves the FFA conversion after 6 hours, it retards the decarboxylation activity by the 2nd hour of the reaction. This observation can be attributed to the production of a more stable form of FFAs (saturated FFAs of C16 and C18) after pre-treating brown grease with H_2. At zero time of the reaction, mainly mono-unsaturated FFAs are present for non-pretreated BG while only saturated FFAs exist for pretreated BG. Since saturated compounds are more stable than unsaturated compounds, pretreated BG shows a lower conversion trend at the beginning of the reaction. It should be noted that the non-pretreated BG batch reaction results are different than the semi-batch study discussed in Section 3.1 where a continuous H_2 flow was operated. In terms of product selectivities, the n-paraffin (n-C13 – n-C18) selectivity is almost the same with and without H_2 pretreatment of BG at 6 hours (Figure 24 and Figure 25). However, the pre-hydrogenation step helps to decrease higher compound (C25+) selectivity and to increase unsaturated C13-C18 selectivity. GC-MS and GC-FID results confirm the formation of C9:0 and C15:0 FFAs for non-pretreated BG and the formation of C11:0, C13:0 and C15:0 FFAs and C6-C11 HCs for H_2- pretreated BG at 2 hours. Formation of C9:0 and C15:0 for non-pretreated BG can be explained by the cleavage of double bonds located at cis-9 for oleic and cis, cis, cis - 9, 12, 15 for linolenic acids. Since C=C bonds are saturated in H_2- pretreated BG, such cleavage is not observed; instead, other FFAs form via cleavage of C-C bonds. This suggests that H_2- pretreatment avoids C=C bond cleavage, but not C-C cleavage. Overall, although the conversion improvement appears to be somewhat minimal, the H_2-pretreatment of BG improves

the diesel selectivity (a combined selectivity of saturated and unsaturated hydrocarbons in diesel

range increases to 100%) and formation of heavy hydrocarbons are eliminated (S_{C25+} decreased

from 23.4% to 0%).
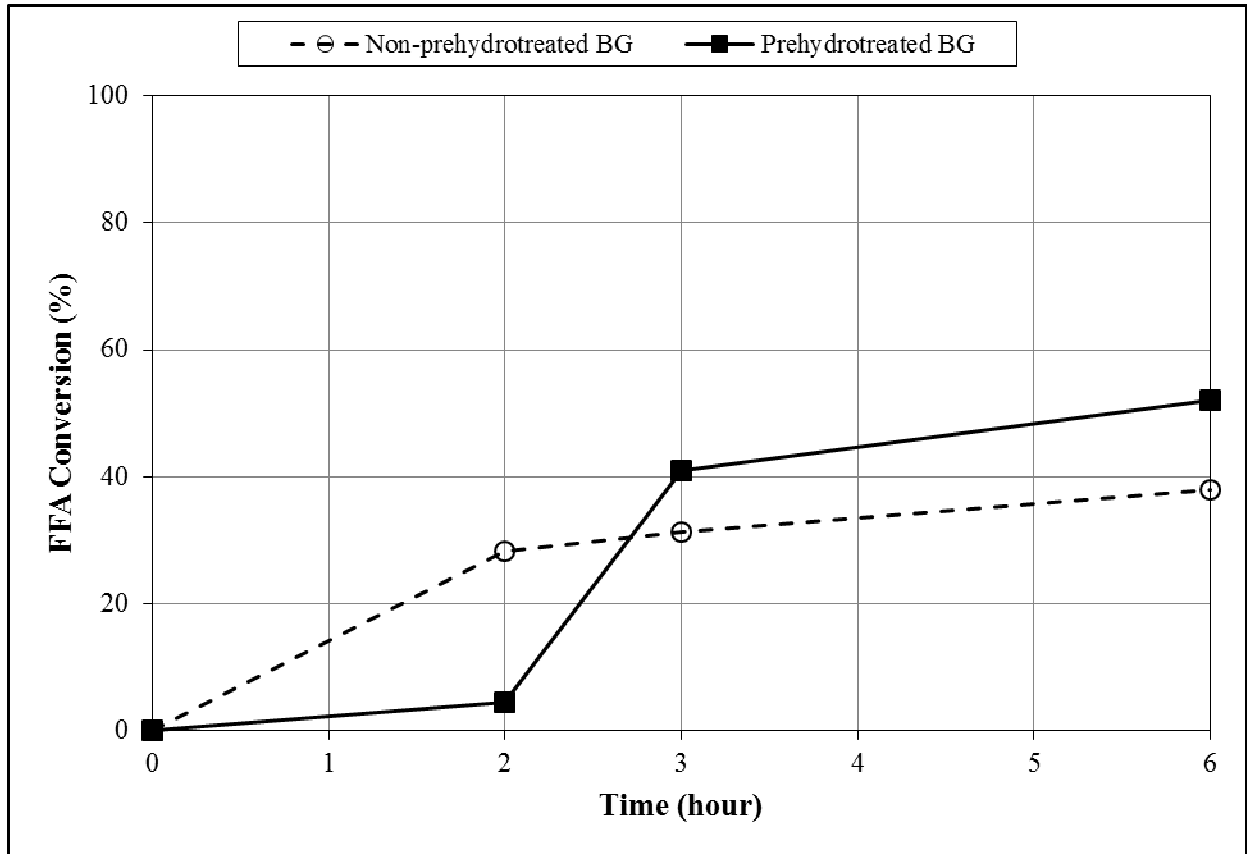
Figure 24. The effect of pre-hydrotreating BG on (a) FFAs conversions
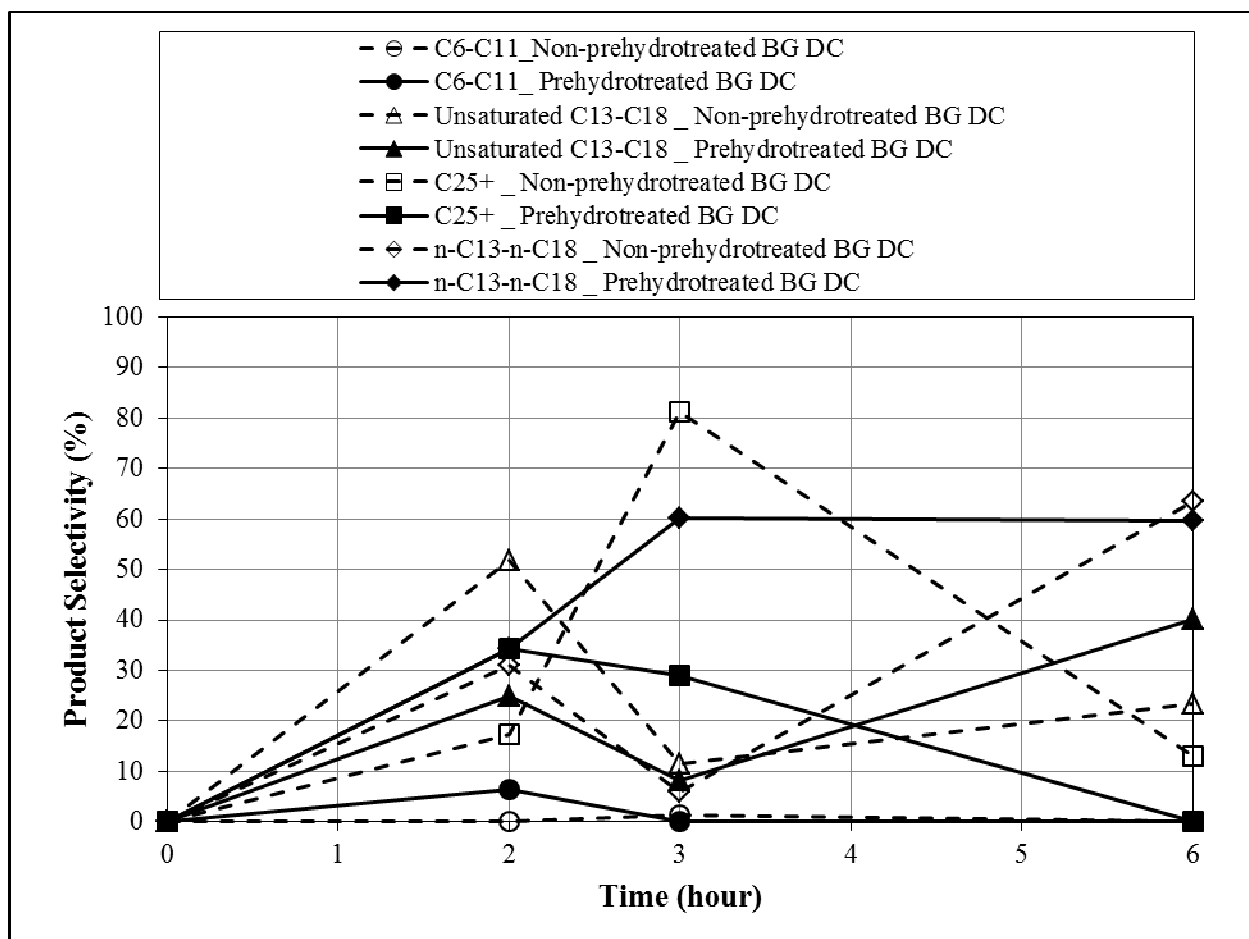
Figure 25. The effect of pre-hydrotreating BG on liquid product selectivities. Reaction

conditions: 5% Pd/C catalyst, BG concentration in solvent=6 wt.%,

catalyst/solvent=66/1(wt./wt.), 300 ^{o}C, 1.5 MPa, 10 vol.%H$_2$-90 vol.%Ar, 6 hours batch reaction.

2.5.4 Effect of H$_2$/BG Ratio

In order to further investigate the limiting effect in decarboxylation activity, H$_2$ partial

pressure was increased 4 times (initial H$_2$/BG ratio: 0.3/1 mol/mol) so that a stoichiometric H$_2$

amount was supplied to saturate C=C bonds in the unsaturated FFA compounds of brown grease

in the batch reactor. In this case, series reactions of partial hydrogenation of C=C double bonds

and decarboxylation reactions were expected in a one stage reaction.

The stoichiometric H_2 amount was calculated based on the fact that 1 mol H_2 is required per mol of C=C. Therefore, one, two and three moles of H_2 are required per mole of oleic, linoleic and linolenic acids, respectively. Based on this calculation, an approximately 1/1 Figure 26 displays the FFA conversion and product selectivities as a function of H_2/BG ratios (0.3/1, 1/1, 2/1 and 3/1) after 6 hours of reaction. Having a H_2/BG ratio of 1/1 mol/mol in the reaction atmosphere improved the FFA conversion by 40% compared with the case where a 0.3/1 ratio of H_2/BG was used. Increasing the H_2 amount to 2/1 ratio of H_2/BG further increased the FFA conversion by 1.3-fold. Interestingly, further increase to 3/1 ratio of H_2/BG does not have a noticeable effect on conversion. Figure 26 also shows that using a stoichiometric H_2 amount leads to a 75% reduction in olefinic hydrocarbon product formation compared with using a 0.3/1 ratio of H_2/BG. Moreover, a high H_2/BG ratio leads to a total elimination in olefin formation when the H_2/BG ratio was increased from 0.3/1 to 3/1 (Olefin selectivity decreases in the order: 0.3/1 > 1/1 = 2/1 > 3/1). There is a slight increase in C-C cracking selectivity under excess H_2 conditions (from 2/1 to 3/1 ratio of H_2/BG) while a significant increase is observed for the stoichiometric condition. An important observation is that the pre-hydrotreated BG decarboxylation (Figure 24) has the same FFA conversion level as that of the decarboxylation of non-prehydrotreated BG under stoichiometric H_2 conditions (Figure 26). However, based on the product selectivities, the most significant difference is the dominant reactions for these two different conditions. While decarboxylation and decarbonylation reactions are the major pathways for pre-hydrotreated BG conversion, decarboxylation and dimerization (high C25+ selectivity) are the major pathways for conversion of non-pretreated BG under a stoichiometric H_2 amount.

For the H_2/BG range in which the reactions were conducted, lower partial pressures of H_2 do not necessarily favor decarboxylation. As Figure 27 shows, HDO selectivity increases in the presence of excess H_2; while excess H_2 does not significantly affect the decarboxylation selectivity. A similar effect of H_2 on HDO selectivity is discussed in Section 3.2. Immer demonstrated that increasing the H_2 partial pressure causes a shift in the reaction pathway to decarbonylation because of the inhibition effect of H_2 and CO on decarboxylation activity [80]. However, inhibition of the decarboxylation pathway with increasing H_2 partial pressure was not observed in this work. In contrast, decarbonylation/dehydrogenation selectivity significantly decreased from 23.4% to 0% by increasing H_2/BG ratio from 0.3/1 to 3/1 (selectivity decreased in the order of 0.3/1 > 1/1 = 2/1 > 3/1) (Figure 27). Theoretically, H_2 partial pressure should not affect the decarbonylation and decarboxylation activities because of the reaction stoichiometry. However, the effect of H_2 on the conversion of carboxylic acids on Pd surface cannot be excluded in a lean H_2 environment due to the dehydrogenation of paraffins [81]. On the other hand, in a rich H_2 environment, it is likely that olefins produced via decarbonylation of FFAs are further hydrogenated to n-paraffins. These n-paraffins can also be perceived as decarboxylation products. Maier [81] inferred that the use of H_2 is necessary to detach the product hydrocarbons from the Pd surface. Our study indicates a low H_2/BG ratio gives the best green diesel selectivity (a combined selectivity of saturated and unsaturated C13-C18 hydrocarbons). However, the conversion is 58% lower than under the excess H_2 condition.
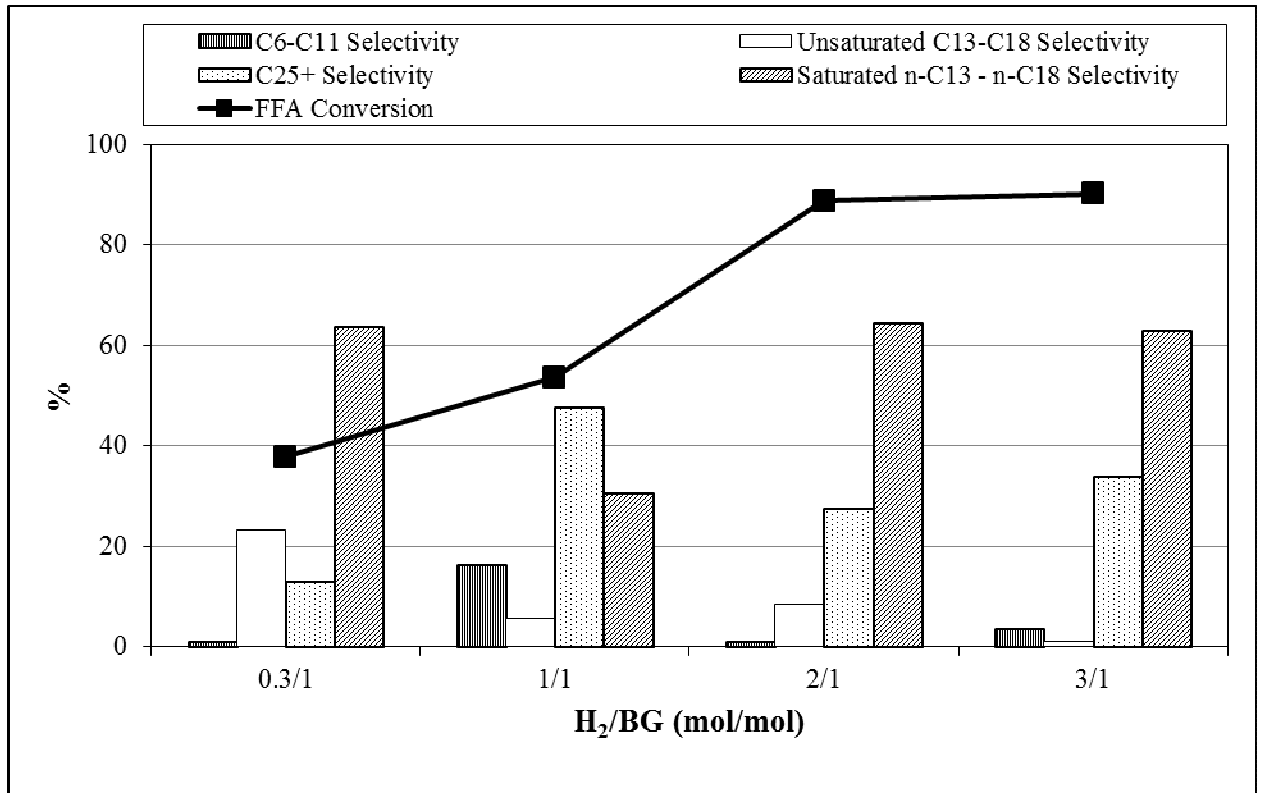
Figure 26. The effect of H_2/BG ratio on liquid product selectivities and FFAs conversions
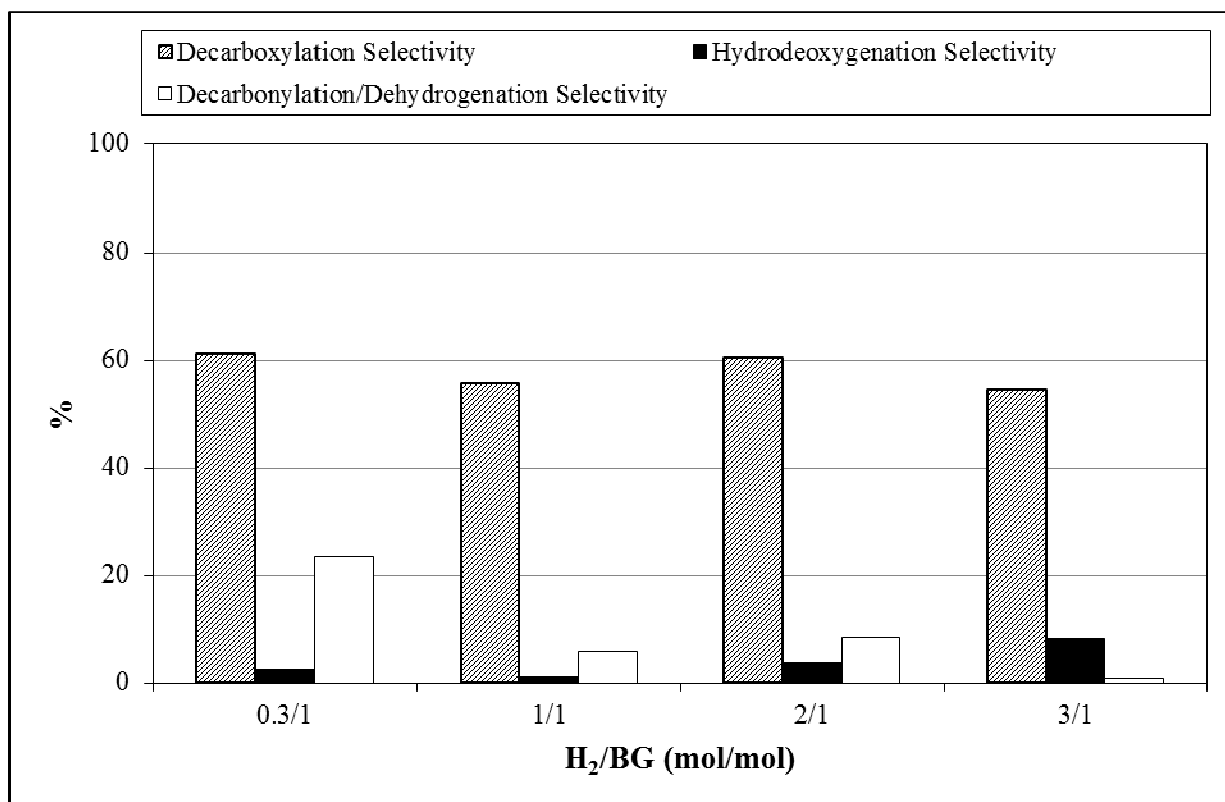
Figure 27. The effect of H_2/BG ratio on (b) Decarboxylation and hydrodeoxygenation (HDO) selectivities. Reaction conditions: BG=6 wt.% in dodecane, solvent/catalyst=66/1 (wt./wt.), 6 hr batch reaction at 300 ^{o}C and 1.5 MPa over 5% Pd/C catalyst.

2.6. Conclusion

The commercial 5% Pd/C catalyst is highly active for the decarboxylation of pure FFAs. Lower activity for BG conversion can be attributed to the unidentified impurities. Solvent dilution as high as 90% is necessary to suppress side reactions and increase diesel yield. Pre-hydrotreated BG results in a 37% increase of conversion with 100% green diesel selectivity. Therefore, such a two-step processing with selective hydrogenation prior to the decarboxylation

of BG improves the product selectivity. The decarboxylation process is a promising alternative to the high temperature and high pressure hydrodeoxygenation of waste oil conversion to diesel fuel.

CHAPTER 3

A Highly Active Nanocomposite Silica-Carbon Supported Palladium Catalyst for Decarboxylation of Free Fatty Acids for Green Diesel Production: Correlation of Activity and Catalyst Properties

A class of Pd catalyst supported on a silica-activated carbon nanocomposite for free fatty acid (FFA) decarboxylation was developed, and displayed excellent activity and operation stability selectively for the green diesel hydrocarbons formation in the absence of H_2 under mild reaction conditions. Six catalysts containing 5 wt% Pd were prepared by systematically varying the silica content in the support. In addition to the effect of particle size, the impact of catalyst preparation method on the activity and selectivity was elucidated. A 5 wt% Pd/Si-C-4 catalyst maintained stable activity for 16 days under reaction conditions of 1.5 MPa and 300 °C. Characterization of the catalyst revealed that the highly active Pd/Si-C-4 catalyst has easily accessible and well-distributed metallic Pd nanoparticles inside the hybrid mesopores.

3.1. Introduction

Environmental awareness and projected increases in the world's energy demand have been the motivation for seeking environmentally friendly, renewable alternative fuels. A large amount of waste cooking oil and grease is produced in the U.S. that can be exploited for liquid biofuel generation. In particular, brown grease, which contains mainly free fatty acids (FFAs), can be a potential inexpensive source for a process to obtain straight chain hydrocarbons in the diesel fuel boiling range (green diesel) via catalytic decarboxylation.

Recently, there has been considerable attention on the development of suitable catalysts for decarboxylation of free fatty acids (FFA) [66,67,82-85]. Most early studies focused on Pd-based catalysts, which exhibit high activity and selectivity for the formation of straight chain hydrocarbons with one carbon number less than the source FFA.[38] However, these supported palladium catalysts readily deactivate even in the presence of H_2. Although a 3 wt% Pd-SBA-15 catalyst was active at 300 °C under 17 bar of 5 vol% H_2 in argon for stearic acid decarboxylation for 5 hours, deactivation was reported due to the formation of unsaturated heptadecene product [67]. A 1 wt% Pd supported on a synthetic mesoporous carbon catalyst showed 23% decrease in the BET specific surface area after decarboxylation of palmitic and stearic acids mixture at 300 °C and 17.5 bar H_2/Ar [66]. In all cases, the extensive catalyst deactivation was attributed to catalyst coking. Snare et al. related the catalyst deactivation to the amount of unsaturated products which further led to catalyst coking specifically for Ru/C and Rh/C catalysts after 6 h of stearic acid decarboxylation.[38] On the other hand, the Pd/C catalyst deactivation was attributed to the reaction atmosphere and degree of unsaturation of the FFA by some researchers [86-88] and to catalyst supports by others [83]. Recently, the Jones group showed that the deactivation of a mesoporous silica supported palladium catalyst occurred during FFA decarboxylation due to the

loss in total surface area, porosity and accessible palladium surface area [84]. Unlike the previously reported literature claim of coke formation, it was claimed that strongly adsorbed reactants and products cause the deactivation.

An ordered mesoporous silica-carbon catalyst support was synthesized as a novel hybrid material [89]. This nanocomposite support has gained increasing attention for catalysis applications in recent years due to several unique features such as high dispersion of palladium nanoparticles (about 3 nm), high surface area, large and tunable pore structure and excellent stability [90,91]. These silica-carbon nanocomposites were produced on the basis of a triblock copolymer templating approach which is a time consuming catalyst preparation technique.

The nature of the surface functional groups on the activated carbon support when modified by oxidative treatments was found to be very important for the catalytic activity of precious metals such as palladium [92,93]. After introducing such oxygen groups, the surface behavior of carbon changes; therefore their catalytic properties differ [94]. The components of activated carbon are disorganized polyaromatic sheets with reactive corner atoms and adsorbent surface atoms. The precursor that is selected for this study, TEOS, is expected to form the templates that contain -OH groups and bridged O atoms in a Si-O-Si structure on the amorphous silica walls, and these groups play a very important role for the incorporation of silica into activated carbon.

In the present work, a new, well-defined and highly efficient Pd/Si-C catalyst was developed for the decarboxylation of FFA. This new nanostructured hybrid catalyst has a well-defined mesoporous structure which allows a better understanding of structure–activity characteristics that are crucial in elucidating the FFA decarboxylation mechanism, unlike an

activated carbon supported palladium catalyst. The decarboxylation reaction of oleic acid was investigated over these catalysts with the aim of producing green diesel in the absence of additional H_2 under mild reaction conditions, elucidating the effects of the nature of the functional groups on the activity and developing a procedure to maintain high catalytic activity.

3.2. Experimental

3.2.1 Materials

The following chemicals were used in this investigation: a commercial activated carbon (Charcoal Norit, Sigma-Aldrich), tetraethyl orthosilicate (TEOS, 99.999%, Sigma–Aldrich), palladium(II) chloride (PdCl$_2$, ≥99.9%, Sigma–Aldrich), oleic acid (technical grade 90%, Sigma-Aldrich, St. Louis, MO), dodecane (anhydrous, ≥99%, Sigma-Aldrich), carbon disulfide (HPLC grade ≥99.9%, Sigma-Aldrich), methyl arachidate (>99%, Nu-Chek Prep Inc., Elysian, MN), Ultra high purity grade argon (Ar), hydrogen (H_2) and nitrogen (N_2) were purchased from Cryogenic Gases (Detroit, MI).

3.2.2. Catalyst preparation

Activated carbon (AC) was immersed in liquid TEOS with varying mass ratios of TEOS to AC. The mixture was stirred vigorously for 2 hours at 120 ^{o}C. Then, it was dried at 105 ^{o}C for 18 hours. Prepared supports were designated as Si-AC-x where x represents the mass ratio of TEOS to AC. During the preparation of Si-AC-0.5 and Si-AC-1, ethanol was added to provide necessary wetness of AC. For comparison, only activated carbon and only silica supported catalysts were also prepared. A support containing only silica was prepared by calcination of the Si-AC-3 support at 550 ^{o}C for 5 hours in air to remove activated carbon. In order to obtain 5 wt% Pd on the support, 1.1 wt% PdCl$_2$ solution was mixed with the support (PdCl$_2$/support=0.088

wt/wt) at room temperature for 24 hours. After each catalyst was dried at 100 $^{\circ}$C for 5 hours, the reduction was carried out under a flow of 10 vol% H_2-90 vol% N_2 at 200 $^{\circ}$C for 3 hours.

3.3. Material characterization

Powder X-ray diffraction (XRD) patterns were obtained on a Rigaku MiniFlex 600 at a scan rate of 3°/min (40 kV, 15 mA). The Scherrer equation and Bragg's law were used to calculate the mean metal particle size and the lattice parameter, respectively.

A Brunauer-Emmett-Teller (BET) analysis was carried out using a Micromeritics TriStar II 3020 (V1.03) surface area analyzer. The samples were degassed in vacuum (P) at 200 $^{\circ}$C for 6 hours prior to analysis. The adsorption/desorption isotherms were acquired at 87.30 K in the relative pressure range of 0.01 to 0.99. The Barrett-Joyner-Halenda (BJH) model was used to derive the pore volumes, average pore diameters and pore size distributions from the desorption branches of the isotherms. A t-Plot was used to calculate the micropore surface areas and micropore volumes.

Catalyst acidity was determined with a Brinkmann/Metrohm 809 Titrando (Westbury, NY) potentiometric titrator. An acid–base technique [95] was performed to determine the total acid number of surface groups reacted in the catalyst slurry of 0.1 g catalyst and 75 mL titration solvent including a mixture of water, propan-2-ol and toluene. A solution containing 0.1 N KOH was used as titrant. The amount of titrant consumed to reach a potentiometric end point (EP) was used to calculate the amount of acidic groups.

Transmission electron microscopy (TEM) was conducted using a JEM-2010 microscope operating at 200 kV. The catalysts that were suspended in ethanol were placed on a carbon coated copper grid.

Fourier transform infrared (FTIR) spectra of powder catalysts were collected on a Spectra 400 spectrometer (Perkin-Elmer, Shelton, CT). Four scans were used to establish an acceptable signal to noise level for each spectrum.

3.4. Decarboxylation procedure

3.4.1 Batch Reactions

The liquid-phase decarboxylation of oleic acid was investigated in a 100 mL Hanwoul (Geumjeong-dong, South Korea) stirred batch reactor. Gas flow rates were controlled by Brooks (Warren, MI) metal sealed mass flow controllers. In all experiments, the catalyst was soaked in dodecane (solvent) prior to the reduction of the catalyst under H_2 flow of 60 mL/ min [88]. During the reduction step the agitation speed was kept at 250 ± 2 rpm, and the pressure was 0.5 MPa. As soon as the desired pressure was reached, the temperature was increased to 200 ^{o}C with a temperature ramp of 10 ^{o}C/min and kept under flowing H_2 for 1 hour at 200 ^{o}C. After cooling the reactor under H_2 flow, excess H_2 was purged with inert gas and oleic acid was fed into the vessel through a one way valve.

For the activity test of each catalyst, 0.45 g catalyst, 2.0 g oleic acid and 30.0 g solvent were used. Throughout the reaction, the agitation speed was kept at 1000 ± 4 rpm. Ar gas was added into the vessel in order to obtain 1.5 MPa total pressure at 300 ^{o}C. After the reaction, the reactor was quenched in an ice bath and the final liquid product was analyzed.

3.4.2 Flow Reactor

The continuous decarboxylation of brown grease was carried out in a fixed bed tubular reactor (40 mL BTRS-Jr, Autoclave Engineers, PA). Two grams of catalyst was placed between glass wool layers. The catalyst was first reduced at 200 ^{o}C and 0.5 MPa under H$_2$ flow. After reduction, the reactor was pressurized to 1.5 MPa under Ar gas and heated to 300 ^{o}C. Oleic acid (0.2 M in dodecane) was continuously fed through the catalyst bed at a volumetric flow of 0.04 mL/min.

3.5 Analysis Method

Liquid samples products were dissolved in carbon disulfide and were analyzed using a Perkin Elmer Clarus 500 gas chromatograph (GC) equipped with flame ionization detector (FID) and an Rtx-65 TG column (length: 30 m, internal diameter: 0.25 mm, phase film thickness: 0.10 μm). The GC oven temperature was programmed as follows: 2 min hold at 80 ^{o}C, 10 ^{o}C/min ramp to 300 ^{o}C, 10 min hold at 300 ^{o}C. The detector temperature was maintained at 300 ^{o}C. Samples (1 μL) were injected into the column with a 50:1 split ratio, and concentrations were determined relative to a methyl arachidate internal standard. In order to identify some of the products, a GC-MS (Clarus 500 GC-MS, Perkin-Elmer) with a capillary wax Rtx-WAX column (length: 60 m, diameter: 0.25 mm, thickness of stationary phase 0.25 μm) was also used.

3.6. Results and discussion

3.6.1 Change in the catalyst structure and the nature of surface groups

The XRD patterns of the fresh palladium catalysts supported on activated carbon, silica and Si-C with four different silica to carbon ratios are shown in Figure 28. For all catalysts except Pd/Si, a broad peak at 2θ of 23.9° and an overlapped broad peak at about 39.8° were

observed, which correspond to the (002) and (100) diffractions of amorphous carbon for Pd/C, respectively [96]. The d spacing of the (002) plane is 0.37 nm for Pd/C which is greater than that of graphitic carbon (0.343 nm), indicating that this catalyst does not contain graphitic carbon [97]. For the Pd/Si catalyst, the broad peak at 22.0° corresponds to amorphous silica [98]. The (002) amorphous carbon diffraction shifted from 23.9° to 23.0° as the Si amount increased. Several well-resolved peaks at 2θ of 40°, 47°, 68° and 82° that are assigned to the (111), (200), (220), and (311) reflections of the face-centered cubic (fcc) Pd lattice are observed in the XRD pattern of samples. Only in the Pd/Si-C-0.5 catalyst, Pd(311) diffraction was not observed. The palladium particle size calculated from the Scherrer formula for each catalyst is 6.7, 5.5, 5.9, 6.3, 6.2 and 4.1 nm for Si, Si-C-4, Si-C-2, Si-C-1, Si-C-0.5 and C supported Pd catalysts, respectively. The larger metal particle sizes for the silica modified samples compared to the activated carbon supported catalyst may be attributed to the nature of the surface groups on the support. It is believed that small metal particles agglomerate to larger particles because they become mobile on the surface when the surface groups thermally decompose during the metal reduction [99].
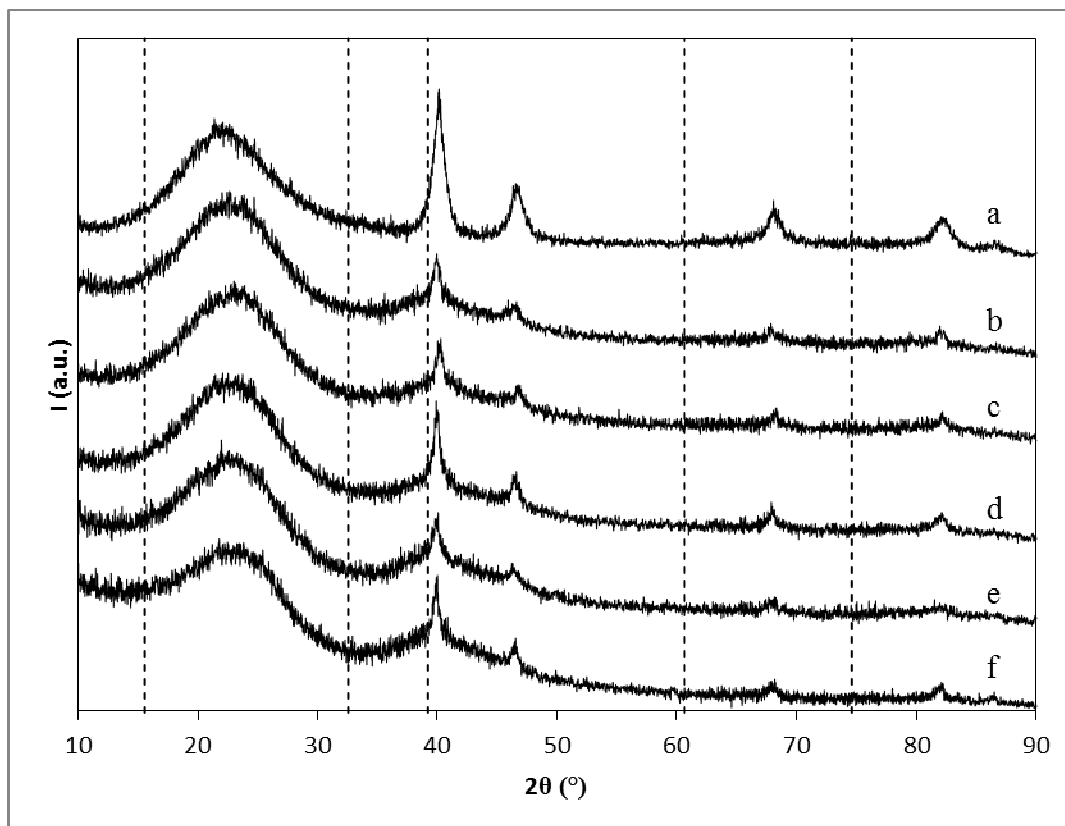
Figure 28. Wide-angle XRD patterns of fresh palladium catalysts supported on: silica (a), SiC(4:1) (b), SiC(2:1) (c), SiC(1:1) (d), SiC(0.5:1) (e), activated carbon (f).

The TEM images of the fresh palladium catalysts supported on silica, Si-C-4, Si-C-2, Si-C-1, Si-C-0.5 and activated carbon are given in Figure 29 (a) – (f). The TEM image of the Pd/Si catalyst (Figure 29(a)) displays a large distribution of sintered Pd particles with an average particle size of 5.3 nm. The larger particle size of Pd/Si catalyst may be due to the lower surface area of Si support and suggests that Pd particles were not stabilized by the oxide support [100]. The inset of the

The TEM images of the fresh palladium catalysts supported on silica, Si-C-4, Si-C-2, Si-C-1, Si-C-0.5 and activated carbon are given in Figure 29 (a) – (f). The TEM image of the Pd/Si catalyst ((a) shows the large silica particles with about 100 nm. Pd/Si-C-4 has fairly narrow Pd particle size distribution with average particle size of 3.0 nm (Figure 29(b)). The Pd metal

appears to be clustered together rather than being spherical in Si-C-1 and Si-C-0.5 (Figure 29(d) and (e)). TEM image of Pd/C (

The TEM images of the fresh palladium catalysts supported on silica, Si-C-4, Si-C-2, Si-C-1, Si-C-0.5 and activated carbon are given in Figure 29 (a) – (f). The TEM image of the Pd/Si catalyst ((f)) shows very fine Pd particles. All the particle sizes observed by TEM images were slightly smaller than those are evidenced by XRD. Nevertheless, both TEM and XRD data confirmed the existence of sintered Pd particles in the Si, Si-C-1 and Si-C-0.5 supported catalysts.
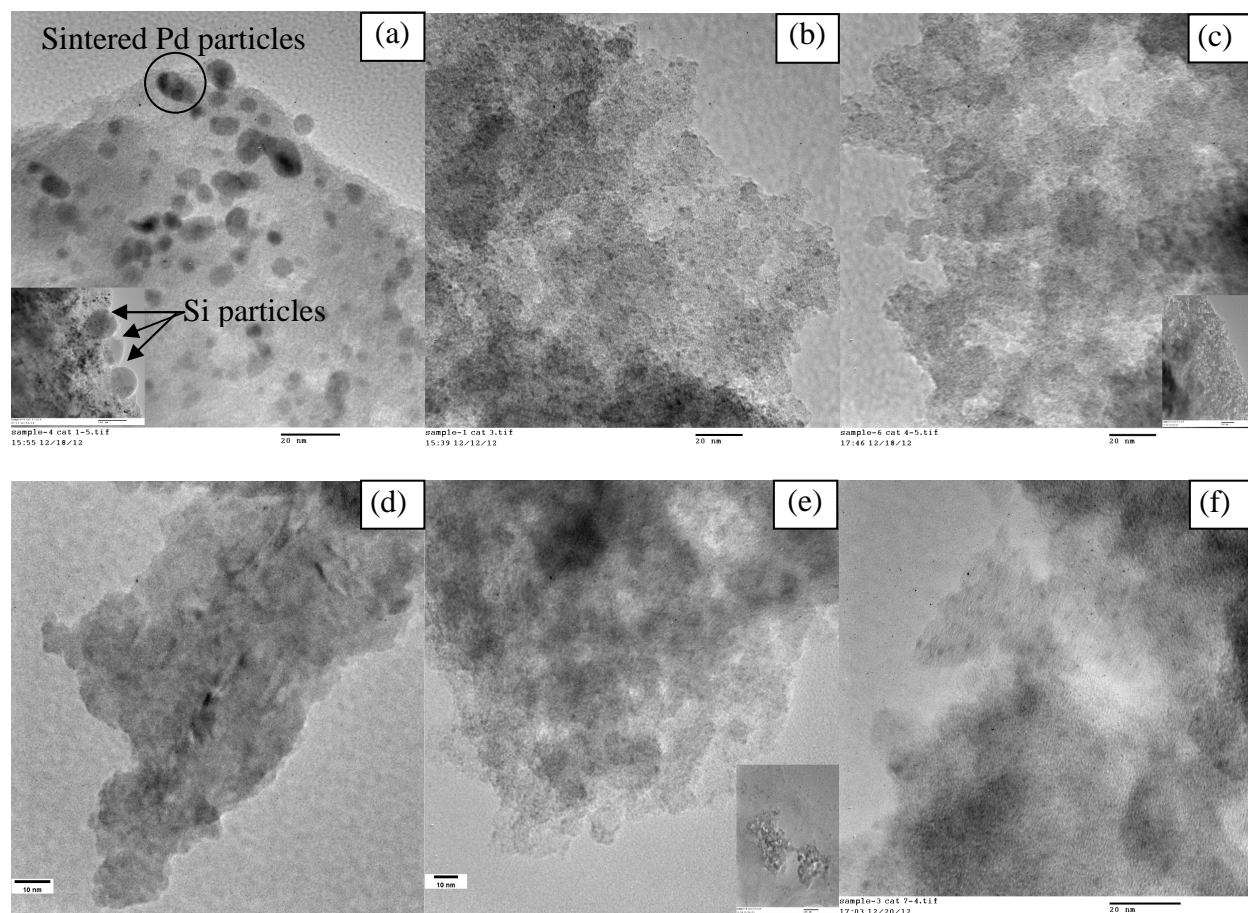
Figure 29. Fresh palladium catalysts supported on: silica (a), Si-C-4 (b), Si-C-2 (c), Si-C-1 (d), Si-C-0.5 (e), activated carbon (f). Insets are the images with 100 nm scale bar.

An H4-type hysteresis loop is also evident, which is often associated with the presence of mesopores with narrow slit-like pores [101]. With increasing carbon content of the support, more obvious hysteresis loops are observed (Figure 30 (d), (e) and (f)). The capillary condensation step shifts to a lower relative pressure in a range of P/P_o =0.44-0.92 for the Pd/Si catalyst, which is related to the pore size reduction to 3.6 nm. This is likely due to shrinkage of the support's framework during the calcination at 550 °C. The silica mesostructure may possibly have been destroyed during the carbon combustion from the Si-C-3 support. Pore size distribution curves of Si-C supported catalysts with different Si content (Figure 31) shows a narrow pore size distribution. The Pd/Si shows bimodal-pores centered at 2.6 nm and 3.8 nm.
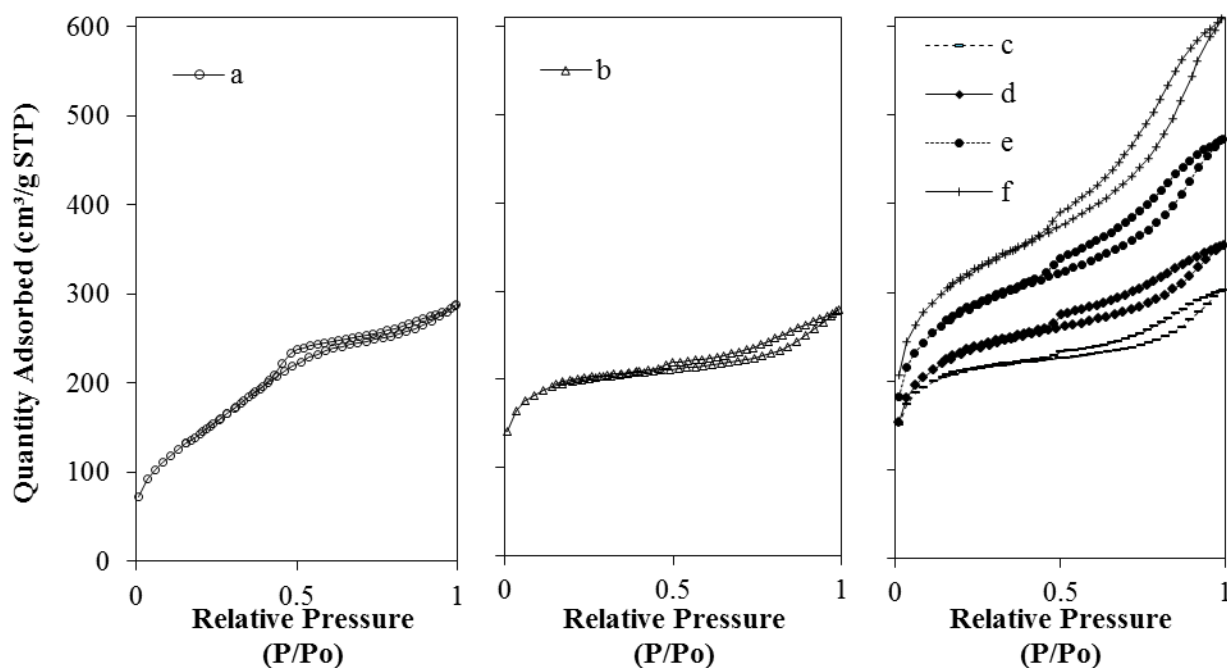
Figure 30. N_2 sorption isotherms of palladium supported on: silica (a), Si-C(4:1) (b), Si-C(2:1) (c), Si-C(1:1) (d), Si-C(0.5:1) (e), activated carbon (f).
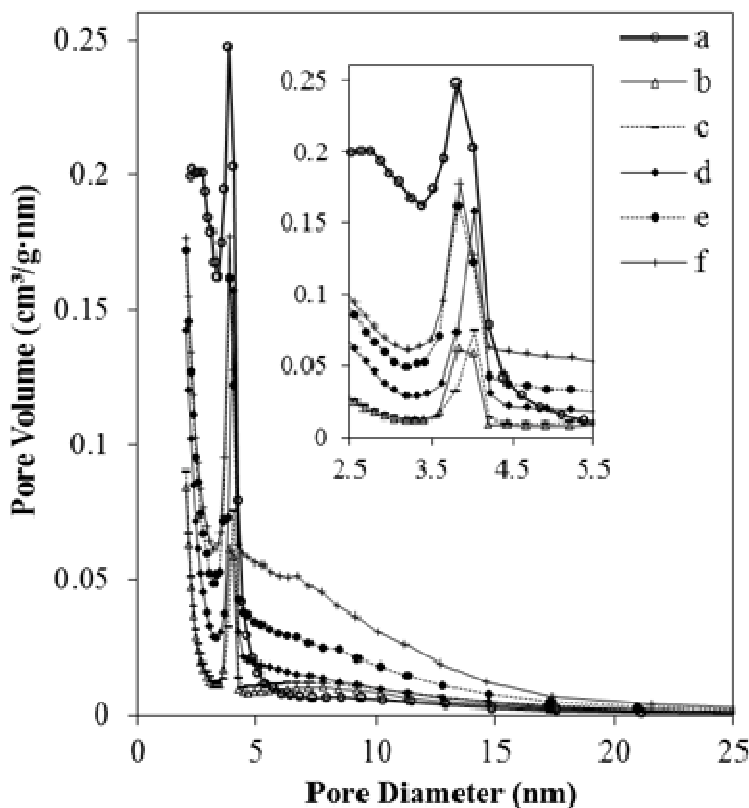
Figure 31. Pore size distribution curves of palladium supported on: silica (a), Si-C(4:1) (b), Si-C(2:1) (c), Si-C(1:1) (d), Si-C(0.5:1) (e), activated carbon (f).

The activated carbon support has a high surface area and a well-developed porosity, with most of the surface area in the micropores. In the modified material, the sol-gel preparation of Pd/Si-C-1 and Pd/Si-C-0.5 (in the presence of ethanol) led to a significant decrease in the micropore volume as well as surface area (Table 8). This can be attributed to pore blockage by the silica particles. On the other hand, the silica content did not contribute to a significant change in the micropore volume of catalysts Pd/Si-C-4 and Pd/Si-C-2. As silica content increases in the support, the BET surface areas and total pore volumes decrease gradually. Yet the average pore diameters do not follow the same trend. For Si-C-2 and Si-C-4 supported catalysts, the pore sizes remain nearly constant at about 5.3 nm, which is the same as that of Pd/C, after Si addition to C. However, pore sizes greatly decreased in Pd/Si-C-0.5 and Pd/Si-C-1, which may be due to

blockage of larger pores. This pore blockage may be due to hydrolysis of TEOS in the presence of ethanol-water mixture followed by a condensation that takes place between a silanol and ethoxy group [102]. Bridging oxygen or silaxane group (Si-O-Si) forms as a result of these reactions where ethanol was used as a solvent during the catalyst preparation. Another explanation for the extensive reduction in pore volumes of Pd/Si-C-1 and Pd/Si-C-0.5 can be due to the silica products covering the micropores of activated carbon. This is possible with the addition of ethanol which causes dissolution of TEOS and subsequent absorption by the micropores of activated carbon during the preparation of Si-C-1 and Si-C-0.5. Capillary condensation may also contribute to this process, which causes the TEOS to more rapidly go deeper inside the pores. This is in contrast to catalysts Pd/Si-C-4 and Pd/Si-C-2 where ethanol was not used and the silica precursor did not fill the micropores. In the absence of ethanol, TEOS is immiscible with water, and the hydrolysis of TEOS does not occur. In this case, thermal decomposition of TEOS to form amorphous SiO_2 is expected with activation energy of -26 kJ/mol while acetaldehyde, formaldehyde, carbon dioxide, water and carbon monoxide formed as decomposition products [103]. TEOS can be completely adsorbed on activated carbon, but not its decomposition products [104]. The possibility of a complete hydrolysis of $Si(OC_2H_5)_4$ to $Si(OH)_4$ to give silicic acid was also considered for Pd/Si-C-0.5 and Pd/Si-C-1. However, such OH groups were not detected in FTIR analysis.

Table 8. Physicochemical Properties

Catalyst	S_{BET} (m^2/g)	S_m (m^2/g)	V_t (cm^3/g)	V_m (cm^3/g)	ΔV (cm^3/g)	D_{BJH} (nm)
Pd/Si	540	-	0.444	-	-	3.6
Pd/Si-C-4	603	381	0.430	0.206	0.224	5.3
Pd/Si-C-2	637	383	0.466	0.211	0.255	5.4
Pd/Si-C-1	717	308	0.544	0.175	0.369	4.5
Pd/Si-C-0.5	882	335	0.730	0.187	0.543	4.7
Pd/C	1002	363	0.941	0.206	0.735	5.3

S_{BET} : BET surface area (t-Plot)

S_m : Micropore surface area (t-Plot)

V_t : Total pore volume of pores at $P/Po = 0.985$

V_m : Micropore Volume (t-Plot)

ΔV : The difference between total and micro pore volumes (mesopore volume)

D_{BJH} : Pore diameter (BJH desorption average pore diameter (4V/A))

Another characteristics of an activated carbon is the surface oxygen groups which determine the hydrophilic/hydrophobic properties of carbon support and make the surface acidic, basic or neutral [105]. These surface groups play a very important role in the dispersion of the active phase, and thus in catalytic activity [106]. The nature of the surface groups was identified by FTIR (Figure 32). None of the samples showed the 2900–3800 cm^{-1} OH absorption stretching band which is associated with hydroxyl groups. However, the development of the 960 cm^{-1} Si–OH stretching band was observed in Pd/Si-C-4 and Pd/Si-C-2. The formation of the silica-carbon nanocomposites may be followed by the appearance of asymmetric stretching vibrations of Si–

O–Si bonds, while incomplete condensation may be revealed by the presence of Si–OH groups [107]. The dominant peak, located at 1056 cm^{-1} in Pd/Si, is due to the Si-O-Si stretching absorption [108]. Although the frequency of the Si-O-Si stretching band increased in Si-C supported catalysts up to 1085 cm^{-1}, it did not change with the Si content of the catalyst. However, the intensity of the peak at 1056 – 1085 cm^{-1} increased significantly with increased Si content. [90]. A broad band between 1300 and 950 cm^{-1} in the Pd/C spectra has a maximum at 1180 cm^{-1} (C–O stretching in acids, alcohols, phenols, ethers and esters) [109] and a shoulder at 991 cm^{-1}. Absorption in this region is usually found in oxidized carbons [110]. Solum et al. [111] reported the appearance of a band at 1203 cm^{-1} due to the formation of phosphoric acid esters. Due to the overlap of absorption bands from Si-O in this region, an unambiguous assignment is difficult. For Pd/Si-C-0.5, C-O stretching vibration (1215 cm^{-1}) is higher than that for Pd/C (1180 cm^{-1}). Such higher absorption frequency is observed in lactones which can be seen as the condensation product of an alcohol group -OH and a carboxylic acid group –COOH [112]. This absorption is not seen for the Si, Si-C-4 and Si-C-2 supported catalysts. The spectra (except for the Pd/Si) have a band between 1600–1580 cm^{-1} due to C=C aromatic ring stretching vibrations enhanced by polar functional groups. While its intensity decreases with increasing Si amount, a small shift in Pd/Si-C-4 and Pd/Si-C-2 indicates an enlargement of the aromatic ring structure [113]. The intensity of aromatic bands is lower for Pd/Si-C-0.5 and Pd/Si-C-1 catalysts than Pd/C while these bands are not seen in Pd/Si-C-2, Pd/Si-C-4 and Pd/Si. This may suggest that substitution of C–H bonds in the aromatic structure takes place and new C–R bonds form for the latter catalysts. For Pd/C, the absorptions at 1702 cm^{-1} (C=O stretch) and 759 cm^{-1} is due to C-H out of plane bending [109]. The C=O stretch frequency is lower than that of a normal ester which is ~1740 cm^{-1}. This change in the C=O stretch frequency can be due to an unsaturation adjacent to the C-O- or α to the C=O [109]. It

can also explain the reason why its frequency is higher (1729 cm^{-1}) for Pd/Si-C-0.5 that that of

Pd/C. The weak intensity of the C=O stretching vibration (1702 cm^{-1}) of Pd/Si-C-4 and Pd/Si-C-2 suggests that these two catalysts contain a small amount of carboxyl groups compared with

Pd/C, Pd/Si-C-0.5 and Pd/Si-C-1. The main observation is that both Pd/Si-C-0.5 and Pd/Si-C-1

have similar surface groups to the Pd/C. On the other hand, Si, Si-C-4 and Si-C-2 supported

catalysts do not contain these interactions.
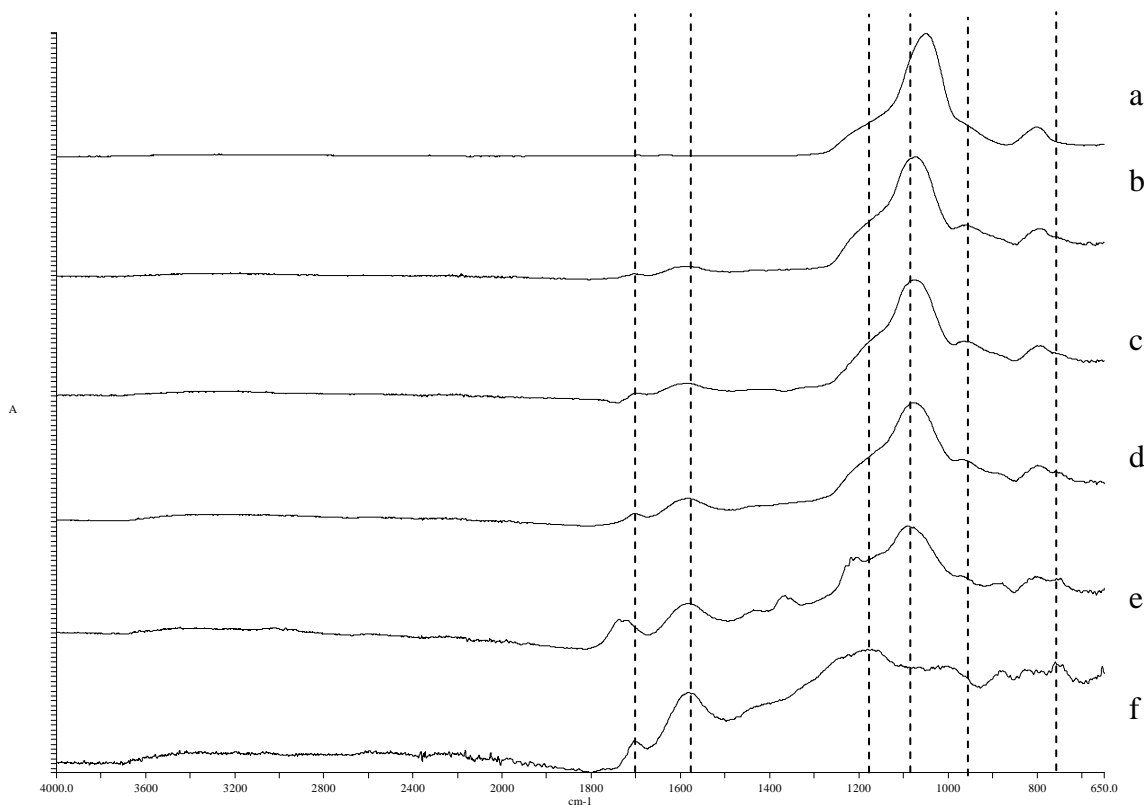
Figure 32. FTIR of fresh palladium catalysts supported on: silica (a), SiC-4 (b), SiC-2 (c), SiC-1 (d), SiC-0.5 (e) and activated carbon (f).

The FTIR spectra of the activated carbon, Si-C-4 and silica supports are shown in Figure

33. The activated carbon support has a broad band between 1000-1300 cm^{-1} which is assigned to

CO bonds such as those exist in ethers, phenols, acids and esters [113,114]. It has another broad band between 1500 and 1750 cm^{-1} that can be assigned to carboxyl groups, quinones, ketones, lactones, diketone and keto-ester, and keto-enol [113,114]. The weak absorptions between 700 and 950 cm^{-1}, assigned to aromatic structures substituted with out-of-plane deformation mode of C–H in variously substituted benzene rings by aliphatic groups [113], appear in the spectra of the AC, but they are absent in Si and Si-C-4 samples. The AC and Si-C-4 supports have 2 bands at 1580 and about 1700 cm^{-1} due to the C=C stretching vibrations in aromatic rings enhanced by polar functional groups [113,114]. However, these absorptions have lower intensity for the Si-C-4. The presence of a band at about 1700 cm^{-1} may be due to the C=O stretching in carboxylic acid groups, esters, lactones and quinones [114]. The AC support spectrum shows a wide absorption band at 3600–3200 cm^{-1} with a maximum at 3404 cm^{-1}. This band can be assigned to the O–H stretching of hydroxyl groups such as alcohols, phenols and adsorbed water [113]. This band is more intense for AC than for Si-C-4 and Si.
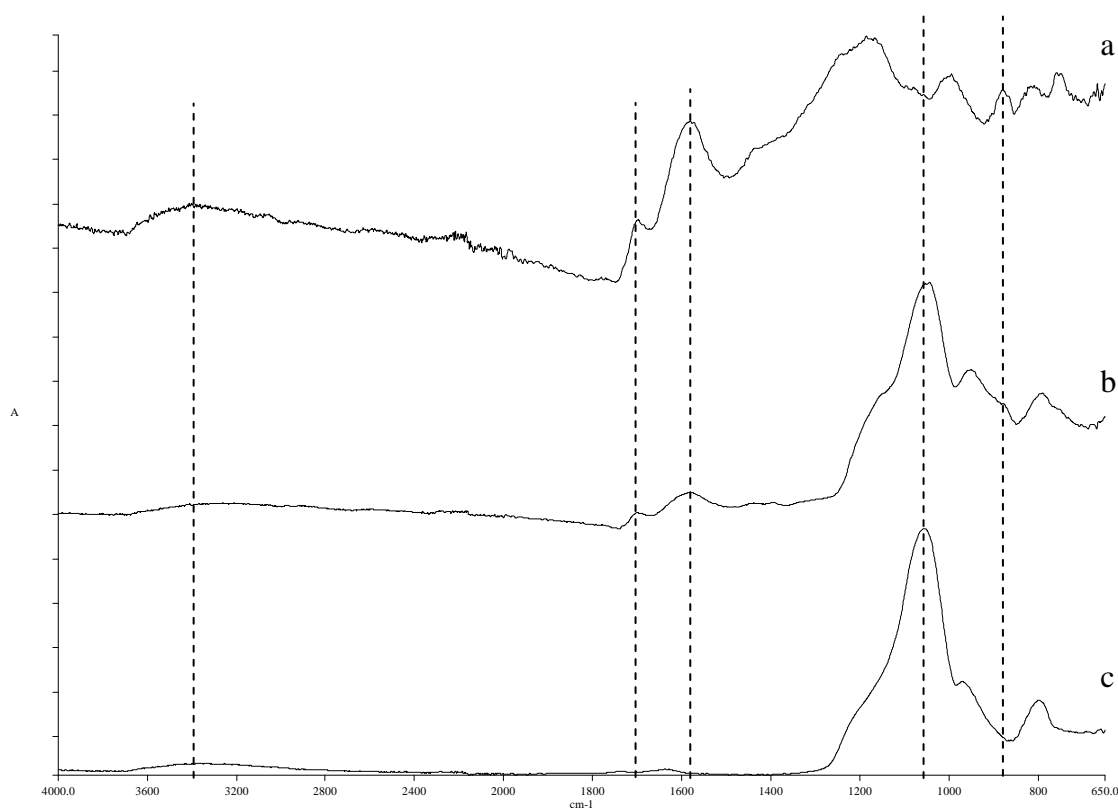
Figure 33. FTIR of supports: activated carbon (a), Si-C-4 (b) and silica (c).

The FTIR spectra for the used catalysts are shown in Figure 34. The absorption bands are similar to the fresh catalyst (Pd/Si-C-4) after reactions but differences are in the relative intensities. The absorption bands at 2867 and 2919 cm^{-1} are observed only in the used catalysts. These peaks can originate from C-H stretching in CH_2 groups [113,114] likely due to the adsorbed reaction products.
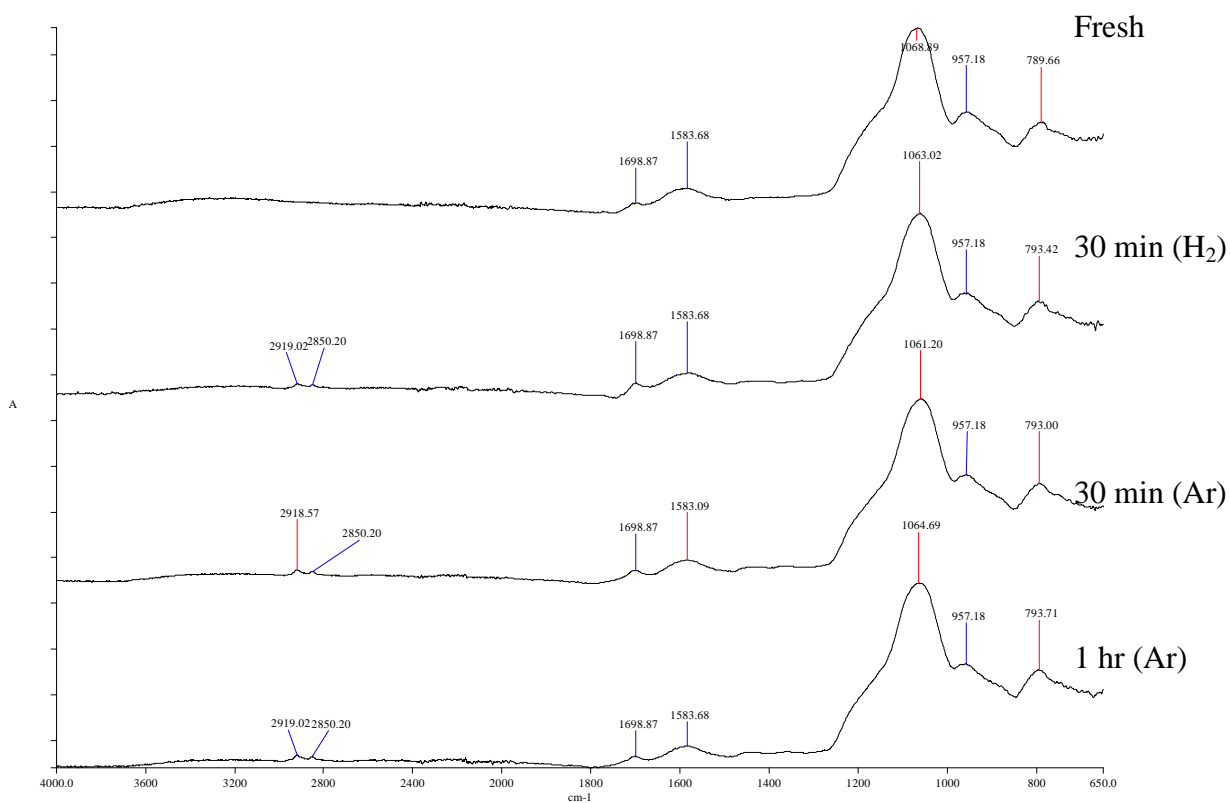
Figure 34. FTIR of the Pd/Si-C-4 catalyst before and after oleic acid batch reaction at 300 °C and 1.5 MPa.

The acid-base titration method gives more information on oxygen surface functionality of the catalysts. According to Boehm [115] the weakly acidic phenolic hydroxyl groups and strongly acidic carboxylic groups are neutralized by NaOH. Therefore, the total acidity is determined by neutralization. The total acid numbers of the catalysts are given in Table 9. The activated carbon supported catalyst shows some acidity which can originate from the surface oxygen groups and also from the storage conditions [94]. When the acidic groups exist on the carbon surface, it becomes more accessible for aqueous metal precursors due to the decrease in the hydrophobicity of the carbon [105]. The Pd/Si catalyst shows the greatest oxygen group content, with a

predominant presence of stronger acidic groups. The Pd/Si-C-0.5 catalyst displayed the lowest total acidity.

Table 9. Acidity of supported 5% palladium catalysts

Catalyst	Acidity (mmol/g_{cat})
Pd/Si	2.36
Pd/Si-C-4	0.34
Pd/Si-C-2	0.33
Pd/Si-C-1	1.53
Pd/Si-C-0.5	0.12
Pd/C	1.65

3.6.2 Relationship between catalyst support, physiochemical properties, acidity and catalytic activity

The silica modification of the activated carbon surface produced significant changes in carbon porous texture and the surface chemistry; thus it can have dramatic effects on the catalytic activity. The analysis of the surface functionality by FTIR shows that the novel Pd/Si-C-4 catalyst has fewer surface interactions than the Pd/C catalyst, which makes it a more inert support.

Table 10 shows the correlation between Pd particle size and the catalytic properties for oleic acid decarboxylation. Both Pd/Si-C-4 and Pd/C showed high conversion of oleic acid while Pd/Si-C-4 exhibited the highest selectivity (31%) to n-heptadecane (n-C17). A high conversion of oleic acid was also observed for the Pd/Si-C-4 catalyst. However, the ability of

Pd/Si in activating oleic acid to give a significant selectivity of the desired hydrocarbon products was inconsiderable (Table 10). According to the TEM, XRD and FTIR the catalysts Pd/Si-C-1 and Pd/Si-C-0.5 have s similar morphology, particle size and surface groups. These catalysts exhibit similar catalytic activity for the decarboxylation of oleic acid, which indicates that the particle size of Pd can influence the catalytic activity. The high activity of Pd/Si-C-4 catalyst can be attributed to accessible, small and well-distributed metallic Pd nanoparticles inside hybrid mesopores. In addition, having low acidity and less surface interaction on Pd/Si-C-4 catalyst rendered it more inert and led to higher catalytic activity.

Table 10. Correlation between Pd particle size and catalytic properties in oleic acid decarboxylation. Batch reaction for 1 hr.

5%Pd Catalyst	d_{Pd} (nm)	C18:1 Conversion (%)	Selectivity (%)						
			C18:0	C18:2	n-C17	Unsaturated C17	n-C18	Unsaturated C18	Others*
Si	6.7	15	<0.05	<0.05	0.0	1.0	0.0	0.0	99
Si-C-4	5.5	87	<0.05	5.6	31.0	53.5	2.2	7.7	<1
Si-C-2	5.9	74	15.0	5.4	13.4	56.7	1.9	7.7	<1
Si-C-1	6.3	42	3.5	19.8	11.6	35.6	0.9	3.5	25.1
Si-C-0.5	6.2	45	2.1	22.5	12.6	32.7	1.3	3.8	25
C	4.1	94	<0.05	1.8	19.2	71.7	1.6	5.7	0

d_{Pd}: Pd metal particle size (XRD)

3.6.3 Decarboxylation Activity of Pd/Si-C-4 in the absence of H_2

The dependence of the reactant conversion and product selectivity as a function of reaction time at 15 bar and 300 ^{o}C over 5% Pd metal supported on Si-C-4 are displayed in Figure 35. At the beginning of the reaction, unsaturated C-17 selectivity was almost 100%. When conversion reaches about 80%, unsaturated C-17 selectivity decreased and saturated n-C17 selectivity increased. This indicates that the C=C double bond hydrogenation is taking place after decarboxylation of oleic acid under the reaction conditions. Unlike Pd/C, which was reported to catalyze the oleic acid C=C bond via hydrogenation prior to decarboxylation of the resultant saturated FFA (stearic acid)[69], Pd/Si-C-4 catalyst follows a different reaction route. This hybrid Si-C supported Pd catalyst favors a direct decarboxylation of oleic acid instead of C=C double bond hydrogenation. By eliminating the hydrogenation of oleic acid, the reaction steps are reduced. The selectivity to stearic acid was less than 0.05 wt% even after 1 hour reaction over Pd/Si-C-4 (Table 10) while Pd/C is reported to have 60% selectivity to stearic acid at 74 % conversion of oleic acid.[69] The existence of 8 and 1- heptadecenes was also identified with GC-MS. The formation of 8-heptedecene suggests the direct decarboxylation of oleic acid while formation of 1-heptedecene indicates the dehydrogenation of n-heptadecane and decarbonylation of oleic acid.
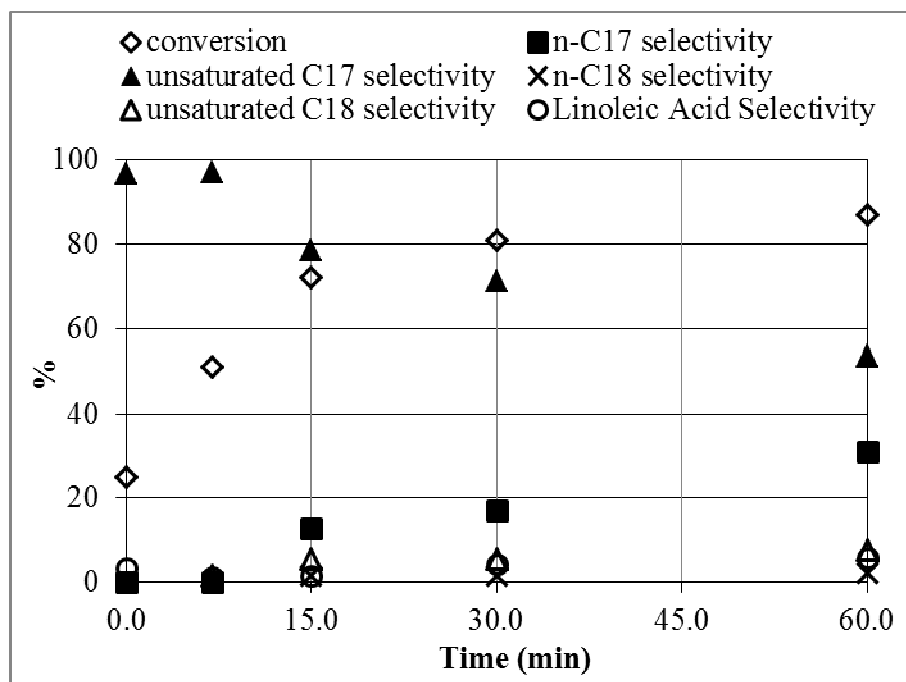
Figure 35. Oleic acid conversion and product selectivity in batch reaction at 300 $^{\circ}$C, 1.5 MPa on Pd/Si-C-4 catalyst.

3.6.4 Stability of Catalyst

The stability of the Pd/Si-C-4 catalyst was investigated in a continuous flow reactor. The oleic acid conversion over 16 days of operation is shown in Figure 36. Although there is a slight decrease in conversion after 3 days of reaction, the addition of 10% H_2 to the gas stream restored the conversion back to 100%. While the catalyst is stable for conversion of oleic acid for 16 days over Pd/Si-C-4 catalyst, there is a dramatic decrease in diesel hydrocarbon (HC) selectivity after 3 days of reaction (Figure 37). After introducing 10% H_2 in the gas stream for 4 days, diesel HC selectivity increased to 55%. This selectivity was maintained in the absence of H_2. However, switching the gas flow back to 10% H_2-90% Ar resulted in a decrease in diesel selectivity. Figure 38 shows the impact of removing the H_2 from input on the selectivity of decarboxylation

products (n-C17 and unsaturated C17 isomers). It is clearly seen that switching back to an Ar gas stream yields double the n-C17 selectivity. Murzin's group indicated that the presence of H_2 in small quantities in the liquid phase helps to preserve the activity of the Pd/C catalyst. However, the silica modified AC supported Pd catalyst stability study showed that the addition of 10% H_2 does not necessarily favor the formation of decarboxylation products, but an H_2 treatment helped to regenerate the decarboxylation sites of the catalyst. Therefore, a regeneration step to clean the adsorbed reactants from the active metal surface can be suggested instead of a continuous H_2 feed into the system. Ziemecki observed the decomposition of the bulk PdC_x phase of Pd/C at 150 ^{o}C in H_2 [116] and this decomposition was observed at 427 ^{o}C in an inert atmosphere by others [117]. Such regeneration can help if the interstitial C in the Pd crystallites forms during the reaction. However, the XRD study of used Pd/Si-C-4 catalyst revealed that there is no lattice expansion after reaction which would indicate the presence of a PdC_x phase. A detailed study is necessary to understand the function of H_2 to prevent the fast deactivation of supported Pd catalyst.
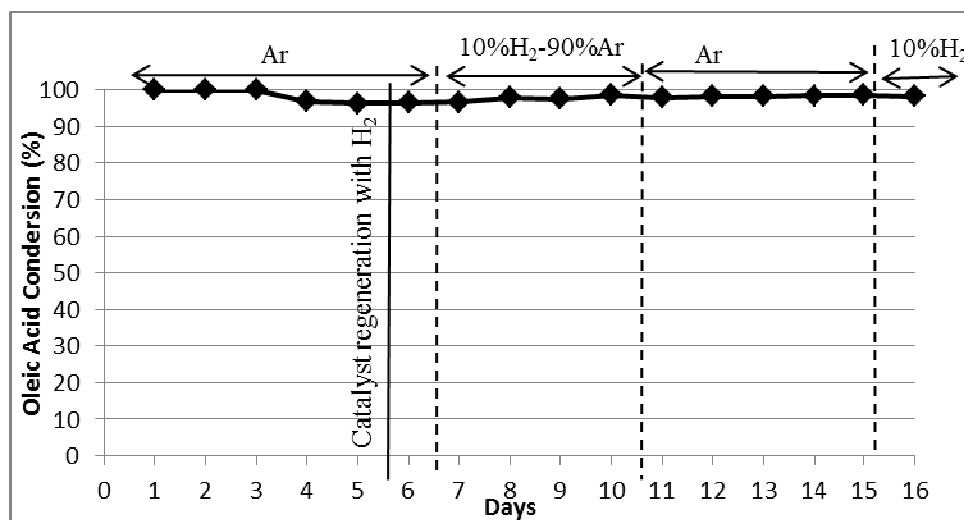
Figure 36. Oleic acid conversion in flow reaction at 300 ^{o}C, 1.5 MPa on Pd/Si-C-4 catalyst with LHSV 1 hr^{-1}
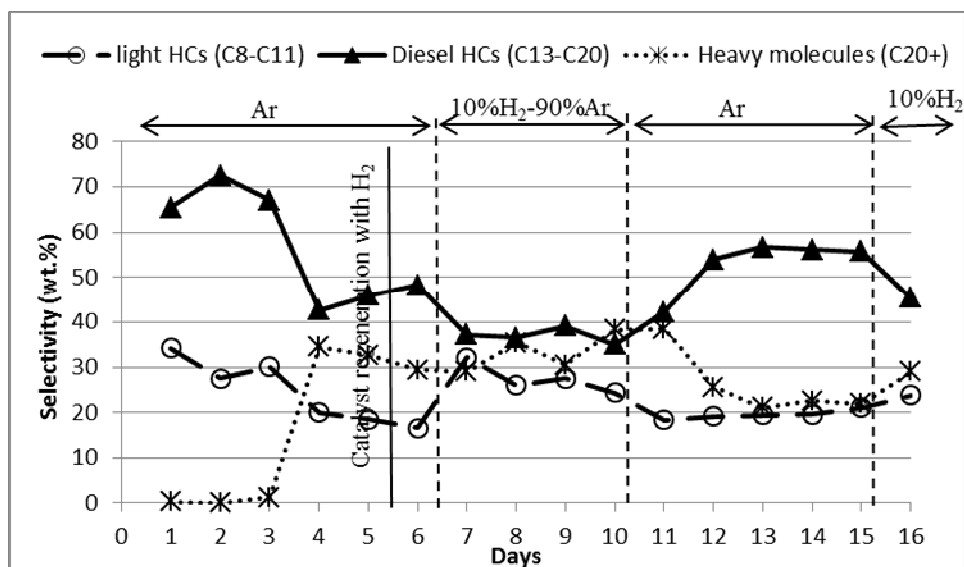
Figure 37. Product selectivity in flow reaction of oleic acid at 300 ^{o}C, 1.5 MPa on Pd/Si-C-4 catalystwith LHSV 1 hr^{-1}
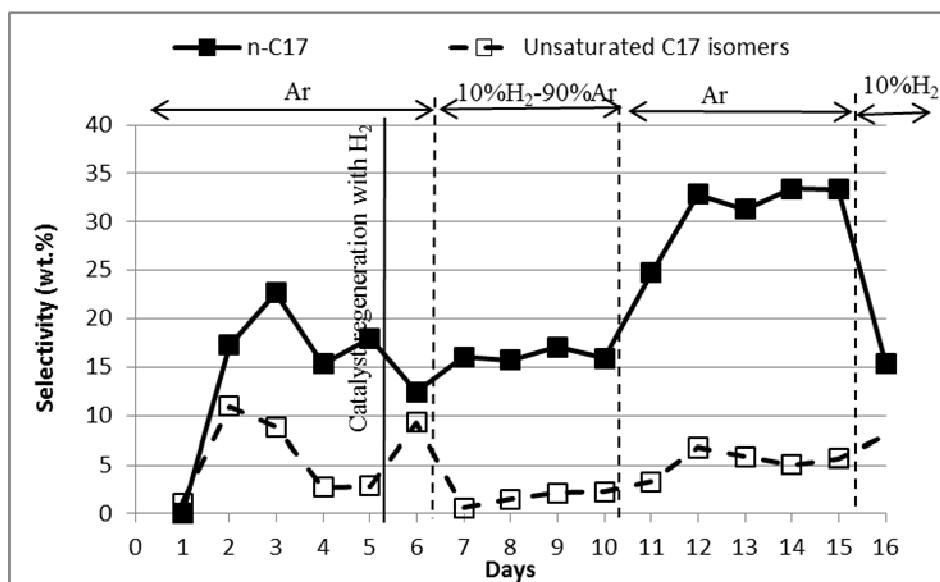
Figure 38. n-C17 (saturated) and unsaturated C17 isomers selectivity in flow reaction of oleic acid 300 ^{o}C, 1.5 MPa on Pd/Si-C-4 catalyst with LHSV 1 hr^{-1}

The Pd/Si-C-4 catalyst maintained the highest reported conversion up to 16 days on stream towards selective decarboxylation of FFA on a supported Pd catalyst under similar reaction conditions without assistance of H_2 input. For example, Pd/C (Sibunit) catalyst showed stable activity only up to 45 h by maintaining 15% conversion of concentrated stearic acid at 360 °C under 1 MPa 5 vol % H_2 in argon while a commercial Pd/C catalyst maintained its stability up to 92 h at 40% conversion [87]. A mesoporous 1% Pd/C (egg-shell) catalyst was deactivating slowly and was rather stable at around 10% conversion up to 5 days at a 0.5 mol/L saturated FFA feed with WHSV 1.7 h^{-1} [86].

3.7. Conclusions

A novel process was proposed for nanocomposite silica-carbon supported catalyst synthesis in which precursors of the raw materials are mixed with activated carbon powder. The characteristic of this technique is to employ a low-temperature procedure which saves energy and time in the catalyst preparation.

The decarboxylation activities of different amount of silica containing catalysts were investigated in a batch reactor under inert gas. Among them, the formulation with the fewer oxygen surface groups (less carboxyl group, C=O) (Pd/Si-C-4) was the most active catalyst for the decarboxylation of an unsaturated FFA in the absence of H_2. The high activity of the Pd/Si-C-4 catalyst is attributed to its accessible and well-distributed metallic Pd nanoparticles inside hybrid mesopores as well as to its low acidity, weak surface interactions and inertness. The novel catalyst was capable of catalyzing a decarboxylation reaction from an unsaturated FFA in the absence of H_2, and was highly stable for oleic acid conversion selectively for green diesel production. Thus, Pd supported on carbon modified with silica may be regarded as a prospective

decarboxylation catalyst for the removal of oxygen from vegetable oil/animal fat without the need of additional H_2.

CHAPTER 4

Diesel Production from Hydrothermal Catalytic Decarboxylation of Oleic Acid in Super-Critical Water and Effect of Pd-Co Alloy on the Catalytic Activity and Diesel Yield

A variety of catalysts and supports were studied for decarboxylation of oleic acid to produce diesel range hydrocarbons in super-critical water. NaOH and $Ca(OH)_2$ alkali metal salts tend to form complexes with oleic acid and hinder the oleic acid decarboxylation. Although $NiMo/Al_2O_3$ metal oxide catalyst showed significant initial decarboxylation activity, change of structure in water presents a challenge in the hydrothermal conversion processes. A Si-C support seems to be more effective than activated carbon itself for both decarboxylation of oleic acid and hydrogenation of alkenes in super-critical water. A systematic study of Pd loading on Si-C support showed that higher Pd loading leads to higher conversion, however, the lowest oxygenated products and highest diesel hydrocarbons yields were obtained on 3% Pd/Si-C. In order to reduce the amount of Pd in the catalyst, Pd_2Co/C catalysts with various Pd content were prepared and the catalytic activity study showed that 0.5 wt% Pd_2Co/C catalyst performs better than a 7 wt% Pd/C catalyst. Pd and Co metals were very well dispersed and formed fine clusters, which led to a higher active metal surface area and hence favored the decarboxylation of oleic acid. The reduction temperature was found to be an important factor to control metal particle size.

4.1. Introduction

Increases in petroleum prices, projected increases in the world's energy demand and environmental awareness have shifted research efforts to explore alternative fuel technologies. In particular, green diesel which displays similar properties as petroleum diesel and can be used as a drop-in fuel, has drawn great attention.[118] This second generation liquid biofuel can be obtained

from triglycerides and fatty acid containing feedstocks such as vegetable oil, animal fat and waste oil/grease. However, converting waste oil/grease, particularly brown grease which possesses 50-100% fatty acid content, into biofuels is more advantageous because it is a waste, inexpensive and non- food competing feedstock. In the U.S. alone, 3800 million pounds of brown grease is generated every year.[119]

There has been considerable attention on the production of green diesel from vegetable oil and fat.[120-124] Most early studies focused on deoxygenation (selectively decarboxylation) of fatty acids in dodecane solvent over Pd-supported catalysts. [66,67,69,125,126] These studies demonstrated milder reaction conditions and elimination of hydrogen consumption can be possible compared with the current commercial process (hydrotreating) (Eq I-III). However, these supported palladium catalysts readily deactivate due to the formation of unsaturated heptadecene product leading to catalyst coking,[67,125] the high unsaturation level of the fatty acids,[64] lack of H_2 in the reaction atmosphere,[127,128] decrease in the BET specific surface area,[66] loss in porosity and accessible palladium surface area.[83,129]
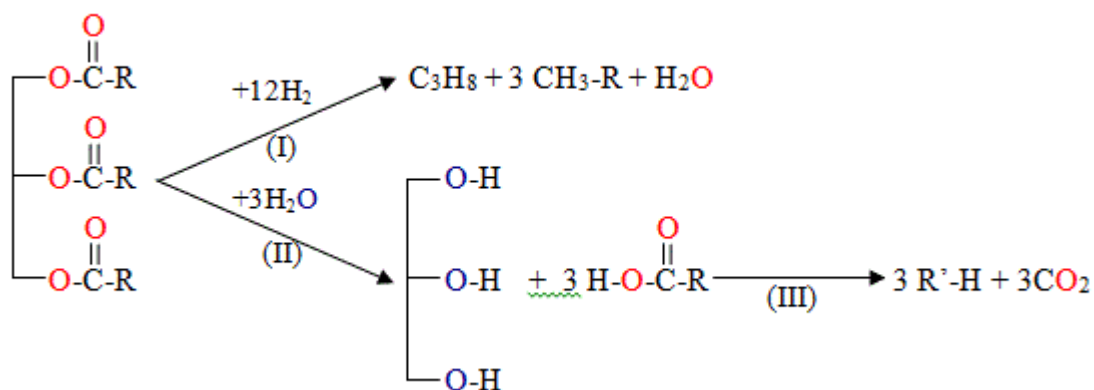
(I). Hydrotreating = Hydrocracking of triglycerides + Hydrodeoxygenation
(II). Hydrolysis of triglycerides
(III). Decarboxylation of fatty acids

Recently, studies of fatty acid deoxygenation have been conducted in aqueous media under sub- and super-critical water conditions. The advantage of water as the reaction media is not only the use of an environmentally benign solvent in the process but also the avoidance of a water removal step after biomass conversion or triglyceride hydrolysis that generates fatty acids in an aqueous stream.[130,131] It was shown that both Pd/C and Pt/C catalysts are active for a saturated fatty acid (palmitic acid) decarboxylation with 76 % molar yield to pentadecane in subcritical water at 370 °C.[132] However, Pt metal dispersion exhibited a significant reduction (from 38.9% to 0.8%) after the reaction. Fu et al. showed that activated carbon itself can catalyze both saturated and unsaturated fatty acids to produce hydrocarbons in sub- and super-critical water as an alternative to the expensive noble metal catalyst.[133] However, the major product from oleic acid conversion was stearic acid with 24% molar yield while the decarboxylation product yield was only 6% after 3 hours reaction at 370 °C.

It was also shown that Pd/C catalyst behaves differently in sub-critical water[132] than in organic solvent[38] for fatty acid decarboxylation.

A decarboxylation study of acetic acid, one of the simplest carboxylic acid, conducted on ZrO_2 in super-critical water at 400 °C, showed that ZrO_2 is an active catalyst for CO_2 removal from acetic acid, however, it selectively produces acetone (ketone).[134] Moreover, a structure change of the zirconia catalyst was observed during acetic acid conversion in super-critical water. The conversion of stearic acid in the presence of oxide catalysts (CeO_2, Y_2O_3 and ZrO_2) was reported as 30%, 62% and 68%, respectively in super-critical water at 400 °C in 30 minutes.[135] Similar to the acetic acid hydrothermal reaction, stearic acid reaction produced ketone ($C_{17}H_{35}OCH_3$) in addition to hydrocarbons. Again, a structure change of the oxide catalysts after the reaction was reported. Structure change of another oxide catalyst was also

observed in a solvent free oleic acid decarboxylation reaction by Na et al.[136] Na and his co-workers investigated the decarboxylation activity of hydrotalcites catalysts with various MgO/Al_2O_3 ratios in a solvent free atmosphere. It was reported that a MgO loading of more than 63% and reaction temperature of 350 °C is needed to obtain deoxygenated hydrocarbon products selectively and with oleic acid conversion more than 98% in 3 hours. More importantly, there was no significant change of the MgO structure in the hydrotalcite catalyst. Although percentage peak areas of GC-MS for the major liquid products and the oxygen content of the products are given, the hydrocarbon yields are not reported in their study.

Stearic acid thermal decomposition was observed by Watanabe et al.[135] with 50% conversion at 400 °C under Ar atmosphere in 30 minutes while its hydrothermal conversion was 2% in super-critical water under the same reaction conditions. Stearic acid conversion was enhanced by adding NaOH or KOH in super-critical water, but the hydrocarbons yield was not reported.

Fu et al.[137] investigated the effect of degree of fatty acid unsaturation on the decarboxylation over Pt/C catalyst in sub-critical water at 330 °C. It was reported that unsaturated fatty acids possess much lower heptadecane yield and selectivity than saturated fatty acids (molar yield of more than 80 % to heptadecane from stearic acid vs. less than 20% from oleic acid) in 2.5 hours reaction. Because Pt/C catalyst was found to be more active and selective for decarboxylation of palmitic (a saturated) acid compared to Pd/C in sub-critical water,[132] oleic acid decarboxylation over Pt/C catalyst was investigated.[137] However, saturated and unsaturated fatty acids behave differently under hydrothermal reaction conditions. Since our ultimate goal is conversion of waste oil/grease which mainly contains unsaturated fatty acids, we investigated oleic acid (the major component of waste oil) conversion on Pd metal supported catalyst.

In order to design a suitable catalyst for conversion of brown grease to green diesel, a systematic study of the model compounds is necessary to understand the reaction pathways in super-critical water. Therefore, the decarboxylation reaction of oleic acid was investigated on various catalysts in super-critical water with the aim of producing hydrocarbons in the diesel range in the absence of H_2 and to improve the catalytic decarboxylation activity and selectivity of the carbon supported catalyst.

4.2. Experimental

4.2.1 Materials

The following chemicals were used in this investigation: NaOH, $Ca(OH)_2$, MgO, γ-Al_2O_3, $NiMo/Al_2O_3$ (Haldor Topsoe), activated carbon (Charcoal Norit, Sigma-Aldrich), palladium(II) chloride ($PdCl_2$, ≥99.9%, Sigma–Aldrich), cobalt, ethylene glycol, oleic acid (technical grade 90%, Sigma-Aldrich, St. Louis, MO), ultra high purity grade hydrogen (H_2) and nitrogen (N_2) were purchased from Cryogenic Gases (Detroit, MI).

4.2.2. Catalyst preparation

For Pd/Si-C catalyst preparation, activated carbon (C) was immersed in liquid tetraethyl orthosilicate (TEOS) with a mass ratio of 2.86 TEOS to C. The mixture was stirred vigorously for 2 hours at 120 ^{o}C. Then, it was dried at 105 ^{o}C for 18 hours. In order to obtain 1, 3, 5 and 7 wt% Pd on the support 0.2, 0.6, 1.1 and 1.6 wt% $PdCl_2$ solution was mixed with 20 g support at room temperature for 24 hours, respectively. After the catalyst was dried at 100 ^{o}C for 5 hours, the reduction was carried out under a flow of 10 vol% H_2-90 vol% N_2 at 200 ^{o}C for 3 hours.

Pd_2Co/C catalysts with 0.5, 1, 3 and 5 wt% Pd were prepared by modifying the preparation technique described by Zhang et al.[138] Activated carbon was suspended in deionized (DI) water with a mass ratio of 40/1 C to DI water prior to mixing with 1.1 wt% $PdCl_2$ and 0.01

M $CoCl_2$ solutions. A 0.04 M NaOH solution was added until the pH of the mixture reaches to 11. As a mild reducing agent, ethylene glycol was added to the mixture with an excess molar ratio of ethylene glycol to metal. The mixture was stirred at 80 °C followed by stirring at room temperature for 12 hours. After drying at 100 °C, catalysts were washed multiple times with DI water. Then, they were dried at 80 °C for 10 hours. Two different temperatures (200 °C and 300 °C) for heat treatment were conducted in a tube furnace under 120 mL/min gas flow of 10 vol% H_2 balanced with N_2 for 3 hours.

4.2.3. Material characterization

Powder X-ray diffraction (XRD) patterns were obtained on SmartLab Guidance and MDI Jade 8 by a Rigaku RU2000 (Rigaku Americas Corporation, TX) at a scan rate of 3°/min and a step size of 0.02° (40 kV, 44 mA). The Scherrer equation and Bragg's law were used to calculate the mean metal particle size, the lattice parameter and bond distance.

Scanning electron microscopy (SEM) was conducted using an FE-SEM microscope operating at 15.0 kV and X-ray Energy-Dispersive Spectrometer (EDS) were used for elemental spectra and mapping.

4.2.4. Reaction procedure

The catalytic hydrothermal conversion of oleic acid was investigated in 1.52 mL stainless steel batch reactors assembled from 3/8-in. Swagelok port connectors.[133] For the activity test of each catalyst, 10 mg catalyst, 0.156 mmol oleic acid and 0.642 mL water were loaded in the reactors and the reactors were sealed in a glove box. Reactors were placed in a pre-heated furnace set at 400 °C. Time required to reach isothermal conditions was 30 minutes for each reactor. After the reaction, the reactors were quenched in a water bath and the liquid product was analyzed.

4.2.5 Analysis Method

In order to identify the products, a GC-MS (Clarus 500 GC-MS, Perkin-Elmer) with a capillary wax Rtx-WAX column (length: 60 m, diameter: 0.25 mm, thickness of stationary phase 0.25 μm) was used. In order to quantify the liquid products, the product was diluted to 5 mL with heptane and the organic phase was analyzed using a Perkin Elmer Clarus 500 gas chromatograph (GC) equipped with a flame ionization detector (FID) and an Rtx-65 TG column (length: 30 m, internal diameter: 0.25 mm, phase film thickness: 0.10 μm). For fatty acids separation, the GC oven temperature was programmed as follows: 2 min hold at 80 ^{o}C, 10 ^{o}C/min ramp to 200 ^{o}C, 5 min hold at 200 ^{o}C, 10 ^{o}C/min ramp to 260 ^{o}C, 3 min hold at 260 ^{o}C. The detector temperature was maintained at 370 ^{o}C. Samples (1 μL) were injected into the column with a 10:1 split ratio. For hydrocarbons analysis, the GC oven temperature was programmed as follows: 2 min hold at 40 ^{o}C, 10 ^{o}C/min ramp to 300 ^{o}C, 5 min hold at 300 ^{o}C. . The injector and detector temperatures were 250 ^{o}C and 300 ^{o}C, respectively, and the split ratio was 5:1. Concentrations were determined by external standard method. The molar yield was calculated from the following formula:

$Molar\ Yield$ (%)= ($No.\ of\ moles\ of\ product$) / ($Initial\ no.\ of\ moles\ of$ oleic acid) x 100

4.3. Results and discussion

4.3.1 Effect of Absence of Catalyst in Supercritical Water on Oleic Acid Conversion

In order to understand the effect of catalyst on the oleic acid conversion, the hydrothermal reaction of oleic acid in super-critical water was conducted both in the absence and presence of the catalyst. As shown in Table 11, without the catalyst, oleic acid conversion was only 4% at 5 hour. Decomposition products were mainly heavy molecules (C>25) and n-alkane

molar yield was 14.7%. Watanabe et al. [134] also showed that acetic acid (CH_3COOH) and stearic acid ($C_{17}H_{35}COOH$)[135] are stabilized in supercritical water (negligible conversion).

Table 11. Oleic acid 5 hours reaction

Catalyst	Conversion	Molar Yield (%)					OLP Yield (wt%)
		n-alkanes (C10-C18)	alkenes (C17-C18)	C17 aromatics	C8-C13 aromatics	Oxygenated products	
-	4	14.7	0	0	0	96.5	108
NaOH	85	6.6	11.4	5.7	0.1	38.0	53
$Ca(OH)_2$	92	6.8	6.6	0	2.7	52.5	54
MgO	97	4.8	8.0	2.8	5.4	10.4	19
γ-Al_2O_3-NaOH	93	2.8	11.6	5.9	0.5	6.3	11
$NiMo/Al_2O_3$	81	30.7	41.4	0.2	0	23.0	86
NiWC/Al-SBA-15	76	21.2	24.1	0	0.5	31.6	92
Activated Carbon	90	33.3	16.3	6.2	7.9	17.1	65
Pd/C	99	36.6	15.4	6.7	5.2	0.44	49

4.3.2 Effect of Anion/Salt on Oleic Acid Conversion

Belsky et al. showed that the decarboxylation of acetic acid derivatives in sub-critical water was enhanced by adding NaOH.[139] It is believed that the sodium salts of these acids which form anionic carboxylic acids in water are more reactive than the corresponding non-ionic carboxylic acids. In this study, the effect of oleic acid anion in super-critical water on the product yield and selectivity was investigated by using a strong and a medium strength base, NaOH and $Ca(OH)_2$, respectively. It is seen in Table 11 that oleic acid is not stable when NaOH and $Ca(OH)_2$ were added in the super-critical water. Although deoxygenated hydrocarbons yield is higher in NaOH containing super-critical water than in that of $Ca(OH)_2$, in both cases the organic

liquid product (OLP) yield is about 50%. Although GC-FID analysis showed 85% oleic acid conversion in NaOH and 92% in $Ca(OH)_2$, after separating the organic and aqueous phases, white solid formation was observed. Observation of these solid materials suggested that the remaining portion of oleic acid might form complexes with NaOH and $Ca(OH)_2$. This may explain why the OLP yield is very low. When $Ca(OH)_2$ was used, no heavy molecule (>C25) formation was observed and the main products were shorter chain fatty acids such as C10, C11, C13, C14, C15, C16 and C17 fatty acids. This suggests that for $Ca(OH)_2$ there is a high selectivity towards hydrocracking with minimal decarboxylation activity.

4.3.3 Effect of Oxide Support on Oleic Acid Conversion

With MgO catalyst, no shorter chain fatty acids were formed, but solid product formation was observed just like in the reactions with NaOH and $Ca(OH)_2$ catalysts. The solid was clearly phase separated at the interface of water and organic phase while some MgO settled on the bottom of the tube. Also the OLP yield for this experiment was only 19%. This suggests that a significant amount of products that are not soluble in heptanes were generated during the reaction, and were not included in GC-FID analysis. Moreover, GC-FID analysis revealed 97% oleic acid conversion while the n-alkanes molar yield was only 4.8%. This result supports the claim that oleic acid and MgO undergo saponification reaction as shown in Eq. (IV).[136] Although Na et al.[136] claimed that the saponification of MgO and fatty acid can be inhibited if the reaction temperature is above 350 °C, in our study the MgO and oleic acid saponification was observed at 400 °C. One possible reason that they do not observe MgO-fatty acid complex at 400 °C might be attributed to water free environment on hydrotalcite ($MgO-Al_2O_3$) catalyst. On the other hand, the hydration of MgO in the presence of water is well-known,[140,141] and the formation of

$Mg(OH)_2$ may explain why the oleic acid hydrothermal conversion results were similar to those of other hydroxide salts (NaOH and $Ca(OH)_2$) used in this study (Eq. V).

$$2R\text{-}COOH + MgO \longrightarrow Mg(OOC\text{-}R)_2 + H_2O \qquad\qquad (IV)$$

$$MgO + H_2O \longleftrightarrow Mg(OH)_2 \qquad\qquad (V)$$
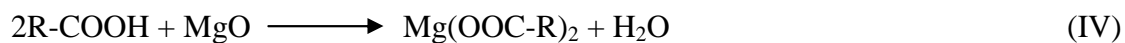
It is known that few transition metals react with sodium hydroxide and generate H_2.[142] Using NaOH:γ-Al_2O_3 (1.5:1 molar ratio) as catalyst for the hydrothermal conversion of oleic acid in super-critical water, NaOH is available to react with the surface hydroxyl groups to form Al-O-Na. In this step, H_2 necessary to saturate C=C double bonds of oleic acid can be generated according to the Eq. VI while alumina can act as a deoxygenation catalyst. Due to the presence of alumina, NaOH is not expected to take part in the oleic acid reaction but only attack to alumina.[143] However, product selectivity (Table 1) showed even lower n-alkane yield (2.8%) than the reaction with NaOH alone in super-critical water. Also, the OLP yield was only 11%, indicating that water-soluble products, which was phase separated from the organic phase that was injected to GC, formed during this reaction. Having observed a white color water phase after the reaction is a hint of alcohol formation. It is possible that the Al-O-Na structure can catalyze deoxygenation of oleic acid as well as alcohol formation. Thus, the deoxygenation active sites of aluminum oxide catalyst may be deactivated by doping with NaOH.

$$2\,Al + 2\,NaOH + 2\,H_2O \rightarrow 2\,NaAlO_2 + 3\,H_2 \qquad\qquad (VI)$$
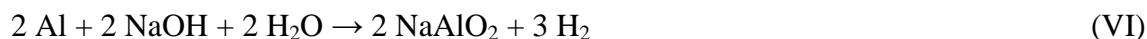
A conventional hydrotreating catalyst, Ni-Mo/Al$_2$O$_3$, was also tested for oleic acid decarboxylation activity in super-critical water. Although the oleic acid conversion (Table 1) was lower compared to the reactions with hydroxide salts, MgO and Al$_2$O$_3$-NaOH, both n-alkane and alkenes yields were greatly improved. While high yield to C17-C18 alkenes (41.4%) shows that Ni-Mo/Al$_2$O$_3$ catalyst has active sites responsible for deoxygenation of fatty acid, high yield of n-alkanes (30.7%) and formation of stearic acid indicate that the catalyst also possesses a C=C double bond hydrogenation function. In addition, the OLP yield was 86% in this experiment. Considering the oxygen removal in the gas phase, the organic liquid yield must be about 85 wt% for 100% conversion, which shows that the OLP yield from this experiment was consistent with the theoretical value. The 5-hour hydrothermal reaction of oleic acid in the presence of Ni-Mo/Al$_2$O$_3$ catalyst showed that this conventional and inexpensive catalyst can be considered as an option to produce green diesel without H$_2$ addition. However, one should consider the stability of Ni-Mo/Al$_2$O$_3$ catalyst in super-critical water and should alter the catalyst to avoid the undesirable structure change of the support from γ-Al$_2$O$_3$ to boehmite (γ-AlO(OH)).[144]

4.3.4 Effect of Carbide Catalyst on Oleic Acid Conversion

When NiWC/Al-SBA-15 catalyst was used, both deoxygenation and hydrogenation activities, similar to Ni-Mo/Al$_2$O$_3$were observed (Table 11). Moreover, formation of C9 fatty acid (molar yield of 3.3%) showed that the carbide catalyst has some cracking activity. However, the conversion and hydrocarbon yield were significantly lower than those obtained with Ni-Mo/γ-Al$_2$O$_3$ catalyst. Although, Al-SBA-15 supported catalyst exhibited a lower fatty acid conversion and a lower yield to deoxygenated products, it is believed to possess a higher hydrothermal stability than the conventional hydrotreating catalyst supports.[145] Therefore, Al-

SBA-15 can be considered as a promising stable support in super-critical water as an alternative to γ-Al$_2$O$_3$ supported catalyst.

4.3.5 Activated Carbon Support

When activated carbon was used in the oleic acid hydrothermal conversion, the yield to n-alkenes was lower but the yield to n-alkanes was higher compared to carbide and oxide catalysts (Table 11). This shows that activated carbon has a higher activity for C=C double bond hydrogenation in addition to a higher activity for fatty acid deoxygenation (oxygenated product molar yield of 17.1%) than those obtained with carbide and oxide catalysts. On the other hand, a lower mass balance (65%) was observed when activated carbon was used. Fu et al.[137] also reported a low mass balance (75%) for unsaturated fatty acids hydrothermal conversion on an activated carbon supported catalyst, and the low mass balance was attributed to the possible formation of high molecular weight compounds that can-not be detected from GC analysis.[69,135]

4.3.6 Palladium on Activated Carbon Support

When activated carbon supported palladium catalyst was used, the oleic acid conversion was already 99% after 1 hour (Table 11). Although the deoxygenation activity was very high (oxygenated product molar yield of 0.44) on Pd/C catalyst, the OLP yield was only 49%.

4.3.7 Si-C Support and Effect of Pd Loading on Oleic Acid Conversion

Table 12 shows the results from 5 hours oleic acid reactions in super-critical water over Si-C supported palladium with various metal loadings. Compared to the activated carbon discussed in the previous section, Si-C support showed higher yield to oleic acid deoxygenation products (37.8% yield to alkenes) in addition to higher hydrogenation activity (42.4% yield to n-alkanes). No aromatics between C8-C13 formed with Si-C support. Table 13 represents the 1 hour data for the same set of catalyst. At 65 % conversion, having alkene yields higher than the

n-alkane yields for 0 and 1% Pd/Si-C indicates the direct decarboxylation of oleic acid. Possibly these alkenes are further hydrogenated to n-alkanes and cracked to obtain n-alkanes in the C10-C18 range. However, the same conclusion cannot be drawn for 3, 5 and 7% Pd/Si-C catalysts because the oleic acid conversion on these catalysts was already more than 80% after 1 hour reaction. It is seen that the n-alkane, alkene and C17 aromatics yields increased as conversion increased for 0, 1 and 7 % Pd loaded catalysts as the reaction proceeds from 1 to 5 hours. On the other hand, 3 and 5% Pd/Si-C catalysts follow a different route. Although oxygenated products yield significantly decreased between 1 and 5 hours, n-alkene yields decreased for 3 and 5% Pd/Si-C catalysts. For these two catalysts, C8-C13 aromatics formation and the alkenes yield decrease while deoxygenation increases at 5 hours, which indicates that the alkenes are further reacted to form shorter chain aromatics. These two catalysts clearly promoted the aromatization reaction. Yin et al.[146] also reported that 5% Pd/C is an effective catalyst for aromatics production from alkanes selectively towards alkylbenzenes at 400 °C. Overall 3% Pd/Si-C shows the best performance due to the low oxygenated product yield and its total hydrocarbon yield is comparable to that obtained on 7%Pd/Si-C catalyst.

Table 12. **Different Pd loading on Si-C, 5 hours reaction**

Pd wt% on Si-Catalyst	Conversion	Molar Yield (%)					OLP Yield (wt%)
		n-alkanes (C10-C18)	alkenes (C17-C18)	C17 aromatics	C8-C13 aromatics	Oxygenated products	
0	92	42.4	37.8	9.1	0	13.0	90
1	98	49.1	37.5	9.4	0.3	8.6	88
3	100	42.8	20.7	8.4	7.1	4.9	66
5	100	39.5	19.9	8.0	7.5	3.0	60
7	100	56.6	33.3	12.5	0.1	5.2	95

Table 13. Different Pd loading on Si-C, 1 hour reaction

Pd wt% on Si-C Catalyst	Conversion	Molar Yield (%)					OLP Yield (wt%)
		n-alkanes (C10-C18)	alkenes (C17-C18)	C17 aromatics	C8-C13 aromatics	Oxygenated products	
0	65	16.8	24.9	6.1	0	45.8	94
1	65	19.3	25.8	6.6	0	42.4	90
3	89	40.3	26.0	10.2	0.1	17.3	82
5	84	42.0	30.7	9.6	0.2	28.7	99
7	92	45.5	27.8	10.6	0	20.6	92

Table 14 shows the n-alkane distribution in the organic liquid product at 1 hour. For all the catalysts, n-C17 was the main n-alkane, indicating the main reactions were decarboxylation of oleic acid followed by hydrogenation to n-heptadecane. Note that not all the alkenes are hydrogenated under the reaction conditions (Table 12 and Table 13). In addition, the 3, 5 and 7% Pd containing catalysts possess cracking activity which was drawn from formation of shorter chain n-alkanes. On the other hand, the oleic acid used in the experiments contains C16 fatty acid as an impurity (up to 10%). The n-C15 and n-C16 alkanes are the decarboxylation and hydrodeoxygenation products of C16 fatty acid for 0 and 1% Pd catalysts.

Table 14. n-alkane product distribution on Pd supported Si-C Catalyst, 1 hr

Pd wt% on Si-Catalyst	Molar Yield (%)								
	n-C10	n-C11	n-C12	n-C13	n-C14	n-C15	n-C16	n-C17	n-C18
0	0	0	0	0	0	1.8	4.1	6.7	4.2
1	0	0	0.6	0	0	1.2	4.4	8.9	4.3
3	1.2	0.7	0.8	0.5	0.5	3.0	7.6	21.8	4.0
5	0.9	0.5	0.8	0	0.6	2.1	7.3	25.5	4.3
7	0.7	0.6	0.8	0	0.6	3.7	8.4	26.3	4.4

4.3.8 Pd-Co Alloy on Activated Carbon

Oleic acid conversion and the liquid product yields, obtained with various Pd loaded Pd$_2$Co alloys on activated carbon after 1 hour in super-critical water, are given in Table 15. 5%Pd on activated carbon is also shown as a comparison. Conversion for each catalyst was more than 89 % after 1 hour reaction. Even the low metal loaded Pd$_2$Co alloy catalysts showed better performance in terms of both conversion and hydrocarbon yield compared with only Pd on activated carbon or Si-C. When the Pd loading was 5% in the Pd$_2$Co/C catalyst, decarboxylation (alkenes) yield only slightly increased compared to Pd only on carbon. For these two catalysts, a lower reduction temperature showed a slight improvement on the catalytic activity. 3% Pd$_2$Co/C-200 catalyst surprisingly showed the highest yield to oxygenated products and lowest yield to hydrocarbons. In the previous section, 3%Pd/Si-C shows high deoxygenation activity which is very different than 3%Pd in Pd$_2$Co/C-200. The morphology obtained by XRD (Table 6) shows that average metal particle size is smaller on Pd/Si-C than Pd$_2$Co/C. The larger metal particle formation can be attributed to alloy formation. For 5% Pd/C the Pd(111) phase appeared at 2θ=39.8° while it shifted to 40.1° for 5% Pd$_2$Co/C-300, 5% Pd$_2$Co/C-200 and 3% Pd$_2$Co/C-300, and to 40.0° for 3% Pd$_2$Co/C-200 catalysts (Figure 39).

Table 15. Different Pd loading in Pd$_2$Co alloy supported on C, 1 hour reaction

Pd$_2$Co/C-*x* (Pd wt%)	Conversion	Molar Yield (%)					OLP Yield (wt%)
		n-alkanes (C10-C18)	alkenes (C17-C18)	C17 aromatics	C8-C13 aromatics	Oxygenated products	
0.5% Pd$_2$Co/C-200	93	51.7	43.1	12.5	0.1	10.0	102
0.5% Pd$_2$Co/C-300	100	31.8	26.2	8.4	0	16.3	73
1% Pd$_2$Co/C-200	89	44.4	38.5	11.6	0.1	18.1	100
1% Pd$_2$Co/C-300	99	38.0	30.7	10.6	0.7	8.2	75
3% Pd$_2$Co/C-200	93	29.8	25.4	8.6	0.6	34.3	88
3% Pd$_2$Co/C-300	93	31.1	28.1	8.6	0	19.1	77
5% Pd$_2$Co/C-200	92	39.0	32.8	10.1	0.5	18.5	86
5% Pd$_2$Co/C-300	94	31.7	26.8	8.9	2.3	16.3	74
5% Pd/C	89	41.4	26.3	11.0	0.2	21.1	88

x= Reduction temperature (°C)
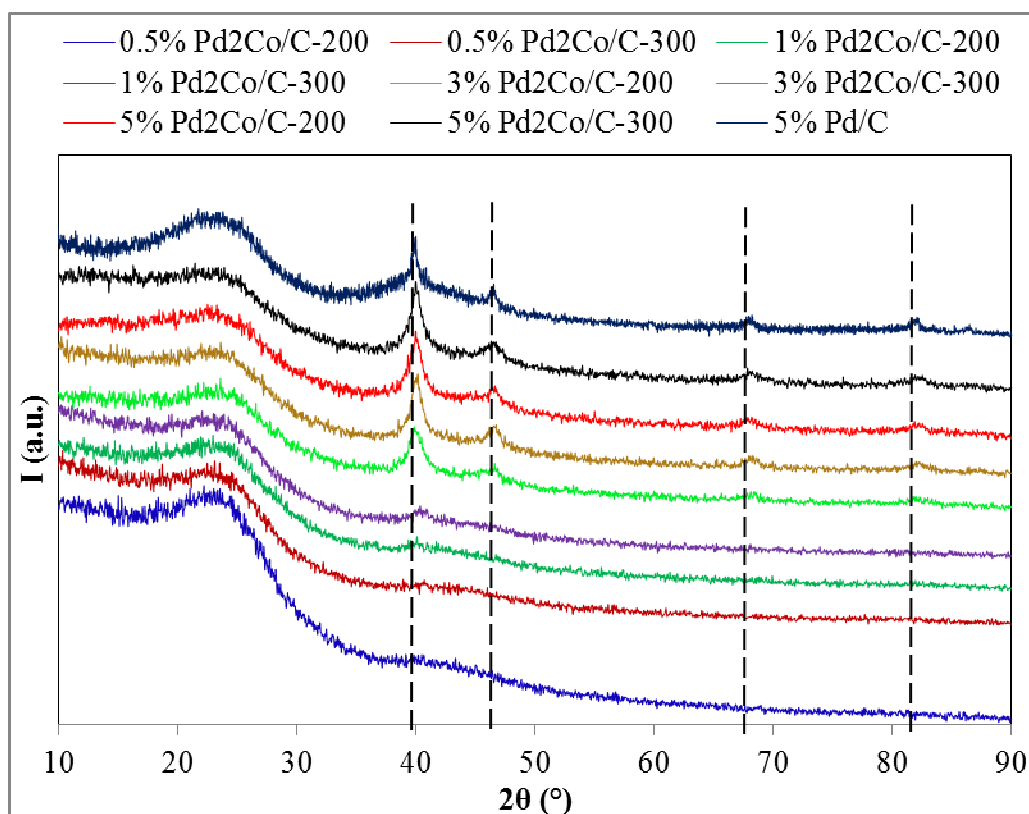
Figure 39. XRD of Pd$_2$Co/C and Pd/C catalysts

The atomic ratios of Pd and Co metals in the catalysts that were reduced at 300 °C are shown in Table 16. These values were calculated by EDAX, and the values shown in parenthesis represent the actual atomic ratios. For the catalysts 1% Pd_2Co/C and 5% Pd_2Co/C-300, EDAX results are fairly close to the actual atomic ratio of 68% Pd- 32% Co. This means the metal particles are well distributed. However, EDAX shows almost 50% Pd - 50%Co for 0.5% Pd_2Co/C-300 and 3% Pd_2Co/C-300 catalysts. This suggests possible segregation of Pd and Co particles on the carbon support for these 2 different metal loadings. On the other hand, SEM images and the metal mapping (Figure 40) show that none of the catalysts have metal aggregation.

Co   Pd
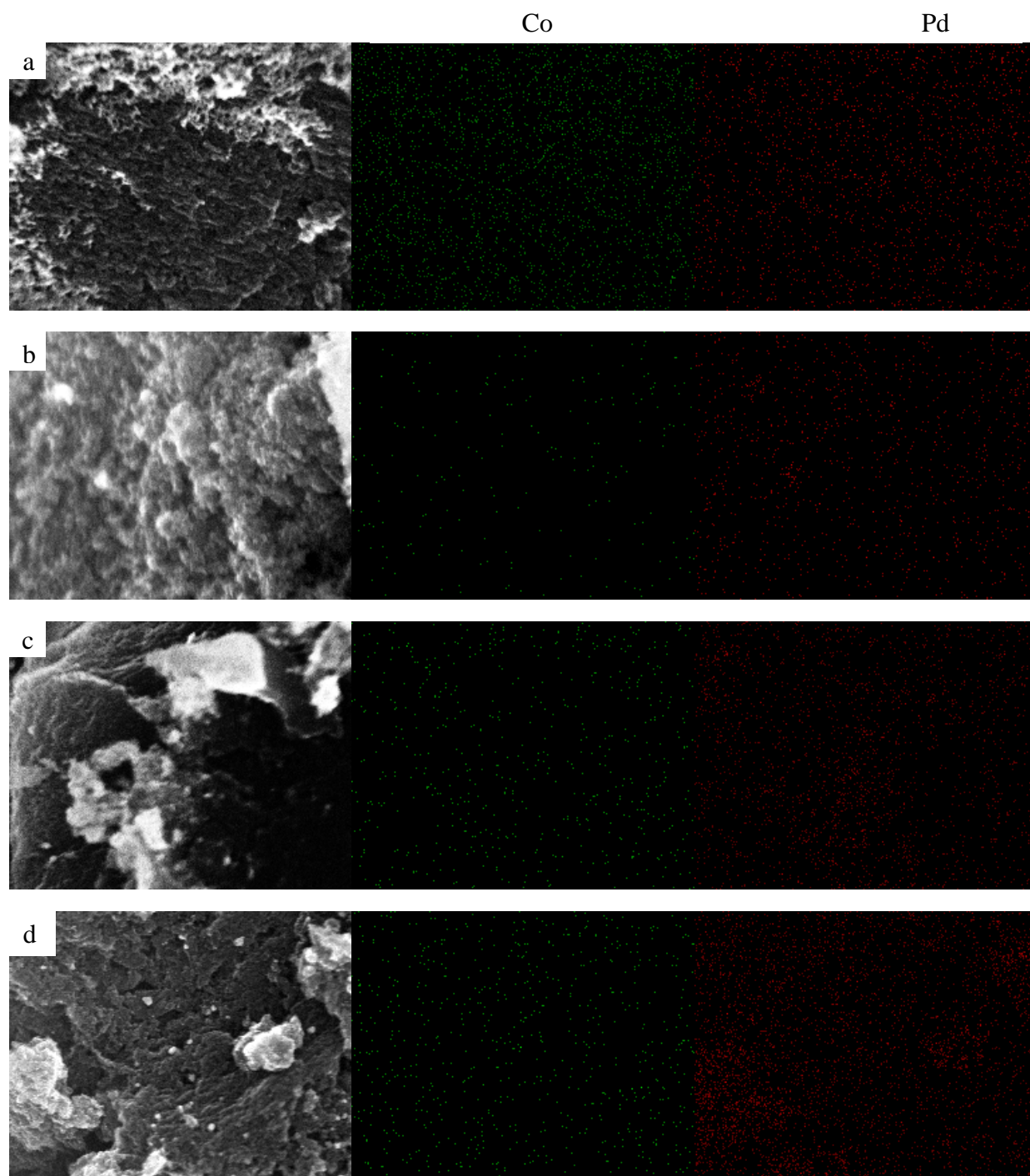
Figure 40. SEM images and metal particle mapping of samples Pd$_2$Co/C-200 with various Pd

loading: 0.5% (a), 1% (b), 3% (c) and 5% (d)

Table 16. Atomic ratios of Pd and Co metals in $Pd_2Co/C-300$ catalysts.

Element	At%[*]			
	0.5% Pd_2Co/C-300	1% Pd_2Co/C-300	3% Pd_2Co/C-300	5% Pd_2Co/C-300
PdL	47.30 (69%)	60.37 (68%)	48.56 (68%)	71.04 (68%)
CoK	52.70 (31%)	39.63 (32%)	51.44 (32%)	28.96 (32%)

[*]Atomic % of metals were calculated by EDAX
At% shown in parenthesis are the actual values

0.5% Pd_2Co/C-200 catalyst showed the best performance with low oxygenated product molar yield (10%), and with significantly high n-alkane, alkene and aromatic yields (Table 15). The XRD pattern does not show any Pd or Co metal phases, so it is hard to make a conclusion about its morphology. One possibility is that the Pd (0.5 wt%) and Co (0.1 wt%) metal concentrations are lower than the detection limit for XRD. Another possibility is that the Pd and Co metals are very well dispersed small clusters which agrees with the SEM images (Figure 40a-b).

With the exception of the 3% Pd_2Co/C-200 catalyst, all the catalaysts that were reduced at 200 °C showed better decarboxylation (alkene product) yield in comparison with the same metal loading containing catalysts that were reduced at 300 °C (Table 15). This can be attributed to the smaller particle size at lower heat treatment (Table 17). It is clear that the smaller particle size led to a higher active metal site surface area which was responsible from high decarboxylation activity. On the other hand, the effect of the alloy homogeneity on the support to the catalytic activity can not be ignored as discussed above. Additionally, the Pd-Pd bond distance (Table 6) and the decarboxylation performance of the catalysts (Table 15) are in good agreement. While 3% Pd_2Co/C-300, 5% Pd_2Co/C-200 and 5% Pd_2Co/C-300 all have similar

bond distance and show similar decarboxylation activity, the 3% Pd_2Co/C-200 catalyst shows a higher bond distance which can be related with its lower decarboxylation activity.

Table 17. Metal particle size calculated from XRD diffractions

Pd_2Co/C-x	Particle size, d_p (nm)	Lattice parameter, a (nm)	Pd-Pd bond distance (nm)
0.5% Pd_2Co/C-200	n.d.	n.d.	n.d.
0.5% Pd_2Co/C-300	n.d.	n.d.	n.d.
1% Pd_2Co/C-200	n.d.	n.d.	n.d.
1% Pd_2Co/C-300	n.d.	n.d.	n.d.
3% Pd_2Co/C-200	6.0	2.6001	2.2518
3% Pd_2Co/C-300	7.8	2.5951	2.2475
5% Pd_2Co/C-200	6.5	2.5959	2.2477
5% Pd_2Co/C-300	7.3	2.5956	2.2479
5% Pd/C	4.1	2.6119	2.2619

4.4. Conclusions

Both activated carbon and Si-C supports are highly active for oleic acid hydrothermal decarboxylation in super-critical water. These supports became much more active after Pd loading. A 0.5 wt% Pd_2Co/C catalyst showed even higher hydrocarbon yield than a 7 wt% Pd/C catalyst. The reason for the significantly high selective decarboxylation being promoted on Pd-Co alloy catalyst with a low Pd content was attributed to the well dispersed Pd and Co metal cluster formation, which led to a higher active metal surface are. The reduction temperature was an important factor to form smaller metal particle size. This study shows that an alloy of Pd on carbon with a significantly low Pd content is much more active and selective to diesel hydrocarbons production from an unsaturated fatty acid in super-critical water. Thus, Pd-C alloy

on carbon may be regarded as a prospective feasible decarboxylation catalyst for the removal of

oxygen from vegetable oil/animal fat without the need of additional H_2.

APPENDIX

ABBREVIATIONS

AC	Activated carbon
AMS	α-Methylstyrene
BET	Brunauer-Emmett-Teller
BG	Brown grease
bio-MTBE	Bio-methyl tert-butyl ether
BJH	Barrett-Joyner-Halenda
C18:0	Stearic acid
C18:1	Oleic acid
C18:2	Linoleic acid
C18:3	Linolenic acid
CCS	CO_2 capturing and storage
$C_{i,t}$	Concentration of product i at time t
DI	Deionized
EDS	Energy-Dispersive Spectrometer
EPA	Environmental Protection Agency
ETBE	Ethyl tert-butyl ether
FAME	Fatty acid methyl ester
FFA	Free fatty acid
FTIR	Fourier transform infrared
GC-FID	Gas chromatograph- flame ionization detector
GC-MS	Gas chromatograph-mass spectroscopy

GHG	Greenhouse gas
GTL	Gas to liquid
HC	Hydrocarbon
HC	Hydrocarbons
HDM	Hydrodemetalization
HDN	Hydrodenitrogenation
HDO	Hydrodeoxygenation
HDRD	Hydrogenation-derived renewable diesel
HDS	Hydrodesulfurization
LHSV	Liquid hour space velocity
NOx	Nitrogen oxides
OLP	Organic liquid product
PM	Particulate matter
S	Selectivity
SEM	Scanning electron microscopy
TAG	Triacylglycerol
TEM	Transmission electron microscopy
TEOS	Tetraethyl orthosilicate
XRD	X-ray diffraction

REFERENCES

(1)   *International Energy Agency. World Energy and Economic Outlook. International Energy Outlook 2009*, DOE/EIA, 2009.

(2)   *Statistical Review of World Energy 2009*. Available from. <http://www.bp.com/liveassets/bp_internet/globalbp/globalbp_uk_english/reports_and_publications/statistical_energy_review_2008/STAGING/local_assets/2009_downloads/statistical_review_of_world_energy_full_report_2009.xls#'Primary>. Accessed October 24, 2009.

(3)   *International Energy Agency, World Energy Outlook 2006*, Available from. <http://www.eia.doe.gov/oiaf/ieo/world.html>. Accessed December 9, 2011.

(4)   *Basic Research Needs: Catalysis for Energy*, U.S. Department of Energy, 2007.

(5)   Nylund, N. O.; Saksa, P. A.; Sipila, K. *Status and Outlook for Biofuels, Other Alternative Fuels and New Vehicles*, Espoo 2008. VTT Tiedotteita- Research Notes 2426.

(6)   *Inventory of U.S. Greenhouse Gas Emissions and Sinks: 1990-2007*, EPA, April 25, 2009.

(7)   Specht, M.; Zuberbuhler, U.; Bandi, A. *Why Bio-Fuels? - An Introduction into the Topic*, Centre for Solar Energy and Hydrogen Research.

(8)   Smith, B.; Greenwell, H. C.; Whiting, A. *Energy & Environmental Science* **2009**, *2*, 262.

(9)   Knothe, G.; Gerpen, J. V.; Krahl, J. *The Biodiesel Handbook*; AOCS Press, 2005.

(10)   Dale, B. *Journal of Agricultural and Food Chemistry* **2008**, *56*, 3885.

(11)   Schwietzke, S.; Ladisch, M.; Russo, L.; Kwant, K.; Makinen, T.; Kavalov, B.; Maniatis, K.; Zwart, R.; Shahanan, G.; Sipila, K.; Grabowski, P.; Telenius, B.; White, M.; Brown, A. *Analysis and Identification of Gaps in Research for the Production of Second- Generation Liquid Transportation Biofuels*, IEA Bioenergy, 2008.

(12)   Hoekman, S. K. *Renewable Energy* **2009**, *34*, 14.

(13)   Lynd, L. R. *Annu. Rev. Energy Environ.* **1996**, *21*, 403.

(14)   Malca, J.; Freire, F. *Energy* **2006**, *31*, 3362.

(15)   Toran, L.; Lipka, C.; Baehr, A.; Reilly, T.; Baker, R. *Water Res* **2003**, *37*, 3756.

(16)   *Wisconsin Biorefining Development Initiative. Fermentation of lignocellulosic biomass. http://www.wisbiorefine.org/proc/fermlig.pdf*.

(17)   Malloy, D.; Mayowski, K. In *Ninth Annual freshman Conference* University of Pittsburgh, 2009.

(18)   Muller, M.; Yelden, T.; Schoonover, H. In *Can both win in the era of ethanol?*; Policy, I. f. A. a. T., Ed. Minneapolis, 2007.

(19)   *Sustainable biofuels: prospects and challenges*, The Royal Society, 2008.

(20)   Achten, W. M. J.; Mathijs, E.; Verchot, L.; Singh, V. P.; Aerts, R.; Muys, B. *Biofuels, Bioproducts and Biorefining* **2007**, *1*, 283.

(21)   *Jet Fuel. http://www.algaelink.com/jet-fuel.htm*.

(22)   Leonard, C. In *The Washington Post*; Associated Press: 2007.

(23)   B. Freedman, M. O. B. *Journal of the American Oil Chemists' Society* **1989**, *66*, 1601.

(24)   Demirbas, A. *Energy Conversion and Management* **2008**, *49*, 2106.

(25)   Freedman, B.; Pryde, E. H.; Mounts, T. L. *Journal of the American Oil Chemists' Society* **1984**, *61*, 1638.

(26)   Canakci, M.; Gerpen , J. V. *Trans ASAE* **2001**, *44*, 1429.

(27)   Monyem, A.; Gerpen, J. H. V. *Biomass and Bioenergy* **2001**, *20,* 317.

(28)   Simakova, I.; Simakova, O.; Maki-Arvela, P.; Murzin , D. Y. *Catal. Today* **2009**.

(29)   Goguen, S. *Energy Technology Drivers for Change- U.S. DOE Perspective.*, Transportation Technologies and Fuels Forum, June 5-7, 2006.

(30)   *Neste Oil. NExBTL diesel.*

http://www.nesteoil.com/default.asp?path=1,41,11991,12243,12335,12337, 2009.

(31)   *The Integration of Biofuels Inside the Refinery Gate: Implementation, Logistics and Strategies*, The Catalyst Group Resources, February 2009.

(32)   *Alternative & Advanced Fuels.*

http://www.afdc.energy.gov/afdc/fuels/emerging_green_production.html.

(33)   Craig, W. K.; Soveran.D. W. US Patent 4,992,605, February 1991.

(34)   Monnier, J.; Tourigny, G.; Soveran, D. W.; Wong, A.; Hogan, E. N.; Stumborg, M. US Patent 5,705,722, January 1998.

(35)   Immer, J. G., Liquid-phase deoxygenation of free fatty acids to hydrocarbns using supported palladium catalysts. North Carolina State University, 2010.

(36)   Iva Kubickova, M. S., Kari Eranen, Paivi Maki-Arvela,Dmitry Yu. Murzin *Catalysis Today* **2005**, *106*, 197.

(37)   Snare, M.; Kubickova, I.; Maki-Arvela, P.; Eranen, K.; Warna, J.; Murzin, D. Y. *Chemical Engineering Journal* **2007**, *134*, 29.

(38)   Snare, M.; Kubickova, I.; Maki-Arvela, P.; Eranen, K.; Murzin, D. Y. *Ind. Eng. Chem. Res* **2006**, *45*, 5708.

(39)   Lestari, S.; Simakova, I.; Tokarev, A.; Maki-Arvela, P.; Eranen, K.; Murzin. D. Y. *Catal Lett* **2008**, *122*, 247.

(40)   Arnold, E. *Porosity in Carbons*; Hodder Headline Group: London, 1995.

(41)   Garcia-Bordeje, E.; Kapteijn, F.; Moulijn, J. A. *Carbon* **2002**, *40*, 1079.

(42)   Scaroni, A. W.; Jenkins, R. G.; Walker, P. L. *Applied Catalysis* **1985**, *14*, 173.

(43)   Viswanathan, B.; Neel, P. I.; Varadarajan, T. K.; National Centre for Catalysis Research Indian Institute of Technology Madras: Chennai, India, 2009.

(44)   Sing, K. S. W.; Everett, D. H.; Haul, R. A. W.; Moscou, L.; Pierotti, R. A.; Rouquerol, J.; Siemieniewska, T. *Pure & Appl. Chem.* **1985**, *57*, 603.

(45)   Heiszwolf, J. J. 2000; Introduction to monoliths *<http://www.dct.tudelft.nl/monoliet/Intro/introduction.html>.* Accessed on August 19, 2010.

(46)   Kapteijn, F. In *6th NICE Workshop San Donato Milanese* Italy, 1999.

(47)   Hilmen, A. M.; Bergene, E.; Lindvag, O. A.; Schanke, D.; Eri, S.; Holmen, A. *Catalysis Today* **2001**, *69*, 227.

(48)   Boger, T.; Zieverink, M. M. P.; Kreutzer, M. T.; Kapteijn, F.; Moulijn, J. A.; Addiego, W. P. *Ind. Eng. Chem. Res* **2004**, *43*, 2337

(49)   Kreutzer, M. T.; Heiszwolf, J. J.; Nijhuis, T. A.; Kapteijin, F.; Moulij, J. A.; Delf University of Technology, Department of Chemical Engineering: the Netherlands.

(50)   Nijhuis, T. A.; Beers, A. E. W.; Kapteijn, F.; Moulijn, J. A.; Delft University of Technology, Industrial Catalysis: the Netherlands.

(51)   Boda, L.; Onyestyak, G.; Solt, H.; Lonyi, F.; Valyon, J.; Thernesz, A. *Applied Catalysis A: General* **2010**, *374*, 158.

(52)   Myllyoj, J.; Aalto, P.; Savolainen, P.; Purola, V.-M.; Alopaeus, V.; Gronqvist, J. In *United States Patent Application Publication*; Neste Oil: 2007; Vol. US 2007/0010682 A1.

(53)   McCall, M. J.; Marker, T. L.; Marinangeli, R. E.; KocalJoseph, A. In *United States Patent Application Publication* US, 2009; Vol. 0162264.

(54)   Mikulec, J.; Cvengros, J.; Porikova, L.; Banic, M.; Kleinova, A. In *44th International Petroleum Conference* Bratislava, Slovak Republic, 2009.

(55)   PPRC *Can Brown Grease be Used for Biodiesel Manufacturing in the Puget Sound?. Available from.*

<http://www.pprc.org/research/rapidresDocs/BrownGreaseforBio-Diesel.pdf>. Accessed December 10, 2010, 2008.

(56)   Canakci, M.; Gerpen, V. J. *American Society of Agricultural Engineers* **2001**, *44*, 1429.

(57)   Wang, Z. M.; Lee, J. S.; Park, J. Y.; Wu, C. Z.; Yuan, Z. H. *Korean J. Chem. Eng.* **2008**, *25*, 670.

(58)   Nu-Energie 2008.

(59)   Myllyoj, J.; Aalto, P.; Savolainen, P.; Purola, V. M.; Alopaeus, V.; Gronqvist, J. 2007.

(60)   Kim, M.; DiMaggio, C.; Yan, S.; Wang, H.; Salley, S. O.; Ng, K. Y. S. *Bioresource Technology* **2011**, *102*, 2380.

(61)   Tiwari, R.; Rana, B. S.; Kumar, R.; Verma, D.; Kumar, R.; Joshi, R. K.; Garg, M. O.; Sinha, A. K. *Catalysis Communications* **2011**, *12*, 559.

(62)   Strege, J. R.; Oster, B. G.; Pansegrau, P. D.; Wocken, C. A.; Aulich, T. R. 2010.

(63)   Maki-Arvela, P.; Kubickova, I.; Snare, M.; Eranen, K.; Murzin, D. Y. *Energy & Fuels* **2007**, *21*, 30.

(64)   Immer, J. G.; Kelly, M. J.; Lamb, H. H. *Applied Catalysis A: General* **2010**, *375*, 134.

(65)   Simakova, I.; Simakova, O.; Maki-Arvela, P.; Murzin, D. Y. *Catal. Today* **2010**, *150*, 28.

(66)   Simakova, I.; Simakova, O.; Maki-Arvela, P.; Simakov, A.; Estrada, M.; Murzin, D. Y. *Applied Catalysis A: General* **2009**, *355*, 100.

(67)   Lestari, S.; Maki-Arvela, P.; Eranen, K.; Beltramini, J.; Lu, G. Q. M.; Murzin, D. Y. *Catal Lett* **2010**, *134*, 250.

(68)   Lestari, S.; Simakova, I.; Tokarev, A.; Maki-Arvela, P.; Eranen, K.; Murzin, D. Y. *Catal Lett* **2008**, *122*, 247.

(69)   Snare, M.; Kubickova, I.; Maki-Arvela, P.; Chichova, D.; Eranen, K.; Murzin, D. Y. *Fuel* **2008**, *87*, 933.

(70)   Bernas, A.; Myllyoj, J.; Salmi, T.; Murzin, D. Y. *Applied Catalysis A: General* **2009**, *353*, 166.

(71)   *Fatty Acids in Industry*; Johnson, R. W.; Fritz, E., Eds.; Marcel Dekker, Inc.: New York, 1988.

(72)   Tolvanen, P.; Maki-Arvela, P.; Kumar, N.; Eranen, K.; Sjoholm, R.; Hemming, J.; Holmbom, B.; Salmi, T.; Murzin, D. Y. *Applied Catalysis A: General* **2007**, *330*, 1.

(73)   Elsasser, F. A.; Mccargar, L. A. 2001.

(74)   Simakova, I.; Rozmysłowicz, B.; Simakova, O.; Maki-Arvela, P.; Simakov, A.; Murzin, D. Y. *Top Catal* **2011**, *54*, 460.

(75)   Zahedi, G.; Yaghoobi, H. *International Journal of Chemical and Biological Engineering* **2008**, *1*, 114.

(76)   Bhasin, M. M.; McCain, J. H.; Vora, B. V.; Imai, T.; Pujado, P. R. *Applied Catalysis A: General* **2001**, *221*, 397.

(77)   Augustine, R. L. *Heterogenous Catalysis for the Synthetic Chemist*; Marcel Dekker: New York, 1996.

(78)   Padmavathi, G.; Chaudhuri, K. K.; Rajeshwer, D.; Sreenivasa, R. G.; Krishnamurthyb, K. R.; Trivedic, P. C.; Hathic, K.; Subramanyamc, N. *Chemical Engineering Science* **2005**, *60*, 4119

(79)   Kubickova, I.; Snare, M.; Eranen, K.; Maki-Arvela, P.; Murzin, D. Y. *Catalysis Today* **2005**, *106*, 197.

(80)   Immer, J. G.; Lamb, H. H. *Energy and Fuels* **2010**, *24*, 5291.

(81)   Maier, W. *Chemische Berichte* **1982**, *115*, 808.

(82)   Simakova, I.; Simakova, O.; Maki-Arvela, P.; Murzin, D. Y. *Catalysis Today* **2010**, *150*, 28.

(83)   Ping, E. W.; Wallace, R.; Pierson, J.; Fuller, T.; Jones, C. W. *Microporous and Mesoporous Materials* **2010**, *132*, 174.

(84)   Ping, E. W.; Pierson, J.; Wallace, R.; Miller, J. T.; Fuller, T. F.; Jones, C. W. *Applied Catalysis A: General* **2011**, *396*, 85.

(85)   Arend, M.; Nonnen, T.; Hoelderich, W. F.; Fischer, J.; Groos, J. *Applied Catalysis A: General* **2011**, *399*, 198.

(86)   Bernas, H.; Eranen, K.; Simakova, I.; Leino, A. R.; Kordas, K.; Myllyoja, J.; Maki-Arvela, P.; Salmi, T.; Murzin, D. Y. *Fuel* **2010**, *89*, 2033.

(87)   Lestari, S.; Maki-Arvela, P.; Bernas, H.; Simakova, O.; Sjoholm, R.; Beltramini, J.; Lu, G. Q. M.; Myllyoja, J.; Simakova, I.; Murzin, D. Y. *Energy & Fuels* **2009**, *23*, 3842.

(88)   Immer, J. G.; Kelly, M. J.; Lamb, H. H. *Applied Catalysis A: General* **2010**, *375*, 134.

(89)   Liu, R.; Shi, Y.; Wan, Y.; Meng, Y.; Zhang, F.; Gu, D.; Chen, Z.; Tu, B.; Zhao, D. *J. Am. Chem. Soc.* **2006**, *128*, 11652.

(90)   Wan, Y.; Wang, H.; Zhao, Q.; Klingstedt, M.; Terasaki, O.; Zhao, D. *J. Am. Chem. Soc.* **2009**, *131*, 4541.

(91)   Anderson, M. L.; Stroud, R. M.; Rolison, D. R. *Nano Lett.* **2002**, *2*, 235.

(92)   Radkevich, V. Z.; Senko, T. L.; Wilson, K.; Grishenko, L. M.; Zaderko, A. N.; Diyuk, V. Y. *Applied Catalysis A: General* **2008**, *335*, 241.

(93)   Pradhan, B. K.; Sandle, N. K. *Carbon* **1999**, *37*, 1323.

(94)   Polovina, M.; Babi, B.; Kaluderovi, B.; Dekanski, A. *Carbon* **1997**, *35*, 1047.

(95)   Markus, H.; Plomp, A., J. ,; Maki-Arvela, P.; Bitter, J. H.; Murzin, D. Y. *Catalysis Letters* **2007**, *113*, 141.

(96)   Yang, H.; Yan, Y.; Liu, Y.; Zhang, F.; Zhang, R.; Meng, Y.; Li, M.; Xie, S.; Tu, B.; Zhao, D. *J. Phys. Chem. B* **2004**, *108*, 17320.

(97)   Park, K.-W.; Sung, Y.-E. *J. Phys. Chem. B* **2004**, *108*, 939.

(98)   Kragten, D. D.; Fedeyko, J. M.; Sawant, K. R.; Rimer, J. D.; Vlachos, D. G.; Lobo, R. F. *J. Phys. Chem. B* **2003**, *107*, 10006.

(99)   Gurrath, M.; Kuretzky, T.; Boehm, H. P.; Okhlopkova, L. B.; Lisitsyn, A. S.; Likholobov, V. A. *Carbon* **2000**, *38*, 1241.

(100)   Krishnankutty, N.; Vannice, M. A. *Journal of Catalysis* **1995**, *155*, 312.

(101)   Sing, K. S. W.; Everett, D. H.; Haul, R. A. W.; Moscou, L.; Pierotti, R. A.; Rouquerol, J.; Siemieniewska, T. *Pure & Appl. Chem.* **1985**, *57*, 603.

(102)   Klein, L. C. In *Thin Film Processes II*; Vossen, J. L., Kern, W., Eds.; Academic Press, Inc.: San Diego, CA, 1991, p 501.

(103)   VAN-DER-VIS, M. G. M.; CORDFUNKE, E. H. P.; KONINGS, R. J. M. *Jornoul De Physique IV Colloque C3, supplement au Journal de Physique 11* **1993**, *3*, 75.

(104)   Fukunaga, A.; Okayasu, Y.; Patent No. EP0495392A1 (22 July 1992), Ebara Corporation: Japan; Vol. EP 0495392 A1.

(105)   Tseng, H. H.; Wey, M. Y. *Chemosphere* **2006**, *62*, 756.

(106) Toebes, M. L.; Dillen, J. A.; De Jong, K. P. *Journal of Molecular Catalysis A: Chemical* **2001**, *173*, 75.

(107) Tripathi, B. P.; Shahi, V. K. *Progress in Polymer Science* **2011**, *36*, 945.

(108) Seco, A. M.; Goncalves, M. C.; Almeida, R. M. *Materials Science and Engineering* **2000**, *B76*, 193.

(109) Silverstein, R. M.; Webster, F. X. In *Spectrometric Identification of Organic Compounds*; Sixth ed.; John Wiley & Sons, Inc: New York, 1998, p 71.

(110) Vinke. P. ; Van Der Eijk. M.; Verbree. M. ; Voskamp. A.F. ; Van Bekkum. H. *Carbon* **1994**, *32*, 675.

(111) Solum, M. S.; Pugmire, R. J.; Jagtoyen, M.; Derbyshire, F. *Carbon* **1995**, *33*, 1247.

(112) Smith, M. B.; March, J. *March's Advanced Organic Chemistry: Reactions, Mechanisms, and Structure* 5th ed.; Wiley-Interscience, 2001.

(113) Puziy, A. M.; Poddubnaya, O. I.; Martinez-Alonso, A.; Suarez-Garcia, F.; Tascon, J. M. D. *Carbon* **2002**, *40*, 1493.

(114) de Celis, J. P.; Villaverde, M. S.; Cukierman, A. L.; Amadeo, N. E. *Latin American Applied Research* **2009**, *39*, 165.

(115) Boehm, H.-P. *Angew. Chem. Internat. Edit.* **1966**, *5*, 533.

(116) Ziemecki, S. B.; Jones, G. A.; Swartzfager, D. G.; Harlow, R. L. *J. Am. Chem. Soc.* **1985**, *107*, 4547.

(117) Lamber, R.; Jaeger, N.; Schulz-Ekloff, G. *Surf. Sci.* **1990**, *227*, 15.

(118) Hallen, R. T.; Albrecht, K. O.; Brown, H. M.; White, J. F.; Battelle Memorial Institute, Richland, WA: USA, 2013.

(119) ShaineTyson K.; National Renewable Energy Laboratory: 2002.

(120) Koivusalmi E.; Jakkula J.; Neste Oil Oyj: USA, 2007.

(121) Jakkula J.; Niemi V.; Nikkonen J.; Purola V.; Myllyoja J.; Aalto P.; Lehtonen J.; Alopaeus V.; Fortum OYJ: USA, 2007.

(122) Faraci, G.; Gosling, C.; Holmgren, J.; Marinangeli, R.; Marker, T.; Perego, C. *Hydrocarbon Processing* **2007**, 67.

(123) Simacek, P.; Kubicka, D.; Sebor, G.; Pospisil, M. *Fuel* **2010**, *89*, 611.

(124) Kubicka, D.; Kaluza, L. *Applied Catalysis A: General* **2010**, *372*, 199.

(125) Snare, M.; Kubickova, I.; Maki-Arvela, P.; Eranen, K.; Murzin, D. Y. *Ind. Eng. Chem. Res.* **2006**, *45*, 5708.

(126) Roberts, W. L.; Lamb, H. H.; Stikeleather, L. F.; Turner, T. L.; North Carolina State University: USA, 2010.

(127) Bernas, H.; Eranen, K.; Simakova, I.; Leino, A. R.; Kordas, K.; Myllyoja, J.; Maki-Arvela, P.; Salmi, T.; Murzin D.Y. *Fuel* **2010**, *89*, 2033.

(128) Lestari, S.; Maki-Arvela, P.; Bernas, H.; Simakova, O.; Sjoholm, R.; Beltramini, J.; Lu, G. Q. M.; Myllyoja, J.; Simakova, I.; Murzin, D. Y. *Energy & Fuels* **2009**, *23*.

(129) Ping, E. W.; Pierson, J.; Wallace, R.; Miller, J. T.; Fuller, T. F.; Jones, C. W. *Applied Catalysis A: General.* **2011**, 85.

(130) Huber, G. W.; Dumesic, J. A. *Catalysis Today* **2006**, *111*, 119.

(131) Idem, R. O.; Katikaneni, S. P. R.; Bakhshi, N. N. *Energy & Fuels* **1996**, 1150.

(132) Fu, J.; Lu, X.; Savage, P. E. *Energy Environ. Sci.* **2010**, *3*, 311.

(133)   Fu, K.; Shi, F.; Thompson, L. T.; Lu, X.; Savage, P. E. *ACS Catal.* **2011**, *1*, 227.

(134)   Watanabe, M.; Inomata, H.; Smith, R. L.; Arai, K. *Applied Catalysis A: General* **2001**, *219*, 149.

(135)   Watanabe, M.; Iida, T.; Inomata, H. *Energy Conversion and Management* **2006**, *47*, 3344.

(136)   Na, J. G.; Yi, B. E.; Kim, J. N.; Yi, K. B.; Park, S. Y.; Park, J. H.; Kim, J. N. *Catalysis Today* **2010**, *156*, 44.

(137)   Fu, K.; Lu, X.; Savage, P. E. *ChemSusChem* **2011**, *4*, 481.

(138)   Zhang, L.; Lee, K.; Zhang, J. *Electrochimica Acta* **2007**, *52*, 7964.

(139)   Belsky, A. J.; Maiella, P. G.; Brill, T. B. *J. Phys. Chem. A* **1999**, *103*, 4253.

(140)   Roy, D. M.; Roy, R.; Osborn, E. F. *American Journal of Science* **1953**, *251*, 337.

(141)   Giauque, W. F. *. Am. Chem. Soc.* **1949**, *71*, 3192.

(142)   Reynolds, W.; Robinson, R. L. 1952.

(143)   Deo, A. V.; Lana, I. G. *J. Phys. Chem.* **1969**, *73*, 716.

(144)   Ravenelle, R. M.; Copeland, J. R.; Kim, W. G.; Crittenden, J. C.; Sievers, C. *ACS Catal.* **2011**, *1*, 552.

(145)   Suresh, C.; Santhanaraj, D.; Gurulakshmi, M.; Deepa, G.; Selvaraj, M.; Rekha, N. R. S.; Shanthi, K. *ACS Catal.* **2012**, *2*, 127.

(146)   Yin, M.; Natelson, R. H.; Campos, A. A.; Kolar, P.; Roberts, W. L. *Fuel* **2013**, *103*, 408.

ABSTRACT

**GREEN DIESEL PRODUCTION VIA CATALYTIC
HYDROGENATION/DECARBOXYLATION OF TRIGLYCERIDES AND FATTY
ACIDS OF VEGETABLE OIL AND BROWN GREASE**

by

ELVAN SARI

August 2013

Advisor: K. Y. Simon Ng, PhD

Co-Advisor: Steven O. Salley, PhD

Major: Chemical Engineering

Degree: Doctor of Philosophy

Increase in the petroleum prices, projected increases in the world's energy demand and environmental awareness have shifted the research interest to the alternative fuel technologies. In particular, green diesel, vegetable oil/animal fat/waste oil and grease derived hydrocarbons in diesel boiling range, has become an attractive alternative to biodiesel— a mixture of fatty acid methyl esters, particularly due to its superior fuel properties that are similar to petroleum diesel. Hence, green diesel can be used as a drop-in fuel in the current diesel engines. The current technology for production of green diesel- hydrodeoxygenation of triglycerides and fatty acids over conventional hydrotreating catalysts suffers from fast catalyst deactivation in the absence of hydrogen combined with high temperatures and high fatty acid content in the feedstock. Additionally, excess hydrogen requirement for hydrodeoxygenation technique leads to high production costs. This thesis proposes a new technology- selective decarboxylation of brown grease, which is a mixture of fats and oils collected from waste water trap and rich in fatty acids,

over a supported noble metal catalyst that overcomes the green diesel production challenges. In contrast to other feedstocks used for liquid biofuel production, brown grease is inexpensive and non- food competing feedstock, therefore the process finds solution to waste management issues, reduces the renewable fuel production cost and does not add to the global food shortage problems. Special catalyst formulations were developed to have a high activity and stability in the absence of hydrogen in the fatty acid decarboxylation process. The study shows how catalyst innovations can lead to a new technology that overcomes the process challenges.

First, the effect of reaction parameters on the activity and the selectivity of brown grease decarboxylation with minimum hydrogen consumption over an activated carbon supported palladium catalyst were investigated. A 90% conversion of brown grease in a semi-batch mode was obtained in 7 hours. In contrast, in a batch reaction the conversion was roughly 40% in the same reaction time. However, by pre-treating the "as received" brown grease with H_2, the conversion in a batch reactor was increased 1.4-fold; and when the H_2 to BG ratio was increased to 3/1 (mol/mol), the conversion was further improved. Therefore, such a two-step processing with selective hydrogenation prior to the decarboxylation of BG improves the product selectivity. The commercial 5% Pd/C catalyst was highly active for the decarboxylation of brown grease to green diesel at 300 ^{o}C and 1.5 MPa.

Second, a class of Pd catalyst supported on a silica-activated carbon nanocomposite for free fatty acid decarboxylation was developed, and displayed excellent activity and operation stability selectively for the green diesel hydrocarbons formation in the absence of hydrogen under mild reaction conditions. The decarboxylation activities of different amount of silica containing catalysts were investigated in a batch reactor under inert gas. Among them, the formulation with the fewer oxygen surface groups (Pd/Si-C-4) was the most active catalyst for

the decarboxylation of an unsaturated fatty acid. The high activity of the Pd/Si-C-4 catalyst is attributed to its accessible and well-distributed metallic Pd nanoparticles inside hybrid mesopores as well as to its low acidity, weak surface interactions and inertness. Thus, Pd supported on carbon modified with silica may be regarded as a prospective decarboxylation catalyst for the removal of oxygen from vegetable oil/animal fat without the need of additional hydrogen.

Third, in order to design a suitable catalyst for conversion of brown grease to green diesel, a systematic study of the model compounds- oleic acid was conducted on various catalysts in super-critical water to understand the reaction pathways in the absence of hydrogen. A Si-C support was more effective than activated carbon itself for both decarboxylation of oleic acid and hydrogenation of alkenes. In an additional effort to reduce Pd amount in the catalyst, Pd_2Co/C catalysts with various Pd content were prepared and the catalytic activity study showed that 0.5 wt% Pd_2Co/C catalyst performs even better than a 5 wt% Pd/C catalyst. Pd and Co alloys were very well dispersed and formed fine clusters, which led to a higher active metal surface area and hence favored the decarboxylation of oleic acid. This study showed that an alloy of Pd on carbon with a significantly low Pd content is much more active and selective to diesel hydrocarbons production from an unsaturated fatty acid in super-critical water and may be regarded as a prospective feasible decarboxylation catalyst for the removal of oxygen from vegetable oil/animal fat without the need of additional hydrogen.

AUTOBIOGRAPHICAL STATEMENT

Name: Elvan Sari

Date of Birth: January 1, 1985

Education:

2011 - M.S. Chemical Engineering, Wayne State University, Detroit, MI 48202

2008 - B.S. Chemical Engineering, Istanbul Technical University, Istanbul, Turkey

Publications:

1. *Catalytic Conversion of Brown Grease to Green Diesel via Decarboxylation over Activated Carbon Supported Palladium Catalyst*. Sari, Elvan; DiMaggio, Craig; Kim, Manhoe; Salley, Steven O.; Ng, K. Y. Simon, Industrial & Engineering Chemistry Research (Accepted on 07/21/2013)

2. *A Highly Active Nanocomposite Silica-Carbon Supported Palladium Catalyst for Decarboxylation of Free Fatty Acids for Green Diesel Production: Correlation of Activity and Catalyst Properties*. Sari, Elvan; Kim, Manhoe; Salley, Steven O.; Ng, K. Y. Simon. Applied Catalysis A: General (Accepted on 07/23/2013)

3. *Diesel Production from Hydrothermal Catalytic Decarboxylation of Oleic Acid in Super-Critical Water and Effect of Pd-Co Alloy on the Catalytic Activity and Diesel Yield*. Sari, Elvan; Alwan, Basem Al; Kim, Manhoe; Salley, Steven O.; Ng, K. Y. Simon. Ready to Submit.

Selected Presentations:

Sari, Elvan; Kim, Manhoe; Salley, Steven O.; Ng, K. Y. Simon. *Si-C Supported Palladium for Liquid Phase Decarboxylation of Oleic Acid to Diesel Hydrocarbons*. 23rd North American Catalysis Society Meeting, Louisville, KY, June 2-7, 2013.

Sari, Elvan; Kim, Manhoe; Salley, Steven O.; Ng, K. Y. Simon. *Effect of Hydrogen on Catalytic Decarboxylation of Brown Grease to Green Diesel*. AIChE Annual Meeting, Pittsburgh, PA, October 28-November 2, 2012.

Sari, Elvan; DiMaggio, Craig; Kim, Manhoe; Salley, Steven O.; Ng, K. Y. Simon. *Production of Green Diesel from Brown Grease via Decarboxylation*. AIChE Annual Meeting, Minneapolis, MS, October 16-21October, 2011.

Sari, Elvan; DiMaggio, Craig; Kim, Manhoe; Salley, Steven O.; Ng, K. Y. Simon. *Production of Green Diesel from Brown Grease via a Two-Step Catalytic Hydrogenation/Decarboxylation*. 22nd North American Catalysis Society Meeting, Detroit, MI, June 5-10, 2011